NOAA Technical Memorandum ERL WPL-7

U.S. DEPARTMENT OF COMMERCE
NATIONAL OCEANIC AND ATMOSPHERIC ADMINISTRATION
Environmental Research Laboratories

Applications of Remote Sensing Techniques to Buoy-Based Environmental Data Gathering

STAFF, WAVE PROPAGATION LABORATORY
V.E. DERR, EDITOR

Wave
Propagation
Laboratory
BOULDER,
COLORADO
September 1972

ONMENTAL RESEARCH LABORATORIES

WAVE PROPAGATION LABORATORY

NATIONAL OCEANIC AND ATMOSPHERIC ADMINISTRATION

U.S. DEPARTMENT OF COMMERCE
National Oceanic and Atmospheric Administration
Environmental Research Laboratories

NOAA Technical Memorandum ERL WPL-7

APPLICATIONS OF REMOTE SENSING TECHNIQUES TO BUOY-BASED ENVIRONMENTAL DATA GATHERING

Staff, Wave Propagation Laboratory
V.E. Derr, Editor

Wave Propagation Laboratory
Boulder, Colorado
September 1972

TABLE OF CONTENTS

APPLICATIONS OF REMOTE SENSING TECHNIQUES TO BUOY-BASED ENVIRONMENTAL DATA GATHERING

National Oceanic and Atmospheric Administration
Wave Propagation Laboratory
Boulder, Colorado
September 29, 1972

Section 1 INTRODUCTION

V. E. Derr, C. G. Little, and C. B. Emmanuel

1.0 The Scope of the Report

1.1 The Status of Various Relevant Remote Sensing Program Within WPL

This report, written by the staff of the Wave Propagation Laboratory (WPL), is in response to a request by the National Data Buoy Project (NDBP) to evaluate the possible remote sensing techniques for the interrogration of both the marine atmosphere and the ocean from buoys. Initially, WPL proposed a three-man year, $90K effort; because of FY 72 fiscal limitations in NDBP, a brief $15K effort was eventually undertaken. This abbreviated study, of course, is far from complete, but it is believed that the principal optical, radio, and acoustic remote sensing concepts relevant to ocean buoys are identified and discussed. The main body of the report discusses existing remote sensing concepts and makes a preliminary evaluation of their potential applicability to the needs and objectives of the National Data Buoy Project.

In recent years, remote sensing of the atmosphere has received new impetus from the development of a wide range of sensing systems which have given excellent capabilities for the remote interrogation of the atmospheric environment. In this area, the Wave Propagation Laboratory has successfully used acoustic sounding, FM/CW radar, optical lidars, and radiometry as well as other radar techniques to map the physical state of the atmosphere. The observational ranges vary with the technique from hundreds to many thousands of meters.

The main objectives of NDBP are the monitoring of the marine atmosphere, the ocean surface and the upper layers of the ocean. In particular, the interrogation involves measurements of the meteorological and ocean variables. In the former category, variables of prime interest are the surface values and the vertical profiles of wind, temperature, and humidity, with secondary interest in precipitation, clouds, and aerosol. In the ocean, the quantities of interest include sea state (especially the wave spectra), surface temperature, salinity, current flow, chlorophyll content, etc. The buoy measurements are designed to increase our knowledge of the present state of the marine atmosphere and the ocean in the vicinity of the buoy in order to help in prediction of their future state. Such information is required for weather forecasting, fisheries, and marine transportation purposes as well as for research use.

This preliminary report addresses itself to the remote sensing needs of the NDBP with particular emphasis on the broad range of technologies available within WPL. The different sections of the report, and their authors, are as follows:

1.	Introduction	V. E. Derr, C. G. Little, C. B. Emmanuel
2.	Acoustic Sounding	F. F. Hall, C. B. Emmanuel, P. A. Mandics
3.	Radar	R. G. Strauch, D. E. Barrick
4.	Lidar	V. E. Derr, R. B. Slusher
5.	Radiometry	M. T. Decker, E. R. Westwater
6.	Line-of-Sight Methods	R. S. Lawrence
7.	Summary and Recommendations	C. G. Little, V. E. Derr

It is recommended that technical questions concerned with specific sections be directed to the principal author of that section, while inquiries relating to the general content of the report should be addressed to V. E. Derr or C. G. Little. Interested readers may find additional information in the following documents: (1) Collected reprints of the Wave Propagation Laboratory, NOAA, November 1971, (2) Potential capabilities of Four Lower Remote Sensing Techniques, Staff, Wave Propagation Laboratory, NOAA, TRERL 227-WPL20, December 1971, (3) Remote Sensing of the Troposphere,

V. E. Derr, NOAA, August 15, 1972, (4) Status of Remote Sensing of the Troposphere, C. G. Little, Bulletin AMS, October, 1972.

1.1 The Status of Various Relevant Remote Sensing Programs Within WPL

The following is a brief summary of the status of various relevant remote sensing programs within WPL.

Acoustic sounding techniques for the interrogation of the atmospheric environment have been shown to hold great promise in planetary boundary layer studies. This is due to the fact that acoustic waves are far more sensitive to fluctuations in wind speed, temperature, and humidity than are electromagnetic waves. To date experimental work carried out by WPL has been very successful in measuring wind, turbulence, and temperature fluctuations. Vertical wind components have been successfully measured to heights of the order 300m, with an accuracy of about 0.2 meters per second, using the acoustic sounder in the monostatic Doppler mode. Operation in the bistatic mode is expected to permit measurement of the horizontal component with an accuracy of approximately 1 m per second to to heights of the order of 1 km. In addition, acoustic sounders have been used to sense the small-scale temperature structure of the atmosphere and although they have not been used to measure temperature profiles directly as yet, their usefulness in sensing the structure of temperature inversions and thermal plumes has been amply demonstrated.

The FM-CW (Frequency Modulated-Continuous Wave) radar has been very successful in monitoring the microstructure of atmospheric radio refractive index. This type of radar does not measure refractive index directly; instead, it measures the intensity of the small-scale ($k = 4\pi/\lambda$) fluctuations in the refractive index, with an unsurpassed height resolution (on the order of 1 m at heights of the order of 1 km). The FM-CW radar, which operates at frequencies near 3 GHz, is more sensitive to humidity fluctuations than temperature fluctuations. Consequently, in conjunction with an acoustic sounder system, one possesses powerful methods for delineating both thermal and humidity fluctuations in the lower atmosphere. Microwave weather radars provide estimates of precipitation rates, total precipitation, and the precipitation coverage over a wide area. Microwave Doppler radar has been used to map the flow of falling snow, rain from stratiform clouds

and thunderstorms, and the air in-flow around forest fires; clear air convection has also been studied using chaff. HF sea scatter has been used to measure sea state and surface currents over large areas of the ocean (up to a few hundred km in the ground wave mode and up to a few thousand km from the transmitter in the ionospherically propagated mode).

Lidar techniques have been used to measure visibility and cloud ceilings. In addition, experimental work has demonstrated the potential of lidar systems to measure vertical profiles of wind, temperature, and humidity. Also, aerosol properties (i.e., type, size distribution, concentration vs. time) may be measured by a combination of on-frequency and off-frequency scattering by tunable lasers. Laboratory research has been performed on ocean constituents such as yellow substance and chlorophyll, and the scattering cross sections indicate that measurements of these quantities in the ocean should be feasible. Other laboratory research indicates that solutes in the ocean may be measured. Furthermore, since the temperature of an air-water interface strongly affects the scattering spectrum of the liquid, the phenomenon leads to a sensitive remote sensing system for the measurement of the interface temperature.

Remote sensing of both temperature and atmospheric water vapor may also be accomplished by radiometric techniques. Temperature profiles may be obtained with the radiometer operating near the 60 GHz oxygen line from measurements of brightness temperatures at a number of different elevation angles, or at a number of different frequencies with a vertical pointing angle (multi-spectral technique). The line integral of atmospheric water vapor has been obtained from radiometer measurements at frequencies near 22.2 GHz; theoretically, water vapor profiles could be obtained by the multi-spectral technique emission measurements.

The turbulent nature of the atmosphere produces fluctuations in both the phase and amplitude of an optical wave. Consequently, in an optical line-of-sight path, the phase and amplitude fluctuations are a measure of the strength of the refractive index fluctuations, while the motion of the turbulent eddies produces effects that permit measurement of the transverse component of the wind velocity, including, for space-to-earth

paths, winds aloft. In addition, the average density of the air along the path affects the phase of the optical wave which permits the measurement of the average air temperature along the beam, and through beam curvature, the vertical temperature gradient.

In the sections that follow, each remote sensing system is discussed in some detail and its potential usefulness in meeting NDBP objectives is evaluated. The environmental difficulties which a system may be expected to experience on the buoy are not treated in depth at this time; such studies must await later investigation.

Finally, in the summary section of this report, the potentials of the different remote sensing systems for NDBP are discussed and compared, and a preliminary set of recommendations presented directed toward the efficient exploration and realization of these potentials.

Section 2 ACOUSTIC ECHO SOUNDING OF THE ATMOSPHERE AND OCEAN FROM DATA BUOYS

Freeman F. Hall, Jr, C. B. Emmanuel and P. A. Mandics

2.0 Introduction

This section of the report considers the application of acoustic echo sounding for sensing temperature structure and winds in the atmosphere from data buoys, and also the application of acoustic sensors under the water for monitoring currents, and structure of the thermocline and the mixed layer. Before considering the environmental data available through acoustic sensing, it is necessary to understand how sound waves interact with the atmosphere and ocean. The remainder of this introductory section will summarize how sound waves can be used for remote sensing, and touch on some of the advantages and problems in their use.

Acoustic energy propagates through a fluid, either the atmosphere or the ocean, as a longitudinal wave of pressure variations. The intensity of a sound wave is defined as the time rate of energy passage through a unit area perpendicular to the direction of propagation. In the MKS system of units, sound intensity is measured as watts per square meter (Wm^{-2}). If resonant interactions with the fluid can be neglected, as is usually the case for frequency ranges of interest for

atmospheric or undersea probing, the attenuation of acoustic waves through the fluid varies with frequency in a continuous, smooth fashion. Therefore, when small frequency ranges are considered, the intensity of a plane wave train I at some distance ℓ from a reference plane where the intensity is I_0 is given by

$$I = I_0 e^{-k\ell} \quad . \tag{2:1}$$

Here, k is defined as the intensity attenuation coefficient. The attenuation coefficient is made up of independent components, representing absorption effects and scattering effects. For example, "classical" attenuation is produced by thermal conductivity and viscosity of the fluid. There are also attenuation effects because of molecular absorption which may be caused by structural or chemical relaxations or possibly resonant absorption in one or more of the fluid chemical species. In addition, scattering of the sound from the incident beam because of propagation speed fluctuations (caused by acoustic index of refraction structure in the fluid) will form a third attenuation term. The attenuation coefficient is the sum of all of these independent components. The frequency which should be chosen for remote sensing will depend upon the nature of attenuation, since to do quantitative work, it is necessary to know accurately how much the sound wave is decreased in intensity by the fluid during transmission to the target volume and return. Molecular absorption effects in the atmosphere dictate acoustic probing be limited to the lower end of the audible frequency range if targets at distances of several hundred meters or more are to be interrogated. In the ocean, somewhat higher frequencies may be utilized because of the decreased attenuation, so that many sonar devices operate at frequencies above the audible range, and even as high as several hundred kilohertz.

Acoustic echo sounding and sonar devices operate in very similar manners. In the usual pulse mode of operation, a short burst of acoustic energy is directed into the fluid being probed, using a transducer which

provides a well defined beam of acoustic energy, so that good spatial resolution is available. For atmospheric probing, specially modified microwave antennas, properly shielded and damped, using high power electrodynamic acoustic transducers at the feed point, have proven quite efficient in providing beams with half power widths of 6^{o} to 8^{o}, for a 1.2m dish aperture at a frequency of 2 kHz. For underwater acoustics, piezoelectric transducers, used singly or in arrays, in a like manner provide well defined acoustic beams.

After the sound pulse is transmitted, the probing system reverts to a passive mode, recording the echo intensities scattered from the interrogated volumes. For the atmospheric case, the same transducer can function as an efficient microphone, and for underwater probing hydrophones designed to have efficient acoustic matching to the water are used to receive the returned signal. The signals are then electronically amplified, possibly compensated for varying reception ranges, and recorded or displayed for evaluation.

Acoustic remote sensing of structural or velocity characteristics of the fluid requires that a certain percentage of the incident acoustic energy be scattered to a receiver from the volume under interrogation. It is emphasized that waves traveling in a perfectly homogeneous and continuous medium are not scattered. There must be variations in the propagation velocity of the wave, that is to say, inhomogeneities in the acoustic refractive index of the fluid, in order to produce scattering.

The velocity of sound waves in a fluid is a function of its density and elasticity. In the atmosphere, the density near the earth's surface is essentially a function of temperature, so that temperature fluctuations are effective in producing scattering centers for sound. In addition, since sound is propagated in the medium, and dragged along with it, velocity fluctuations can also produce scattering, but not directly in the backscatter direction.

In the ocean, density is a function of temperature and salinity and also of depths below the surface since pressure increases rapidly with depth. Fluctuations in temperature, pressure, or salinity can lead to scattering in the sea as can velocity fluctuations, so that scattering in the sea is generally more complex than in the atmosphere. In addition, organic and inorganic material is suspended in the ocean

and these hydrosols are characterized by differences in propagation speed of sound compared to the surrounding water. Because of the lower density of the atmosphere, aerosols are in general so small they do not effectively interact with sound waves with frequencies of importance for remote sensing, although hydrometeors may contribute appreciable scattered energy (Little, 1972).

2.0.1 Scattering of Sound in the Atmosphere

Considering first the problem of determining the acoustic scattering cross section in the atmosphere, if $\Phi(V)$ and $\Phi(T)$ are respectively the three-dimensional spectral densities of wind velocity and temperature, Monin (1962) has shown that the solution for $d\sigma(\theta)/d\Omega$, the power scattered from a unit volume per unit incident flux into a unit solid angle is given by

$$\frac{d\sigma(\theta)}{d\Omega} = \frac{32\pi^5 \cos^2\theta}{\lambda^4} \left[\frac{\Phi(V) \left(\frac{4\pi}{\lambda} \sin\frac{\theta}{2}\right) \cos^2\frac{\theta}{2}}{C_0^2} + \frac{\Phi(T) \left(\frac{4\pi}{\lambda} \sin\frac{\theta}{2}\right)}{4T^2} \right] \quad (2:2)$$

Here λ is the wavelength of the sound for the average atmospheric temperature T, θ is the scattering angle measured from the direction of propagation and the wind end temperature fluctuations are sampled at a spatial scale λ' where

$$\lambda' = \frac{\lambda}{2 \sin\frac{\theta}{2}} \quad . \quad (2:3)$$

For a Kolmogorov spectrum of turbulence, where the scale size of input eddies are many times the probing wavelength, (2:2) becomes

$$\frac{d\sigma(\theta)}{d\Omega} = 0.055 \lambda^{-1/3} \cos^2\theta \left[\frac{C_v^2}{C^2} \cos^2\frac{\theta}{2} + 0.13 \frac{C_T^2}{T^2} \right] \left(\sin\frac{\theta}{2}\right)^{-\frac{11}{3}} \quad . \quad (2:4)$$

Here C_v^2 is the velocity structure parameter, C_T^2 is the thermal structure parameter defined by

$$C_v^2 = \overline{\left[\frac{u(x) - u(x+r)}{r^{1/3}}\right]^2} \quad , \quad C_T^2 = \overline{\left[\frac{T(x) - T(x+r)}{r^{1/3}}\right]^2} \qquad (2:5)$$

A study of (2:4) reveals that the scattered acoustic power is only a weak function of acoustic wavelength, varying as $\lambda^{-1/3}$, that direct backscatter for $\theta = \pi$ is a function of the thermal structure only, that there is no scattering at $\pi/2$, and that there is strong scattering in the forward direction because of the final factor in the equation. The scattering equation obviously cannot be applied for extremely small values of θ, but its general correctness for scattering angles as small as 20^o has been confirmed in experiments by Kallistratova (1961) in the real atmosphere and more recently by Baerg and Swartz (1965) in a wind tunnel.

In addition to acoustic backscatter from random temperature structure in the atmosphere, uniform temperature gradients or turbulence generated in thin shear layers, not characterized by a Kolmogorov spectrum of turbulence, can also contribute to the scattered power. To have a measurable acoustic reflection from a temperature gradient requires a significant change of index of refraction in a small percentage of the acoustic wavelength. Present knowledge of temperature stratification under stable conditions does not yet yield much insight on gradients at such a fine spatial scale. Acoustic echo sounder records indicate, however, an excess return which is frequently observed under stably stratified conditions. Fast response, differential temperature readings, which provide a measure of the random temperature structure, lead to a prediction of smaller acoustic scattering than is actually observed under such conditions. Better backscatter agreement is obtained with predictions from differential temperature readings under convectively unstable conditions, when a more uniformly mixed, isotropic turbulence

condition is more likely to occur. Further research must be done on the relative importance of gradient or partially coherent reflections from the stable atmosphere as compared to acoustic scatter from random fluctuations before the full advantage of acoustic remote atmospheric sensing can be derived.

2.0.2 Scattering of Sound Under the Sea

(This subsection written by C. B. Emmanuel and P. Mandics)*

There is considerable theoretical and experimental work on sound scattering in the ocean. The published work, however, pertains to very general conditions, with particular applications to naval problems, with most results still in the classified literature. Nevertheless, much is known so as to warrant a careful examination of the theory.

The incidence of an acoustic wave upon an object suspended in the ocean results in its oscillation, and consequently the object becomes a secondary source of sound. The amplitude of the oscillation is proportional to the amplitude of the incident wave. Thus, the intensity of the secondary sound is proportional to the incident intensity.

The scattering of sound in a fluid medium of bulk modulus m, and density ρ by a spherical object of volume V, bulk modulus m_o and density ρ_o was first considered by Rayleigh (1896 and 1945). The geometry of the problem is assumed to be the incident wave upon the volume V is a plane, then at a point R from the scattering volume and at an angle θ relative to the direction of propagation of the incident wave, the pressure amplitude of the scattered wave is given (for $D << \frac{\lambda}{\pi}$, where D is the diameter of the scattering sphere) by

$$p_s = p_i \pi \frac{V}{R\lambda^2} \left[\frac{m_o - m}{m_o} - 3 \frac{(\rho_o - \rho)}{2\rho_o + \rho} \cos\theta \right], \quad (2:6)$$

where p_i is the pressure amplitude of the incident wave. The scattered power flux (intensity) is then proportional to

$$\{p_s\}^2 = \left\{ p_i \frac{\pi V}{R\lambda^2} \right\}^2 \left[\frac{m_o - m}{m_o} - 3 \frac{(\rho_o - \rho)}{2\rho_o + \rho} \cos\theta \right]^2 \quad (2:7)$$

*From the report "Acoustic Doppler Remote Current Measurement" submitted to Engineering Development Laboratories, NOS, NOAA, 14 September 1972.

and shows the λ^{-4} dependence of the scattered energy which is characteristic for $\lambda \gg D$.

Integration of the scattered intensity over all angles, defines an average scattering cross section as

$$\sigma_{av} = 4\pi R^2 \frac{\frac{1}{4\pi} \int_0^{2\pi} \int_0^{\pi} I_s(\theta) \sin\theta \, d\theta \, d\phi}{I_i} \qquad (2:8)$$

where $I_s = \frac{p_s^2}{\rho c}$, $I_i = \frac{p_i^2}{\rho c}$, and c is the velocity of sound in water

Upon substitution of (2:7) into the above expressions yields

$$\frac{\sigma_{av}}{0.25\,\pi D^2} = \frac{4}{9}\left[C_o^2 + \frac{3}{4} C_1^2\right]\left(\frac{\pi D}{\lambda}\right)^4 \quad \text{for } D \ll \lambda/\pi, \qquad (2:9)$$

where

$$C_o^2 = \left(\frac{m_o - m}{m_o}\right)^2$$

$$C_1^2 = \left(\frac{\rho_o - \rho}{\rho_o + \rho/2}\right)^2$$

are constants that depend on the elasticity and density of the scattering sphere. Note that (2:9) ignores the angle dependence of the scattering. Some typical values of C_o, C_1 for certain substances are given in Table 2.1 (taken from Principles and Applications of Underwater Sound, Department of the Navy, Headquarters Naval Material Command, Washington, D. C., 1968).

TABLE 2.1

Substance	C_o	C_1
Iron	0.99	0.81
Clay	0.93	0.50
Granite	0.98	0.57
Marble	0.94	0.53
Wood (Balsa)	-3.5	-0.50
Wood (Ironwood)	-0.87	-0.25
Turpentine	-0.43	-0.07

The factor $\frac{4}{9}\left[C_o^2 + \frac{3}{4} C_1^2\right] \approx 1/2$ for most substances (note the exceptions in Table 2.1.

The "target area", or "total scattering cross section" of an object suspended in a medium determines the amount of acoustic power that is intercepted by the object. For example, the target area, σ , of a sphere of diameter $D >> \frac{\lambda}{\pi}$ is given by (Urick, 1967)

$$\sigma = 0.25\ \pi D^2 \quad , \tag{2:10}$$

while the target area of an irregular object will depend upon the shape of the object and the direction of incidence of the sound wave. The target area of a small ($D << \frac{\lambda}{\pi}$) solid or liquid scatterer is much less than its actual cross section (see (2:9), in a ratio which is roughly given by $(\pi D \lambda^{-1})^4$.

A quantitative idea of the reflecting characteristics of an object may be obtained from the definition of a target strength, T. Thus, we have

$$T = 10 \log \left(\frac{\sigma avg}{4\pi}\right) \quad \text{(dB)} \tag{2:11}$$

or, in view of (2:9) ,

$$T = 10 \log \left[\frac{\pi^4 D^6}{36 \lambda^4} \left(C_o^2 + \frac{3}{4} C_1^2\right)\right] \text{(dB)} \tag{2:12}$$

The scattering power of a small target ($D << \frac{\lambda}{\pi}$) is very much affected by the dimensions of the target and the incident wavelength of sound (see (2:9)). A small spherical target, therefore, will scatter short wavelengths more effectively than long. For example, a small spherical target will scatter 10^4 more sound of frequency 24 kHz than of 2.4 kHz.

A sound wave impinging upon a gas bubble embedded in water will cause the bubble to oscillate with a relatively large amplitude. This is due to the greater compressibility of the gas bubble relative to that of the surrounding water. The forced oscillations of the gas in the bubble produce the emission of a secondary sound wave from the bubble which, for all practical purposes, is spherically symmetric.

The scattering cross section of a spherical bubble near resonance and for $\frac{\pi D}{\lambda} \lesssim 0.01$ is

$$\sigma = \frac{\pi D^2}{\left(\frac{f_o^2}{f^2} - 1\right)^2 + \delta^2} \qquad (2:13)$$

where D is the bubble diameter, f is the frequency of the incident sound wave, $f_o = (1/\pi D).\sqrt{3\gamma p_o/\rho}$ is the resonance frequency of the bubble, p_o is the average hydrostatic pressure in the water, $\gamma = C_p/C_v$, C_p and C_v are the specific heats of the gas at constant pressure and constant volume, respectively, ρ is the density of the water, and δ is the damping constant. Although is is possible to calculate the damping constant from a knowledge of the frequency, heat conduction, viscosity, and other parameters, measured values of δ at resonance (where the role of δ is important) turn out to be considerably larger than those predicted by the theory. Consequently, values of δ must be determined empirically.

Scattering cross section of an air bubble becomes very large at resonance ($f = f_o$) or several hundred times its true area, and decreases to its geometrical cross-sectional area, $\sigma = \frac{1}{4}\pi D^2$, for high frequencies

($\frac{\lambda}{\pi} << D$). At low frequencies (well below resonance) the scattering cross section of a bubble follows a $(\pi D/\lambda)^4$ dependence, and it is several orders of magnitude larger than the scattering cross section of a solid sphere of the same size.

The mass of water surrounding the gas bubble coupled with the compressibility of the bubble, will result in a resonance at a frequency f_o, which is found to depend on the diameter of the bubble, D, and on the average pressure, p, of the gas in the bubble. An appriximate relation for this dependence may be written as

$$f_o \simeq \left[3 \frac{\gamma p}{\rho(\pi D)^2} \right]^{1/2} , \qquad (2:14)$$

ρ being the density of the medium. For p in feet of water, f_o in kHz, and D in inches, (2:14) becomes

$$f_o D \simeq 2 \times 10^{-2} p^{1/2} \qquad (2:15)$$

The formulation of a target area for non-spherical objects presents some difficulties. Nevertheless, some estimates may be made, which, on the average are expected to be in error by a factor of 2 or 3. It is unlikely that the error will be by a factor of 10. For example, a fish that is neither flat nor elongated will cast a shadow roughly equal in area to that of a spherical object of the same volume. However, an additional uncertainty is injected into the calculation by our ignorance of the exact reflection coefficient applicable in each case. The reflection coefficient will, of course, depend largely on the compressibility and density of the particular type fish.

Probably the most effective portion of the fish responsible for reflection is the swim bladder (if, indeed, the fish has one). For example, kelp and other forms of marine life possess gas-filled floats, and these are indeed excellent reflectors of sound.

The scattering cross section $\sigma(\theta)$, is defined as

$$\sigma(\theta) = 4\pi R^2 \, I_s(\theta) \, I_i^{-1} \qquad (2:16)$$

where $I_s(\theta)$ is the scattered sound intensity (power per unit area) at the receiver situated a distance R from the scatter as a function of the scattering angle θ, and I_i is the incident intensity at the scatterer. It is assumed that the incident wave is plane and its direction if fixed ($\theta = 0$). Note that $\sigma(\theta)$ is an area such that the product of this area and the incident sound intensity gives a power which, if scattered isotropically, would result in the actual observed sound intensity at the receiver.

However, in order to compare the efficiencies of various scatterer it is convenient to define the scattering cross section per unit volume per unit solid angle, i.e.,

$$\frac{d\sigma(\theta)}{d\Omega} = \frac{R^2}{V} \frac{I_s(\theta)}{I_i}$$

$$= \frac{\sigma(\theta)}{4\pi V} \quad , \qquad (2:17)$$

where V is the scattering volume and $d\Omega$ is an element of solid angle.

2.0.2.1 Scattering Due to Temperature Inhomogeneities In Water

Assuming the Kolmogorov temperature turbulence spectrum

$$\Phi_T(\kappa) = 3.3 \times 10^{-2} \; C_T^{\,2} \; \kappa^{-\frac{11}{3}} \qquad (2:18)$$

to be valid, then the ratio of scattered to incident sound intensity is found to be (Skudrzyk, 1963)

$$\frac{I_s(\theta)}{I_i} = K \frac{V}{2R^2} \, k^{1/3} \left[2 \sin \frac{\theta}{2}\right]^{-\frac{11}{3}} \qquad (2:19)$$

where κ is the spatial wavenumber, C_T is the temperature structure parameter, $k = \frac{2\pi}{\lambda}$ is the acoustic wavenumber (λ is the acoustic wavelength), and K is given by

$$K = 3.3 \times 10^{-2} \; C_T^{\,2} \; \frac{1}{c^2} \left(\frac{\partial c}{\partial T}\right)^2$$

or

$$K \simeq 1.66 \times 10^{-6} \; C_T^{\,2} \quad , \qquad (2:20)$$

(c is the speed of sound in water, T is the absolute temperature, with $T = 288^{\circ}K$ used above). It is assumed that the temperature inhomogeneities are isotropic and that the scatterers of importance lie within the inertial subrange; that is

$$\ell_o < \frac{2\pi}{\kappa} < L_o$$

where ℓ_o and L_o represent, respectively, the inner and outer scales of turbulence.

Comparison of (2:19) with its counterpart for the scattering by temperature inhomogeneities in the atmosphere (Monin, 1962) reveals that an additional angle-dependent term ($\cos^2 \theta$) is missing from (2:19). Consequently, further theoretical work is needed along these lines to determine whether or not this term should be included in (2:19).

Using Equations (2:17, 19, and 20) there results

$$d\sigma(\theta) \simeq 1.53 \times 10^{-6} \; C_T^{\,2} \; \lambda^{-1/3} \left[2 \sin \frac{\theta}{2}\right]^{-\frac{11}{3}} \; d\Omega \quad , \qquad (2:21)$$

and we note that as for the atmospheric case, the intensity of scattering is rather weakly dependent on the propagated wavelength. Similarly, the quantity in the brackets raised to the $-\frac{11}{3}$ power indicates that the scattering is primarily in the forward direction.

The temperature structure parameter C_T varies considerably in the ocean. It is dependent on time, depth, thermal stratification as well as on a number of other parameters. McKean's (1971) measurements indicate that the temperature structure function

$$D_T(r) = \overline{\left[T(\vec{r}_1) - T(\vec{r}_2)\right]^2} = C_T^2 \; r^{2/3} \qquad (2:22)$$

$$r = |\vec{r}_1 - \vec{r}_2|$$

may not be statistically stable. As a result, the use of C_T in (2:21) must be with caution. It appears that further work is needed to resolve this question. Nevertheless, because the acoustic frequencies to be used on data buoys may be quite high (100-400 kHz) and the important scatterers are small (the smaller the scatterer the more likely that it will obey (2:22)), (2:22) may validly describe the turbulent temperature field.

According to several workers (Skudrzyk, 1963; McKean, 1971; Frisch, 1972) C_T varies between 4×10^{-4} and 1.1×10^{-3} $cm^{-1/3}$ near the surface (depth < 100 m). Smaller C_T values are observed at greater depths (McKean, 1971). If we take f = 200 kHz ($\lambda \simeq 0.75$ cm) and consider scattering in the backward direction ($\theta = 180^\circ$), then (2:21) yields for the C_T values quoted above

$$2.1 \times 10^{-14} \lesssim \frac{d\sigma\ (\theta = 180^\circ)}{d\Omega} \lesssim 1.6 \times 10^{-13} \quad cm^{-1}$$

2.0.2.2 Scattering Due to Current Velocity Fluctuations

According to Tatarski (1971) atmospheric scattering of sound waves due to temperature and wind velocity fluctuations are about equal. However, at WPL it has been found C_v scattering usually greatly exceeds that due to C_T in the atmosphere. Because the speed of sound in water is much greater than in air, water current velocity variations may be relatively less important than wind velocity fluctuations in the atmosphere. Scattering due to water current fluctuations may be entirely negligible (Krasilnikov, 1963; Albers, 1965) in the open ocean, but may be important

when using bistatic sounder geometries near known strong currents. More work clearly needs to be done on C_v in the ocean.

2.0.2.3 Scattering Due to Suspended Inorganic and Organic Matter

Studies on suspended particulate matter in coastal regions, where data buoys are planned, have been carried out by a limited number of oceanographic institutions and governmental laboratories. Although not all such studies have been restricted to the coastal regions (see for example, Bassin et al., 1972), the bulk of the published research is restricted to selected regions along both coasts of the United States. Table 2.2 shows the average concentrations of total suspended matter as well as the average proportions of organic suspended matter in estuaries along the eastern seaboard (Meade, 1968).

The total suspended matter along the eastern seaboard ranges from about 0.5 to 8 milligrams per liter; mineral grain sizes range from about 1 to 250 μ (average $\sim$ 15 μ)(Bond and Meade, 1966). There is no particular preference for the suspended matter to possess a certain shape, consequently an average dimension is obtained on the basis of spherical symmetry. Furthermore, a relatively small portion of the suspended matter, $\sim$ 2 to 11% of the total, consists of recognizable mineral grains.

Little information exists on the available living matter suspended in coastal waters. In fact, whatever information exists is for localized areas, and even then there does not appear any conclusive evidence on type, size and total concentration (see for example, Kinzer, 1971; Zeitzschel, 1970).

Suspended organic and inorganic matter in water has been found to possess a great variety of shapes as well as density and compressibility variations. As a first approximation, we shall assume that scattering due to particulate matter can be described adequately by the (non-rigid sphere) scattering theory discussed earlier. (It is assumed that the scatterers are small compared to the acoustic wavelength, that is $D << \frac{\lambda}{\pi}$).

The angular dependence of the scattering may be determined from (2:7) and (2:16). For example, for clay we have from Table 2.1 that

TABLE 2.2

AVERAGE CONCENTRATIONS OF TOTAL SUSPENDED MATTER AND AVERAGE PROPORTIONS OF ORGANIC SUSPENDED MATTER IN ESTUARIES OF THE ATLANTIC SEABOARD

Estuary	Depth	Total Suspended Matter (mg per liter)	Organic Suspended Matter (percent dry weight lost on ignition)
Long Island Sound (Riley, 1959)	Surface	4.5	40
Chesapeake Bay			
(Bond and Meade, 1966)	Surface	2.6	50
(Patten, Mulford, and Warinner, 1963; Patten and Warinner, 1961).	Surface	9.7	34
(Patten, Warinner and Eayrs, 1961; Patten Young, and Roberts, 1963,1966)	Surface	10.0	35
	Bottom	34.9	21
Charleston Harbor (Federal Water Pollution Control Administration,1966)	Surface	32.3	28
	Bottom	51.7	27

(From Meade, R. H., Relations between suspended matter and salinity in estuaries of the Atlantic seaboard, USA, Internat. Assoc. Sci. Hydrology, Gen. Assembly, Bern 1967, vol. 4, (I.A.S.H. Pub. 78), published 1968, pp. 96-109).

$C_o = 0.93$ and $C_1 = 0.50$, leading to little forward scatter, but much stronger backscatter. An examination of Table 2.1 reveals that a similar angular dependence should hold for most "heavy" particles.

By neglecting the angle dependence and ignoring multiple scattering effects, we obtain an average scattering cross section per unit volume per unit solid angle for a number of identical spheres scattering independently from (2:9) and (2:17),

$$d\sigma_{av} = \frac{\pi^4}{36} \frac{D^6}{\lambda^4} N \left[C_o^2 + \frac{3}{4} C_1^2 \right] d\Omega \quad , \qquad (2:23)$$

where N is the number of scatterers per unit volume.

The typical mineral grain sizes vary between 4×10^{-4} and 1.6×10^{-3} cm in near-shore areas of the Atlantic (Manheim et al., 1970). The concentration of these particles is observed to be between 1×10^{-3} and 8×10^{-1} mg/liter. Taking f = 200 kHz $C_o \simeq 0.95$, $C_1 \simeq 0.55$, and using the values just given we obtain from (2:23)

$$4 \times 10^{-19} \lesssim \frac{d\sigma_{av}}{d\Omega} \lesssim 2 \times 10^{-14} \text{ cm}^{-1} \quad .$$

Beamish (1971) reports that typical scattering cross section of zooplanktonic organisms (the euphausiid) is $\sigma \approx 1.4 \times 10^{-4}$ cm^2 at f = 102 kHz. Because four-fifths of the scattering was found to be caused by the compressibility contrast, it is assumed that the scattering is very nearly isotropic. Assuming that the size of these organisms is very small compared to the wavelength, and using the fact that in this case the scattering cross section is inversely proportional to the fourth power of the wavelength, we obtain $\sigma \approx 2.2 \times 10^{-3}$ cm^2 for f = 200 kHz.

According to Kinzer (1971) the concentration of euphausiids in the eastern north Atlantic varies from a maximum of about 1.6/m^3 to less than 0.01/m^3. Scattering due to euphausiids at f = 200 kHz thus will range between

$$1.8 \times 10^{-12} \lesssim \frac{d\sigma}{d\Omega} \lesssim 2.8 \times 10^{-10} \text{ cm}^{-1} \quad .$$

2.0.2.4 Scattering Due to Bubbles

As we have discussed earlier, air bubbles are found to be very efficient scatterers of sound in water, especially near their resonance frequency. Although it is known that large numbers of air bubbles are generated near the surface and in the wake of ships, and that bubbles of a fraction of a millimeter in size exist for some time, practically no information is available on their concentration and size distribution. Consequently, we are unable to estimate the scattering due to air bubbles.

2.1 Atmospheric Studies

With a co-located acoustic transmitter and receiver, the backscatter from the atmosphere is caused only by thermal structure which may be either random temperature inhomogeneities or uniform temperature gradients. This effect has been discussed earlier in connection with (2:4). The temperature structure parameter is not a usually measured atmospheric variable, and we still have much to learn about its magnitude and variation in the atmosphere, especially over the ocean. It is not surprising that considerable temperature structure is observed over land near midday when the atmosphere is convectively unstable, for under such conditions heat is added rapidly to the low lying levels by conduction from the solar heated ground. Similar structures must exist over warm bodies of water. Typical acoustic returns obtained under convective conditions will be discussed next, followed by an investigation of the echo returns from the stably stratified atmosphere.

2.1.1 Convective Plumes

The typical pattern observed on the facsimile recording showing backscattered intensity with height as a function of time, for the unstable atmosphere is shown in (F2.1). This is the thermal plume structure, indicating the rise of heated and thermally nonuniform air parcels from the surface due to heating from solar radiation, and also, probably, from a warm ocean. That the upwelling air is characterized by variation in temperature is well known from investigations with fast response temperature sensors on aircraft, or spaced sensors on towers.

The agreement between in situ measurements of C_T and acoustic sounder derived values is quite good for the convective, unstable atmosphere. With a well calibrated sounder, and if temperature and humidity of the atmosphere are well known, to allow calculation of acoustic attenuation, agreement to within 30% is common. In the generally humid marine boundary layer, attenuation will be less than for most operations WPL has previously undertaken

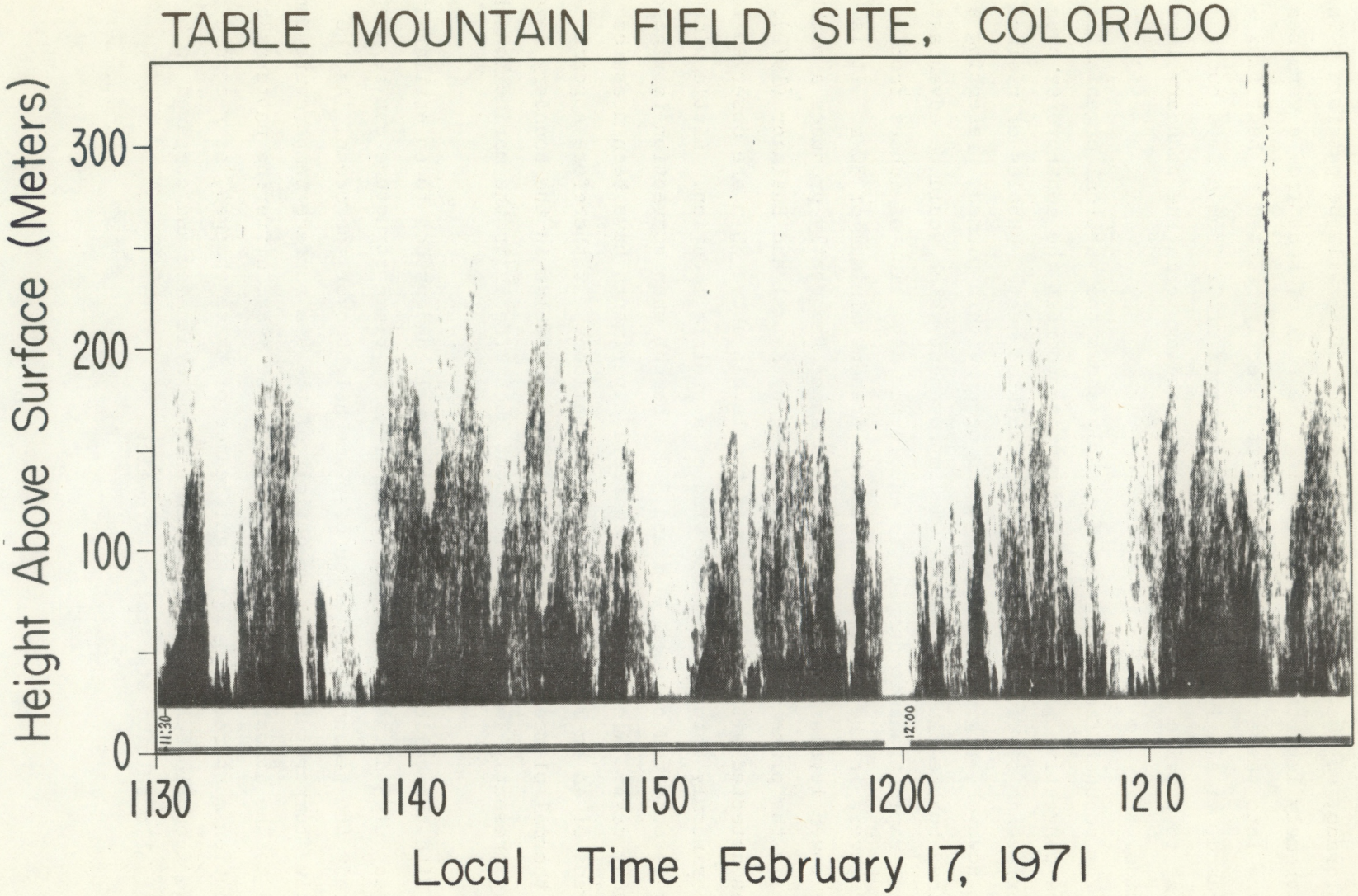

Figure 2.1 Facsimile recording of backscattered acoustic intensity from thermal convective plumes.

in Colorado, so that a more accurate measure of C_T will be possible. This is extremely important in understanding the flux of heat from a warm sea surface into the atmosphere, since C_T is directly related to heat flux (Wyngaard, et al, 1971). Routine measurements of C_T from a data buoy promise to provide significant new understanding to marine boundary layer dynamics.

The sounder facsimile record clearly shows the vertical organization of the convective plumes, seemingly putting to rest the controversy over the existence of plumes as opposed to isolated heated bubbles of rising air. However, regions of higher C_T do occur within plumes, presenting a combined bubble-plume picture. One improvement which would be advantageous is more rapid transmit damping to enable the detection of echoes from lower levels in the atmosphere than the present minimum of 30 m. It is these lower levels below 30 m that wind shear frequently produces a marked slope in the plume structure, as observed by Kaimal and Businger (1970). Plumes detected with the sounder in the levels above 30 m are observed to slope randomly into or with the wind at a prairie location. Little wind shear is observed between 30 m and 300 m height when convection is vigorous on sunny days. Wind data for such field experiments have been measured by means of an anemometer on a tethered balloon. It therefore appears that thermal plumes significantly modify wind fields in the boundary layer, and we presently know very little about such effects in the marine boundary layer.

With the calibration of the sounder well understood to an estimated accuracy of 3 dB, the facsimile recordings of plume structure can be used to study the seasonal variation of plume height over the ocean. As the relative temperature excess or deficit of the sea surface temperature compared to the atmosphere varies throughout the year, differing patterns of convection must result. The significance of these changes, as recorded by the acoustic echo sounder, could then be evaluated and compared to numerical models of atmospheric dynamics.

As an example, we find acoustically measured C_T^2 for the unstable atmosphere to decrease with height approximately as $Z^{-4/3}$ over prairie grassland, at least through the lowest 200 m, as predicted by similarity theory. It is important to determine if a similar decrease occurs over the ocean when convection is present.

The facsimile recordings of C_T such as (F2.1) serve as a useful pictorial representation of the temporal convective structure in the atmosphere, and can be used for semi-quantitative work, as in finding gradients in thermal structure. To assign absolute values to C_T, it is necessary to have a more accurate means of recording the back-scattered sound intensity. Analog signals corresponding to acoustic echo strength could be telemetered from the buoy, or recorded on tape on board. These tape records could be returned to the laboratory for digitization and computer processing, introducing in the computational scheme atmospheric humidity and temperature effects, to account for molecular absorption, and the echo sounder system parameters so that quantitative values of C_T over the ocean could be derived.

2.1.2 Temperature Inversions

A quite different type of acoustic sounder return facsimile display is obtained under stable conditions in the boundary layer. When the surface temperature is below the atmospheric temperature, thermal radiation from the surface results in the ground (or ocean) having a lower temperature than air immediately adjacent to it. This is because the infrared emissivity of the surface is much greater than the atmosphere. The dryer and more clear the atmosphere, the poorer it is as an infrared radiator. Turbulence or molecular conduction within the low lying levels of the atmosphere causes a heat loss to the earth, and a cold layer of air forms just above the surface. As heat conduction losses continue, the depth of this cold layer of air increases. If the conduction of heat occurred principally on the scale of molecular diffusion, one would not expect much random thermal structure, and we might predict that the acoustic sounder would detect only

the temperature gradient separating the cold, surface air from the warmer air above. Under most atmospheric conditions, there is more heat conducted through turbulent eddy diffusion, so that throughout the cooler air a large value of C_T is observed.

A typical acoustic facsimile display illustrating the formation of a nocturnal radiation inversion over land is given in (F2.2). The last vestige of convective plume structure dies away at about 1700 hours and the increase in the radiation iversion depth is indicated by the thickening lower dark trace beginning at 1900 hours. The blanked-out echo in the lowest 30 meters prevents detection before this time. As time progresses, the depth increases through 0200 hours. Minor variations in inversion height are probably caused by changes in wind conditions, and mixing at the top of the temperature inversion. After 0200 it appears there was sufficient mixing, possibly from wind, to dissipate the initially formed inversion structure, and to lead to the formation of yet another nocturnal inversion growing from the surface after 0230.

A second type of temperature inversion is caused by large scale downward motion, or subsidence, within the troposphere. The relatively rapid descent of air parcels in subsidence results in adiabatic heating of the air. By the time a subsiding air mass has approached the surface it's temperature significantly exceeds that of the lower lying levels. This is because typical lapse rates in the atmosphere are less than dry adiabatic. The subsiding air is prevented from reaching the earth's surface by the trapped, stable, lower levels so that horizontal divergence of the subsiding air mass frequently occurs above the low layers, leading to wind shear and turbulent mixing of the warmer upper air with the underlying levels.

The acoustic detection of the formation of a subsidence inversion is also shown in (F2.2), entering the picture at a height of 700 meters at 0240 hours. As the subsidence continues through 0800, the increasingly dark acoustic return indicates an increase in the thermal structure. The wavy nature of the return is probably caused by wind shear induced instabilities or Kelvin-Helmholtz billows. The merging of the subsidence

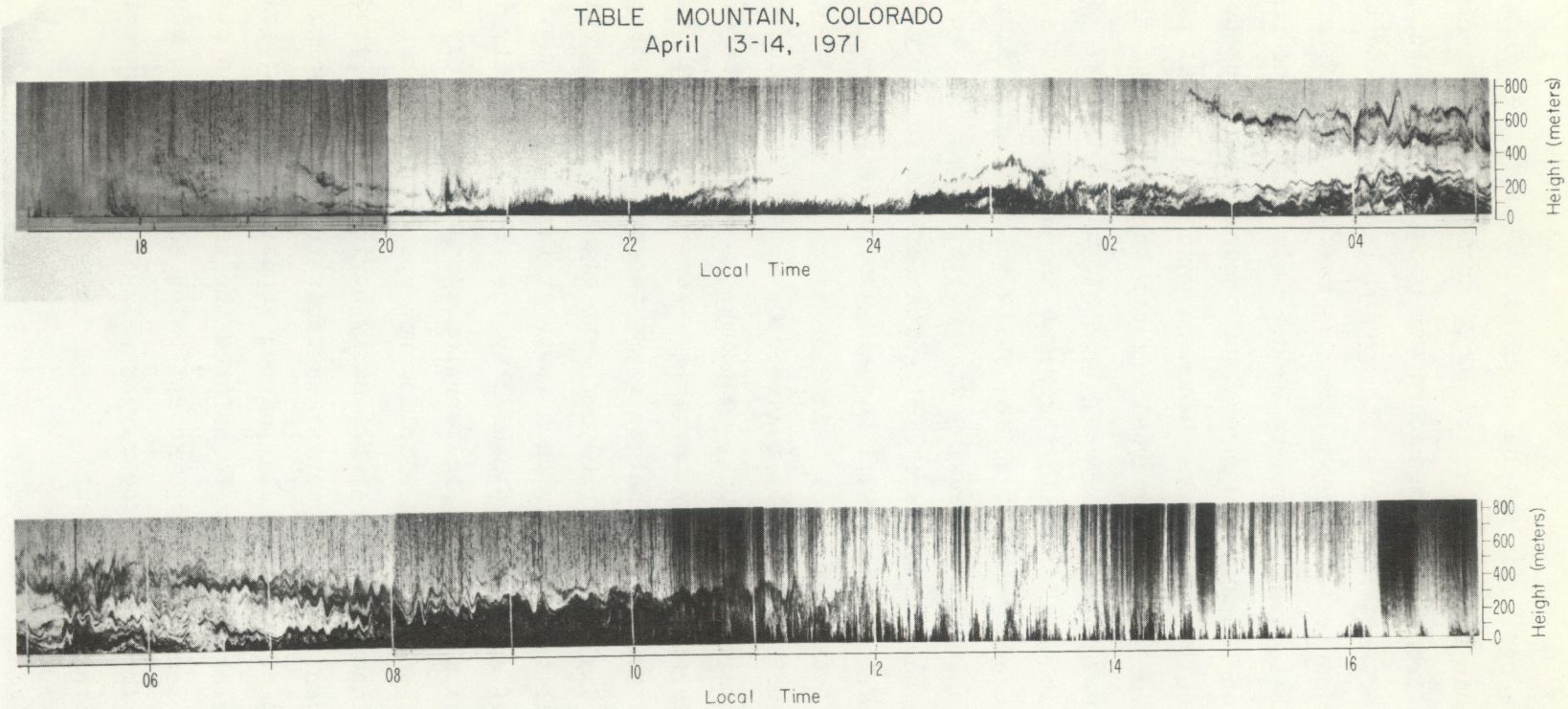

Figure 2.2 Facsimile record of 24 hours of backscattered acoustic intensity, depicting formation, and eventual breakup of a radiation and subsidence inversion.

inversion and the radiation inversion after 0800 resulted in a temperature differential across the inversion of 10°C, as measured by radiosonde ascent in Denver, 40 km from where the record was obtained at Table Mountain, Colorado, just north of Boulder. The eventual weakening and breakup of the inversion by convective thermal plumes may be noted after 1000 with all traces of the inversion gone by 1200. This timing also matched the observed inversion breakup in Denver, and clearly indicates how the sounder may be used to monitor mesoscale phenomena which may affect points separated by many kilometers. At sea, diurnal effects should be less noticeable. Cyclic patterns may result, however, from air mass passage. The dark vertical traces in the facsimile (F2.2) at the upper levels after 1000, and 1400 were caused by insect noise, while the darkening of the trace after 1600 was caused by increasing wind noise. These two sources of background noise sometimes place limitations on acoustically detected atmospheric variables. More will be said about the problem of wind and wave noise on a data buoy in section 2.3.

Comparison of acoustically measured C_T with tower measurements, under temperature inversion conditions, sometimes do not agree as well as when the atmosphere is convectively unstable. When thin, horizontal laminae are present, the acoustic technique seems to estimate consistently too high a value of C_T, sometimes 100 per cent higher than the value measured with differential thermometers on a tower at the same height. It is believed that this lack of agreement is caused by the inadmissability in the scattering theory of assuming isotropic turbulence under the stably stratified inversion conditions, so that a Kolmogorov spectrum of turbulence may not exist. Also, since the layers are nearly horizontal, and gradients of temperature present nearly specular surfaces to the advancing wave fronts in the far field of a vertically pointed acoustic antenna, some partially coherent scattering may occur to enforce the returned echo strength. When sharply defined lamina are not present below an inversion, tower and sounder measured values for C_T agree nearly as well as for the convectively unstable atmosphere or within 50 percent.

2.1.3 Wind Studies by Acoustic Doppler Methods

So far we have considered only the atmospheric structure revealed by the intensity of the backscattered signal. By analyzing the frequency content of the returned signal, and comparing this with the transmitted frequency, one can derive the velocity of the air parcels along the acoustic beam, from the Doppler frequency shift in the scattered sound. Consider a vertically pointed sounder. The vertical velocity, w, of the scattering volume along the direction of the beam is given by

$$w = \frac{c}{2}\left(\frac{\nu_o}{\nu_s} - 1\right) \qquad (2:24)$$

where c is the velocity of sound, ν_o is the transmitted carrier frequency, and ν_s is the frequency of the scattered signal. This equation is correct to first order accuracy, where wind velocity is small compared to the velocity of sound. This is nearly always true for vertical velocities in the atmosphere, and certainly for those velocities measured under nominal convective plume conditions. As pointed out by Beran, et al. (1971), the much slower speed of acoustic waves compared with electromagnetic waves can introduce some errors into the acoustic Doppler measurements. If the total velocity of the medium along the path to the scattering volume is varying with time, which is usually the case in the atmosphere, additional frequency shifts caused by beam bending may be added to the true Doppler shift produced by the radial motion of the target. Fluctuations in the vertical velocity of the air along the vertical path of the sound do not, however, produce spurious frequency shifts, provided that the vertical velocity field does not change between the upward and the downward traverse of the sound pulse through the medium. On the other hand, temperature fluctuations produce phase changes of equal magnitude and sign in both propagation directions, and do not cancel out. Overall, spurious propagation-induced frequency shifts should not produce errors in derived vertical velocities of more than about 0.1 ms^{-1} for the heights which concern us.

The frequency spectrum of the returned signal is compared with that of the original transmitted pulse to obtain the Doppler frequency shift. The method of obtaining the spectra differs slightly in the acoustic and electromagnetic cases, primarily because of the characteristically much higher pulse repetition rate used with electromagnetic radar. The final spectrum generated from a radar return is extracted from information contained in each of many separate pulses and it is this spectrum which is used to reproduce the Doppler frequency; in the acoustic case, a spectrum can be generated for each pulse. The higher pulse repetition rate of the radar does not increase the accuracy if the signal-to-noise ratios and overall duty cycles (fraction of time that the transmitter is on) are equal in the two cases. A further improvement can be made by averaging the acoustic spectra from succeeding pulses, although this reduces the horizontal resolution by increasing the size of the total volume being considered because of the ambient air motion during the time required to collect the sample.

A typical Doppler derived vertical velocity profile for a convective plume is illustrated in (F2.3). On the left is the backscatter intensity depiction of the thermal plume structure and on the right are the profiles of vertical velocity in ms^{-1}.

Studies of the vertical velocity observed under breaking gravity wave conditions when strong temperature inversions are present have revealed vertical velocities of the same order of magnitude as those observed in convective plumes, or several meters per second in both the positive and negative z direction. Further studies of this type over the ocean will add much more to our understanding of the dynamics of such wave motion in the marine boundary layer. The importance of wave energy in boundary layer dynamics has not been extensively investigated but it may turn out that wave energy budgets are of comparable importance to the energy transported through convection or dissipated through turbulence.

By employing three acoustic echo sounders in the geometry illustrated in (F2.4) it is possible to measure the Doppler component along each of the

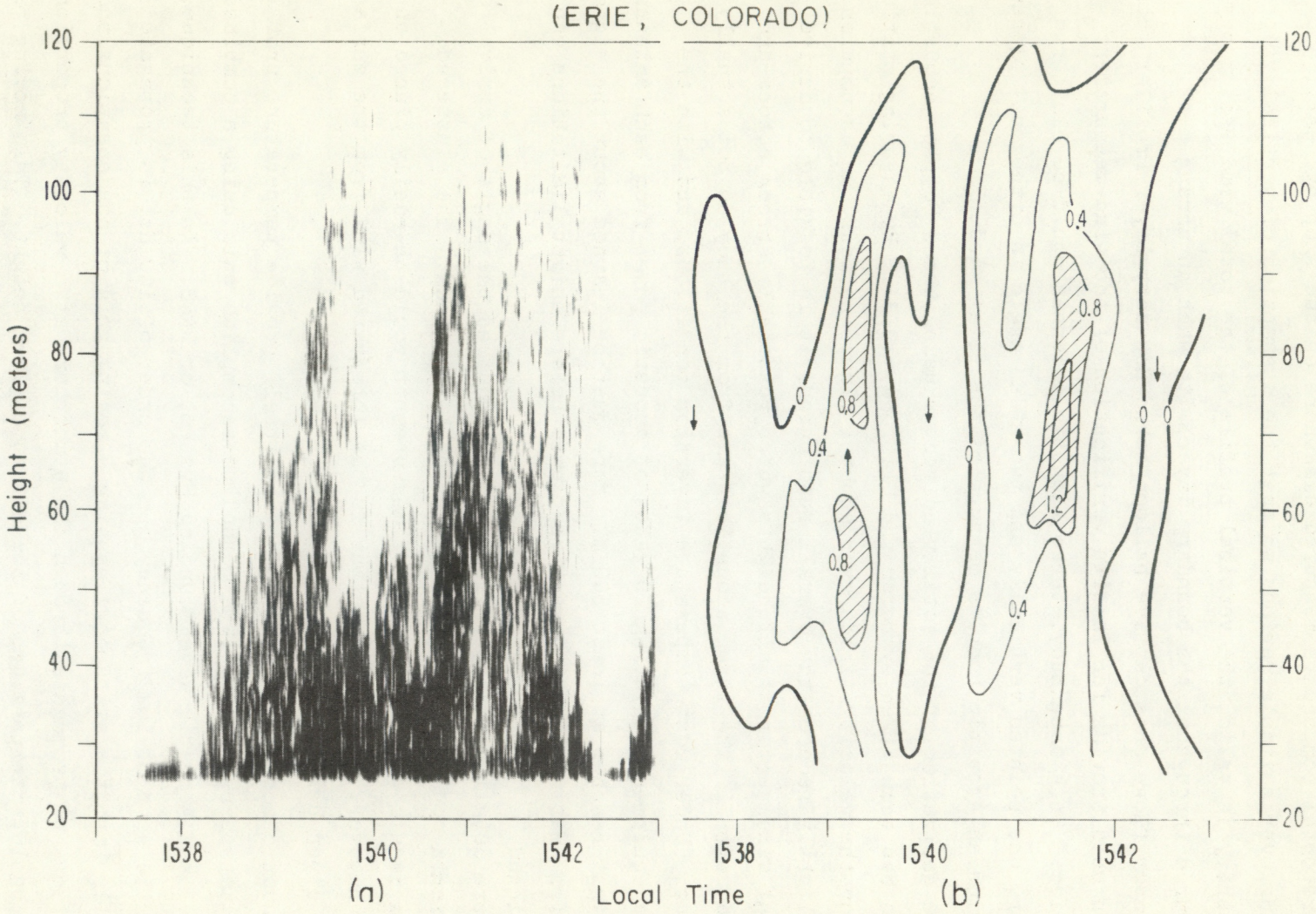

Figure 2.3 (a) Facsimile record of convective plumes, and (b) Doppler detected vertical velocities in ms^{-1}, for the same plumes as in (a).

three beams. In this manner, the total wind vector may be measured in the volume intersected by all three beams. By subtracting the vertical component from horizontal components measured elsewhere on the sloping beams, and averaging over suitable periods so that the assumption of vertical velocity stationarity is valid, the vertical profile of the total wind vector may be measured throughout the boundary layer with such an arrangement. A wind sensor flown on a captive balloon borne Boundary Layer Profiler (BLP) has been used provide for in situ verification of the wind measurement accuracies. On a data buoy, three acoustic antennas could be clustered together, one pointed vertically and two at an angle in orthogonal planes, to provide an acoustic Doppler measure of the total wind.

The derivation of the total wind vector using three Doppler acoustic sounders has been given by Beran and Clifford (1972). By assuming stationarity for the velocity fields over about 1 minute periods, an assumption which slightly reduces the overall resolution, it is possible to derive the total wind vector at all heights where reasonably strong echoes are obtained, even if the three acoustic beams from the buoy do not actually intersect. Under most temperature inversion conditions, and with the acoustic equipment radiating 20 watts of acoustic power from each antenna, this height reaches at least 500 m. More must be learned about the signal return from marine layer convective plumes before height limitations can be predicted.

Where detailed wind profiles are not required, the angle of arrival of phase fronts could be used to measure low level winds. The clustered antennas required for this type of measurement could be easily placed on a buoy, however, the direct output is the integrated wind from the surface to some given height and not a profile.

Acoustic echo sounding does not by itself provide temperature profiles of the atmosphere. There is a method to accomplish this using a combined Radiowave and Acoustic wave Sounding System, or RASS. In this technique, an acoustic wave of low frequency, on the order of 100 Hz, is propagated vertically into the atmosphere causing a moving grid of condensations and rarifactions to propagate through the atmosphere at a velocity proportional to the absolute temperature of the air at a given height. This moving grid of pressure fluctuations can cause coherent backscattering of radio energy if the electromagnetic wavelength is chosen to have just one-half the wavelength of the acoustic energy. For this condition, constructive

interference results, enhancing the reflectivity of the atmosphere. By observing the Doppler shift on the returned radio signal, direct temperature profiles can be measured. This technique is under investigation at the Stanford Electronic Laboratories and has demonstrated capabilities for measuring temperatures through the lowest several hundred meters of the atmosphere. One difficulty with this technique is that as the acoustic wave interacts with turbulence in the atmosphere, the acoustic wavefronts become incoherent so that constructive reinforcement for the radio waves fails to occur after some finite distance of propagation.

2.2 Undersea Studies

The Wave Propagation Laboratory is now beginning to accumulate direct experience in underwater acoustic echo sounding. Introductory studies which have been accomplished, as outlined in Section 2.0.2, show great potential for acoustically investigating the oceans mixed layer, just as has been done in the atmospheric boundary layer. The reverberation of the sea has always presented a background noise problem to sonar operators in their search for point targets. This same reverberation can be a meaningful remote sensing signal for the physical or biological oceanographer, and meteorologist.

NDBP personnel are already familiar with the current sensing capabilities of acoustic Doppler devices, operating in the 300 kHz frequency range. Placing such units on the buoy, and on the mooring cable has the potential of providing a monitor of currents throughout a considerable depth at the buoy. Different operating frequencies, transducer and hydrophone designs, and possibly more advanced signal coding and processing promise significant improvements in the capabilities of such current sensors.

It is well known that reverberation from the surface grazing ray is related to sea state. This is because surface scattering is directly related to the mean-square slopes of the surface waves and to near surface bubbles. Semi-quantitative expressions relating surface backscatter to sea state (Chapman and Scott, 1964) are deserving of further investigation, for there is meaningful information in the intensity of reverberation as

as well as its frequency content, as employed for current sensing.

Investigation of the vertically backscattered sound intensity and frequency promises to provide new information on mixed layer overturning, "salt fingers," and the morphology of vertical motions. When coupled with information on winds, insolation, and air and water temperature, a much improved picture of air-sea interactions should result.

Much of the electronic circuit designs available within WPL for timing, tone bursts, pulse shaping, power amplification, return signal processing, and data evaluation are directly applicable to undersea probing with acoustics. The cross-disciplinary transfer of this technology presents a new and exciting challenge for the personnel in the acoustics program.

2.3 Problem Areas

Acoustic sounding techniques have been successfully employed for the interrogation of the atmospheric environment, especially the lower 1 km, over land. It appears that no further fundamental development or feasibility tests of the method are required to provide wind measurements from a buoy. However, a detailed study of the acoustic environment typical of buoys and their pitch, roll, and yaw properties is necessary. Examination of the acoustic environment will yield information on the amount of antenna shielding and frequency filtering needed to reject the background noise in favor of the returned echo from the atmosphere. Information on the stability of the buoys is necessary to determine the amount of antenna stabilization, or inertial frame reference required, should steerable phased array antennas be used on buoys. In any event, feasibility studies and experiments must be performed to determine whether acoustic echo sounding techniques may successfully be employed on buoys. These include:

1. Determine the acoustic and dynamic environment on a typical buoy.
2. Perform analytical and field studies to determine if the buoy environment allows the efficient use of atmospheric acoustic echo sounders.
3. Perform salt spray tests on echo sounder transducers, to ensure that they will hold up in the marine environment.

For undersea acoustic applications, a careful study of buoy dynamics must also be performed, to determine if proper directional control of the acoustic beams can be obtained. The environmental noise problems must also be studied further for the typical buoy locations.

In the absence of marine life and shipping, the underwater ambient noise level depends primarily on wind force and sea state. This is particularly so in the frequency range 100 Hz to 25 kHz.

The noise level due to oceanic traffic is particularly evident in the 10 to 1000 Hz frequency range. The noise level due to bubbles and spray is confined to the frequency range 50 Hz to 20 kHz, while that due to turbulent pressure fluctuations is confined to the frequency range 1-100 Hz.

It is particularly important to recognize that an oscillating bubble represents an effective source of sound. In the ocean, bubbles are expected to execute both free and forced oscillations, particularly near the surface where agitation occurs due to the wind force. The natural frequency of oscillation for the zero order mode is given by

$$f_o = 3\left[\frac{C_\rho}{C_v}\ \rho_s\ \rho^{-1}\right]^{1/2} (\pi D)^{-1}$$

where p_s is the static pressure, ρ the density of the medium, and D the mean bubble diameter.

Biological noise contributes to the ambient noise level of the ocean, but this appears to be a function of frequency, time, and location. Consequently, the contribution of biological noise to the ambient noise level is difficult to predict and should be measured at buoy locations. However, in some cases, the diurnal, seasonal, and geographical patterns may be predicted if sufficient experimental data are available. In addition, the habits as well as habitats of noise-makers must be known.

The effect of precipitation to the ambient noise level appears to be most noticeable at frequencies above 500 Hz. In the frequency range above

100 kHz, thermal agitation appears to be the most important source of ambient noise. Over the temperature range 0° to 30° C, the thermal noise level L_T is given by (Mellen, 1952).

$$L_T \approx -101 + 20 \log f,$$

where L_T is in dB re 2×10^{-4} dyn/cm for 1 Hz bandwidth and f is in Hz see also Wenz (1962), Kendig (1963).

All of these underwater noise sources will limit the utility of current measuring or the sensing of sea state or mixed layer and thermocline.

2.4 Conclusions

In spite of the potential difficulties with buoy dynamics, which may dictate some stable platform or steerable antenna for acoustic echo sounding, and in spite of the problems of environmental noise on the buoy caused by wind and wave motion, it is concluded that temperature structure and wind sensing using acoustic means from data buoys holds great promise of providing significant atmospheric information. A three antenna cluster, or possibly a flat, steerable phased array capable of producing three acoustic beams simultaneously, could provide wind profiles throughout the marine boundary layer. Such performance would require the use of the on board computer to properly interpret the backscatter Doppler shift, or possibly the raw acoustic data could be telemetered to a shore station for processing. The frequency band widths per Doppler channel are only several hundred Hertz, so such a telemetry link is entirely feasible.

It is concluded that wind sensing may be the first operational use made of atmospheric acoustic echo sounding on data buoys. But, the research value obtained in understanding the structure of the marine boundary layer must be regarded as of equal importance. So little is known of the morphology of convective structures over a warm ocean or of the

nature of stratification, gravity wave energetics, or synoptic influence on the stable marine layer that there would be great value in obtaining a better understanding of the structure of the lower regions of the atmosphere. The advantages to be gained by atmospheric acoustic echo sounding are great enough to warrant considerable effort to overcome the environmental problems which must be faced in placing such equipment on data buoys.

It is also concluded that under water acoustic sensing of currents is essentially feasible, as already investigated by NDBP. Pulsed Doppler acoustic sensors may be located on the buoy or along the mooring cable to sense currents at varying depths below the surface. There is an advantage to spaced sensors along the cable in avoiding refraction effects produced by temperature gradients, if such current sensing were attempted from sensors on the buoy only. It is worthwhile, however, to study further a configured array of sources and hydrophones on the buoy, perhaps operating at lower frequencies than the conventional current sensors, to provide greater range under certain deep water conditions. Careful considerations in this study must be made of refraction, surface and bottom reflections, and reverberations. There is likewise the promise of obtaining interesting new data on the structure of the mixed layers and on temperature gradients below the surface by utilizing undersea acoustic probes on the buoy.

2.5 A Proposed Acoustic Program

In this section of the report a program to establish developmental acoustic sounders, for atmospheric studies and for undersea studies, is proposed. Tasks 1 through 5 involve the deployment of the experimental atmospheric sounders. The end result of these tasks would be the installation of developmental equipment on the buoy, ready for testing of its operability under a variety of environmental conditions. Similarly, Tasks 6 through 10 involve the study and preparation of underwater acoustic sounders for structural and current studies of the mixed layer and possibly into and below the thermocline.

It is anticipated that the sequence of tasks listed would extend over a two year period in time. Tasks 1-3 and 6-7 would occur during the first year, and the remainder during the second year.

A more detailed consideration of the various tasks is now presented. Supplementary budget information follows at the end of this discussion.

The purpose of Task 1 is to determine the acoustic and dynamic environment on a typical buoy, and to establish the design of an atmospheric acoustic echo sounder compatible with this environment. Sub Task 1A would involve the modification of existing WPL sound level meters and tape recorders for installation on a data buoy, to determine the acoustic environment for a variety of conditions. After determining the most expedient method of recording this information in consultation with NDBP personnel, the existing electronics would be modified either for a timed sequence of recordings or for remote command control from shore.

After accomplishing the modification, the sound level meters would be installed on a buoy in Task 1B, and the background noise recorded under calm, quiet conditions and under increasingly more severe conditions up to the maximum presented during the proposed test period of one month's duration. The recordings would be returned to WPL in Task 1C for analysis, with the results being a statistical tabulation of background noise conditions experienced for a variety of meteorological and C state conditions.

Paralleling the first three Sub Tasks A-C, a study would be undertaken under Task 1D to determine the dynamics of the several classes of data buoys contemplated for use by NDBP, most probably through a study of the manufacturer's reports, with supplemental information provided by experience gained in operating the buoys Task 1E would determine the type of antenna stabilization, gimbaling, or phased array steering required to insure that the returned echo was within the beam width of the antenna.

Following the completion of the first five Sub Tasks A-E, the characteristics of an anticipated successful sounder design would be established. A report would be prepared for NDBP, detailing the results of Task 1, determining just what is required for successful atmospheric sounding from a data buoy. Task 1 would be completed in six months time after the beginning of the acoustic project.

Having established the desired operational characteristics of an experimental buoy mounted sounder, it would be required to perform certain environmental tasks on critical components in Task 2A. Such

tests would include humidity tests on exposed components and structures plus salt spray tests on the acoustic transducers.

With the availability of sound level records from the buoy as a result of Task 1B, and the analysis available from the buoy dynamics study, Task 1D, computer simulations of signal plus noise expected in the marine environment, and studies of signal loss from uncompensated or imperfectly compensated antennas on the moving buoy would be performed. The consideration of on board computer processing required for steering acoustic phased arrays would also be accomplished, and bids obtained as a backup from manufacturers of stable platforms for dish type antennas. Task 2 could be initiated after the completion of Task 1A-D and accomplished over a two month period, so that the results could be incorporated into the report which establishes the sounder design. Thus, both Tasks 1 and 2 will be accomplished six months after the starting date.

Task 3 will involve the design and construction of a single channel, vertically directed experimental test model of an acoustic sounder for installation on a buoy. Data obtained from acoustic probing of the marine atmosphere will be stored on a tape recorder housed in the buoy. Either time programmed or remote command recording of data will be employed to acquire data under a variety of environmental conditions. The data will be returned to WPL for analysis, to determine how well the experimental test sounder operated in the buoy environment. Because the work to be accomplished during Task 3 will significantly depend upon the outcome of Tasks 1 and 2, the cost and scheduling of Task 3 are somewhat less well defined. It is believed that Task 3 could be completed 12 months after the beginning of the project.

Having successfully operated the single channel, vertically directed sounder on the buoy, a three axis, total wind sensing Doppler system will be designed, constructed, and installed on a buoy as Task 4. The resulting returns would either be tape recorded or telemetered to shore. This system will undoubtedly require interfacing with the buoy computer and possibly the computation requirements will be such that the wind

sensing sounder will require its own computer. It should be possible to incorporate some of the components from the Task 3 single channel sounder into the wind sensing system so that completion of this task could occur 18 months after the initiation of the project.

Following the operation of the single channel and three channel experimental test models, a developmental model, with much improved reliability and redundancy in its design will be developed and installed on a buoy for an extended period of test operations. The developmental model would be installed two years after the beginning of the project.

The Tasks for undersea acoustic study, investigations, and sounder developments follow a similar sequence to that proposed for the atmospheric sounder. Task 6 would be a study to determine the acoustic environment to be expected near the data buoys. Of paramount importance in this task is the establishment of "need-to-know" for NOAA personnel with the Navy, so that existing measurements of the acoustic environment in locations planned for data buoys may be made available. Even in the preliminary studies leading to this report, the necessity for obtaining access to classified data (and very possibly, unclassified data buried within classified reports) was made apparent. A two man-month effort is proposed to obtain a better understanding of the background noise problem.

Task 7 will supplement the study of Task 6 by investigating the actual acoustic environment on board an operating buoy. The buoy itself will influence the recorded sounds because of its own size and motion in the ocean. It is proposed to construct the simple passive sound recording system capable of recording background noise from 1 kHz through several hundred kHz. The recordings obtained on a WPL furnished tape recorder would be returned to Boulder for analysis.

Based on results of Tasks 6 and 7, the single axis active echo sounder for underwater probing of the mixed layer will be constructed, installed on the buoy, and the results analyzed in a manner similar to that for the Task 3, atmospheric single axis sounder.

During Task 9, a three axis sounder for remote measurements of underwater currents and structure would be designed, constructed, installed,

operated, and the resulting data analyzed. This undoubtedly would be a relatively sophisticated echo sounder, employing a number of simultaneous frequencies or perhaps chirped pulses to obtain echoes from a number of different ranges and perhaps at different angles to allow probing in the mixed layer, the thermocline, and in deeper layers. Following the completion of the successful operation of the experimental units, a high reliability , developmental current sensor would be designed, constructed, and installed on the buoy. Task 6-10 would run concurrently with Tasks 1-5 and the entire acoustic program would be completed approximately two years after the initiation of the project.

On the budget sheets which follow, the funds required for the first task are more accurately identified than those for follow on tasks because of uncertainties in the results of the preliminary investigations. It is believed, however, that the overall level of effort proposed is a realistic one.

Budget - Acoustic Echo Sounding of the Atmosphere and Ocean from Data Buoys

Task	Man months of effort	Other Costs	Funds Required
1A - Modify sound meters	2 - Electronic engineers		3,400
	1 - Technician		1,300
		Electronic components	1,000
		Travel and per diem	400
		Task sub-total	6,100
1B - Record sound levels	0.5 Electronic engineer		850
	1 - Technician		1,300
		Magnetic tape	50
		Travel and per diem	800
		Task sub-total	3,000
1C - Analyze records	1 - Electronic engineer		1,700
	1 - Programmer		1,200
		Task sub-total	2,900
1D - Buoy dynamics study	0.5 Engineer		850
	0.5 Programmer		600
		Task sub-total	1,450
1E - Antenna study	0.5 Engineer		850
	0.5 Programmer		600
		Task sub-total	1,450
1F - Establish sounder design	1.0 Engineer		1,700
	0.3 Draftsman		500
	0.3 Secretarial		350
		Task sub-total	2,550
		Task 1 Total	$17,450

Task	Man months of effort	Other Costs	Funds Required
2A - Environmental tests	0.5 Engineer		850
	1.0 Technician		1,300
		Testing sub-contract	2,000
		Task sub-total	4,150
2B - Computer simulations	2 - Engineer		3,400
	2 - Programmer		2,400
		Computer costs	2,000
		Task sub-total	7,800
		Task 2 total	11,950
3 - Design, construct single channel sounder for buoy; install, operate, analyze data	6 - Engineer		10,200
	3 - Meteorologist		6,000
	10 - Technician		13,000
	3 - Programmer		3,600
		Sounder components	30,000
		Task 3 total	62,800
4 - Design, construct, operate 3 axis wind sensing system			
		Task 4 total	~ 180,000
5 - Develop, install developmental wind sensing system			
		Task 5 total	~ 200,000

Task	Man months of effort	Other Costs	Funds Required
6 - Undersea acoustic environment study	2 - Scientist/engineer		3,400
		Travel and per diem	800
		Task sub-total	4,200
7 - Buoy sound recording	2 - Engineer		3,400
	2 - Technician		2,600
	1 - Programmer		1,200
		Travel and per diem	800
		Hydrophones, components	3,000
		Task sub-total	11,000
8 - Mixed layer sounder (experimental)		Task 8 sub-total	60,000
9 - 3 axis, buoy current sounder (experimental)		Task 9 sub-total	150,000
10 - Developmental current, structure sounder		Task 10 sub-total	200,000
		Total, 2 year program Acoustic tasks 1-10	$897,400

References

Albers, V. M., Underwater Acoustics Handbook - II, The Pennsylvania State University Press, University Park, Pennsylvania, 1965, 356 pp.

Bassin, N. J., J. E. Harris, and A. H. Bouma, Suspended matter in the Caribbean Sea: a gravimetric analysis (letter), Marine Geology, Vol. 12, No. 3, March 1972, pp. M1-M5.

Beamish , P., Acoustic scattering from zooplanktonic organisms, Proceedings of an International Symposium on Biological Sound Scattering in the Ocean, Ed. G. B. Farquhar, March 31 - April 2, 1970, Airlie House Conference Center, Warrenton, Virginia.

Beran, D. W., C. G. Little, and B. C. Willmarth, Acoustic Doppler measurements of vertical velocities in the atmosphere, Nature, Vol. 230, No. 5290, pp. 160-162, March 19, 1971.

Beran, D. W., and S. F. Clifford, Acoustic Doppler measurements of the total wind vector, Proceedings of AMS Second Symposium on Meteorological Observations and Instrumentation, San Diego, Calif., March 27-30, 1972 pp. 100-109.

Bond, G. C., and R. H. Meade, Size distributions of mineral gains suspended in Chesapeake Bay and nearby coastal waters, Chesapeake Science, Vol. 7, No. 4, 1966, pp. 208-212.

Frisch, A. S., Private Communication, 1972.

Kaimal, J. C., and J. A. Businger, Case Studies of a convective plume and a dust devil, J. Appl. Met., 1970, 9, 612-620.

Kendig, P. M., Under Water Acoustics, ed. V. M. Albers, Plenum Press, 1963.

Kinzer, J., On the contribution of euphausiids and other plankton organisms to deep scattering layers in the eastern north Atlantic, Proceedings of an International Symposium on Biological Sound Scattering in the Ocean, G. B. Farquhar, Ed., March 31-April 2, 1970, Airlie House Conference Center, Warrenton, Va., Superintendent of Documents, U. S. Government Printing Office, Washington, D. C., 1971, pp. 476-489.

Krasiluikov, V. A., Sound and Ultrasound Waves in Air, Water and Solid Bodies, third edition, U. S. Department of Commerce, National Technical Information Service, Springfield, Va., 1963, 354 pp.

Little, C. Gordon, On the detectability of fog, cloud, rain and snow by acoustic echo-sounding methods, Jour. Atmos. Sci., Vol. 29, No. 4, May 1972, pp. 748-755.

Manheim, F. T., R. H. Meade, and G. C. Bond, Suspended matter in surface waters of the Atlantic continental margin from Cape Cod to the Florida Keys, Science, Vol. 167, No. 3917, 23 Jan., 1970, pp. 371-376.

McKean, R. S., Lateral Distributions of Thermal Microstructure in the Open Ocean, Rept. No. APL-UW 7115, Applied Physics Lab., University of Washington, Seattle, Washington, March 1971.

Monin, A. S., Characteristics of the scattering of sound in a turbulent atmosphere, Soviet Physics - Acoustics, Vol. 7, No. 4, April - June 1962, pp. 370-373.

Skudrzyk, E. J., Thermal microstructure in the sea and its contribution to sound level fluctuations, in Underwater Acoustics, V. M. Albers, ed. Plenum Press, New York, 1963, pp. 199-233.

Tatarski, V. I., The effects of the turbulent atmosphere on wave propagation, U. S. Department of Commerce, National Technical Information Service, Springfield, Va., 1971, 472 pp.

Urick, R. J., Principles of underwater sound for engineers, McGraw-Hill Book Company, Inc., New York, 1967, 342 pp.

Wenz, G. M., Acoustic ambient noise in the ocean: spectra and sources, The Journal of the Acoustical Society of America, Vol. 34, No. 12, December 1962, pp. 1936-1956.

Wyngaard, J. C., Y. Izumi, S. A. Collins, Jr. Behavior of the refractive index-structure parameter near the ground, J. Opt. Soc. Amer., 61, 1646-1650, 1971.

Zeitzschel, B., The quantity, composition and distribution of suspended particulate matter in the Gulf of California, Marine Biology, Vol. 7, No. 4, 1970, pp. 305-318.

Section 3 APPLICATIONS OF RADAR FOR DATA BUOYS

R. G. Strauch and D. E. Barrick

3.0 Introduction

This section summarizes the applications of radar methods to remote sensing from buoys. The potential role of microwave radar, conventional radar and boundary layer radar, for meteorological measurements and the role of high frequency radar for sea state measurements are explored. Problems associated with buoy operation are discussed and recommendations are made for a program that would lead to the development of radar systems operating unattended from a buoy.

3.1 Meteorological Radar For Data Buoys

Microwave radar has been used for remote sensing of meteorological conditions almost since its invention. Advances in hardware for meteorological radars have followed advances in military radar technology, and as a result, the uses and potential uses of radar in environmental sensing have slowly increased. The most recent developments have led to radars capable of using naturally occuring refractive index fluctuations to monitor processes in the lower troposphere.

3.1.1 Incoherent Pulsed Radar

The incoherent pulsed radar technique has been the conventional weather radar that has been in operational use by NWS for many years. No other remote sensing instrument is as widely used or covers as large a volume of space from a fixed ground location (Atlas, 1964). The weather radar most commonly used operates at 10 cm and is capable of detecting hydrometeors to 400 km. The 10-cm radar systems can measure rainfall rates,

total precipitation, and liquid water content of precipitating clouds. Qualitative information on the sea state may possibly be obtained from the background clutter. Liquid water content of non-precipitating clouds and fogs can be obtained from short wavelength (1.25-cm and 0.86 cm) radars. The shorter wavelength radars also measure precipitation, but the attenuation caused by precipitation reduces the accuracy and range of measurements.

The calibrated weather radar measures the reflectivity (η) of the radar target modified by the total attenuation (two-way) between the radar and the target. The reflectivity is related to the liquid water of content of the target and for spherical drops is given by

$$\eta = \frac{\pi^2 |K|^2}{\lambda^4} Z \qquad (3:1)$$

where λ is the radar wavelength and $|K|^2$ is a dielectric factor given by

$$|K|^2 = \left|\frac{m^2-1}{m^2+2}\right| \qquad (3:2)$$

where m is the complex refractive index. Z, the reflectivity factor is given by $Z=\Sigma D_i^6$ where D is the particle diameter and the summation is over a unit volume of the liquid drops. Empirical relationships relating rainfall rate and liquid water content to Z are used to infer these quantities from measured values of η. Relationships typically used are

$$Z = 200\ R^{1.6} \qquad (3:3)$$

for rainfall where R is the rainfall rate in mm/hour and

$$Z = 0.048\ M^2 \qquad (3:4)$$

for liquid water content where M is expressed in milligrams per cubic meter and Z is expressed in mm^6/m^3.

The conventional weather radar is the most advanced of all meteorological radars and numerous methods of data storage and display are available. A possible mode of operation from a buoy is described below:

The radar would be energized for a single azimuth scan periodically. The periods of active operation would be chosen to utilize power when other sensors were not used. The scans would be infrequent when there were no precipitation echoes (about every 30 min.) and more often when echoes were detected. The time of the next scan would be determined from the data obtained during the previous scan. A digital video integrator would average and quantize data for storage on a digital tape recorder. A 2-meter diameter antenna (10-cm radar) would provide a 4° beamwidth so that by storing only 90-range sweeps a coarse PPI picture of the precipitation would be retrieved. A range resolution of 1 km would then mean that about 15,000 data points per scan would have to be stored for a 150-km maximum range radar. A single tape reel could store the data from an average of 100 sweeps per day for 60 days. An alternative to magnetic tape storage could be storage on film. Intensity levels could be coded so the dynamic range and intensity resolution would be obtained by sequentially photographing data stored in the video integrator, using as many photos as necessary for each scan to obtain the desired resolution. The additional alternative of temporary storage and telemetry readout also exists, as well as other solutions for the data handling problem. The status of conventional weather radar is such that the major problems of this type of radar would be those associated with the buoy environment.

High power 10-cm radars are capable of detecting refractive index fluctuations in the clear air and can also measure liquid water content of clouds, as well as measuring precipitation parameters. The reflectivity for refractive index fluctuations is given by (Ottersten, 1969)

$$\eta = 0.38\lambda^{-1/3}C_n^2 \qquad (3:5)$$

where C_n^2 is the structure constant for refractive index. The high power radar is not envisioned for buoy applications because of power and size considerations.

3.1.2 Pulsed Doppler Radar

The addition of pulse-to-pulse coherence to the conventional weather radar leads to the ability to measure the spectrum of radial velocity as well as the parameters measured by the incoherent radar. These radars are referred to as meteorological Doppler Radars and their utility as a research tool has been demonstrated (Lhermitte, 1970). The value of Doppler capability lies in the ability to measure detailed structure of the motion of hydrometeors inside the radar echo region. The average motion of the echo region can be obtained from incoherent radars. Present pulsed Doppler radars have a maximum range-maximum velocity product given by

$$R_m V_m = \pm \frac{c\lambda}{8} \quad . \tag{3:6}$$

Progress in Doppler capability has been relatively slow because of the data processing needed to obtain the velocity spectrum. Recent advances in data processing will be reflected in new Doppler radar research tools and operational Doppler radars will surely follow.

The Doppler radar measures only the radial velocity component, and techniques for extracting the maximum amount of information from the radial component, including the wind field, have been devised. These techniques often involve assumptions that are not easy to verify. The concept of multiple Doppler radar for obtaining velocity fields was introduced by Lhermitte (1970), and recent Wave Propagation Laboratory experiments have demonstrated the potential of a dual Doppler network (Miller, 1972). Fig. 3.1.1 is a wind field obtained during a snowstorm in Boulder, Colorado using two 3-cm radars. The eddy field (Fig. 3.1.2) is the two-dimensional velocity field after subtracting the mean flow. The pulsed Doppler method has also been applied to clear air returns from high power radars (Browning, 1972).

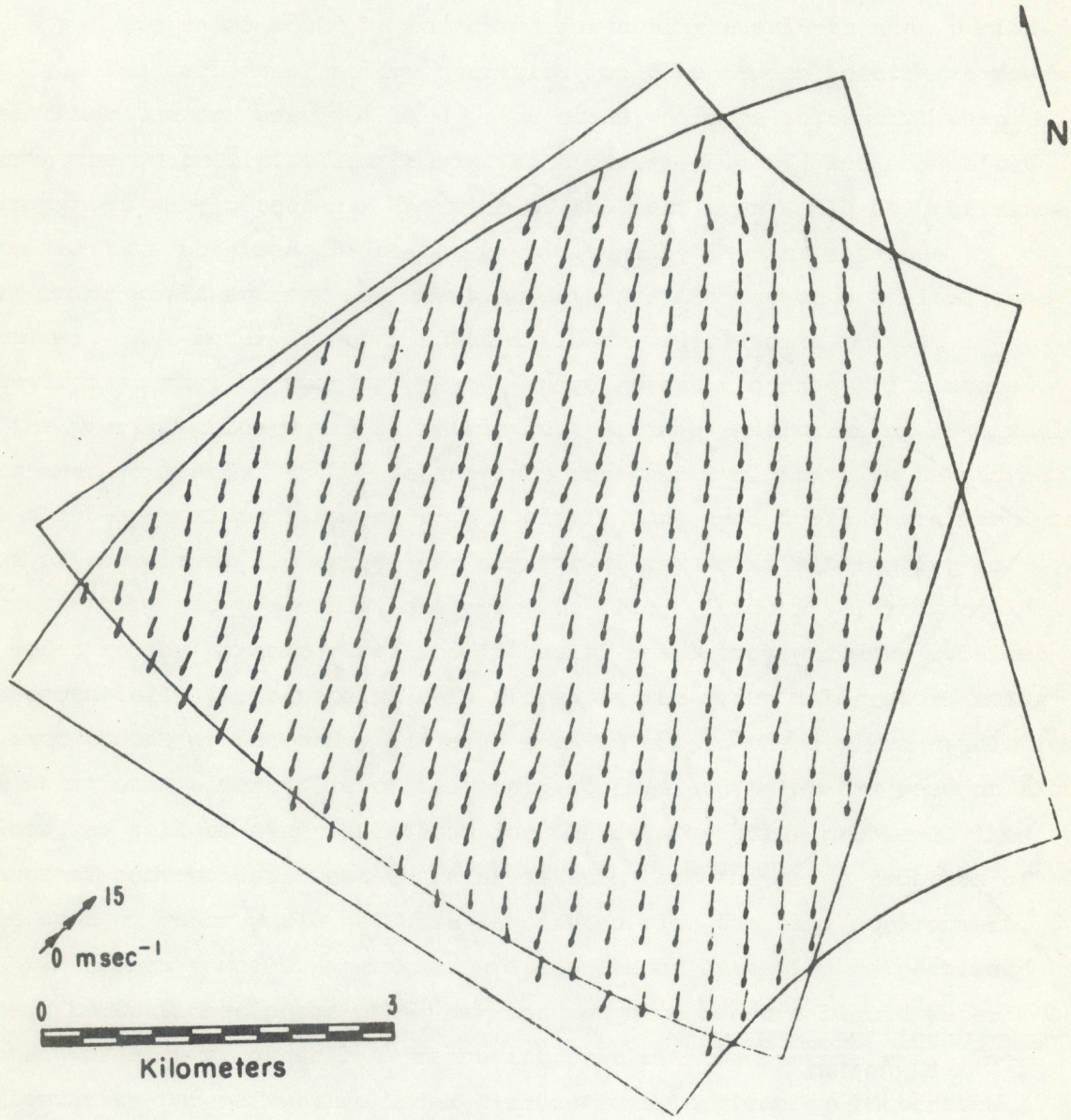

Fig. 3.1.1 Horizontal wind field derived from data taken in snow. Field points are separated by 300 m.

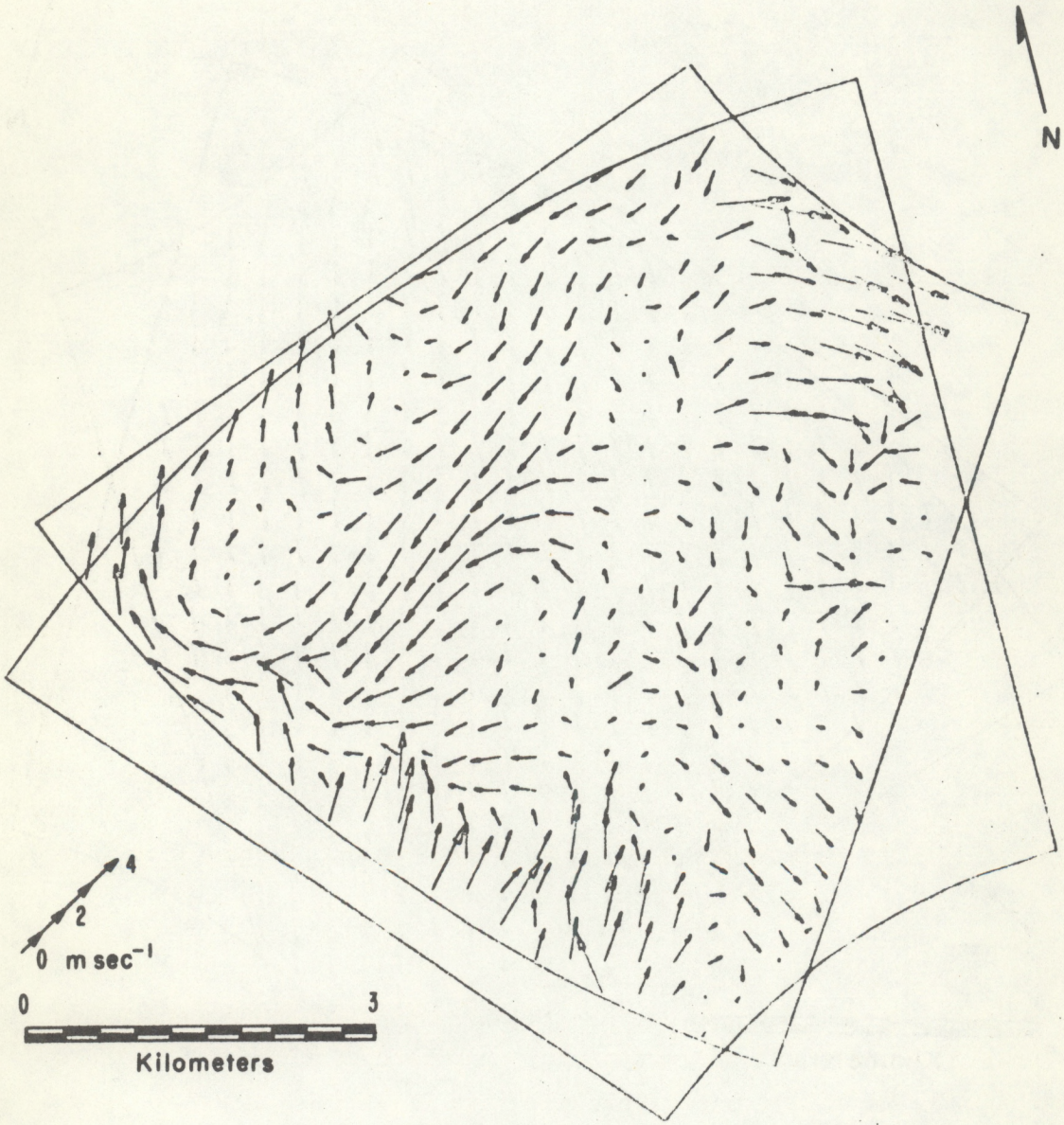

Fig. 3.1.2 Eddy flow field of wind field in Fig. 3.1.1. The mean flow is from 14.8° at 5.5 m/sec^{-1}.

The additional major problem associated with adding Doppler capability to a radar on a buoy is the requirement for extensive data processing equipment for on-line data reduction. Efficient methods of data reduction are now being planned for the next generation of Doppler radars. The actual utility of Doppler capability will be known when these radars are used operationally.

3.1.3 FM/CW Radar

The FM/CW radar has demonstrated the ability to measure refractive index fluctuations (C_n^2) in the clear air (Richter, 1969, Bean *et al*, 1971) utilizing equation 3:5 to obtain C_n^2 from measured radar reflectivity. This radar has proven to be very useful for studying waves and turbulent structure in the clear air. The radar detects echoes which coincide with cloud tops for some types of clouds. Velocity of isolated targets can be measured by this radar (Chadwick and Warner, 1971), but measurement of radial velocity from distributed targets has not been shown. Figure 3.1.3 shows the intensity-time record of a vertically pointing FM/CW radar, revealing the excellent spatial resolution of the device. Separate transmitting and receiving antennas are needed and their isolation must be sufficient to prevent receiver saturation. A scanning antenna system has operated successfully (Richter, 1972). Data storage using film or magnetic tape in conjunction with on-line processing has been utilized.

The extension of the FM/CW technique to include Doppler velocity and precipitation measurements would lead to a versatile boundary-layer radar.

3.1.4 Pseudorandom Coded Radar

An 8.6 mm wavelength pseudorandom coded radar has been under construction at the National Institute for Telecommunications Research, Johannesburg, South Africa for several years (Reid, 1969). This is a CW radar (and thus uses two antennas) with a pseudorandom modulation of the transmitter phase by π radians. It is designed specifically for the analysis of the spectrum of precipitation drops and for the measurement of liquid content of clouds. Doppler velocity is obtained and excellent

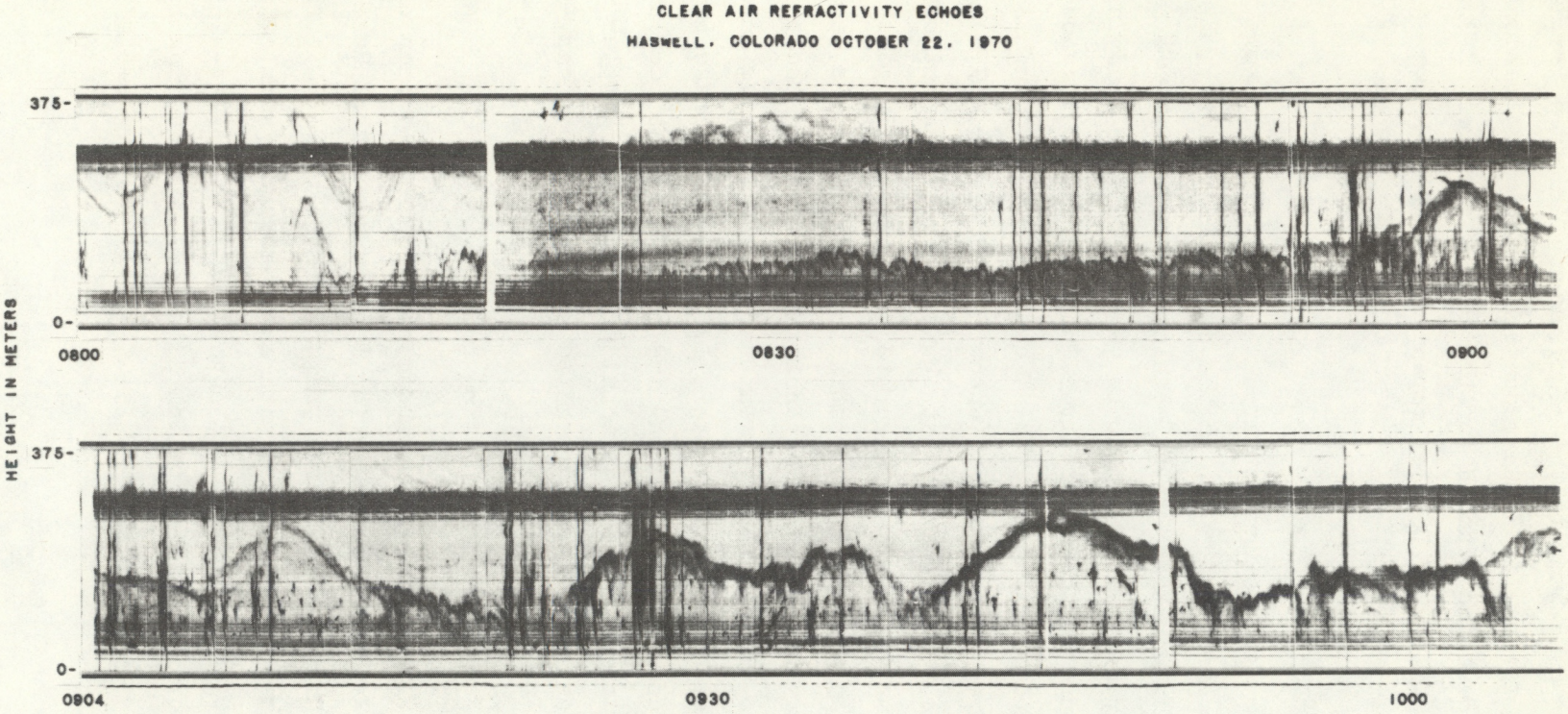

Fig. 3.1.3 Radar record of clear air returns from FM/CW radar

range and velocity resolution are possible by suitably choosing the length and rate of the modulating code. The principle disadvantage of this radar is that a correlation must be performed at each range of interest. Since radar returns from all ranges are received simultaneously, integration times are long so it is not suited for rapid scanning of many radar resolution cells. A 10-cm pseudorandom coded radar for precipitation and refractive index fluctuations could be constructed with sensitivity similar to the FM/CW radar. Note that in the FM/CW radar, targets at different ranges appear at different received frequencies and the FM/CW radar therefore has the advantage of rapid scanning. The advantage of the pseudorandom coded radar is the ease with which Doppler data is obtained.

A 10 cm pseudorandom transmitter and receiver are being utilized by the Institute of Telecommunication Sciences in Boulder, Colorado for tropospheric channel sounding. This device utilizes a 1 kW transmitter and could serve as the transmitter portion of a pseudorandom radar. The range resolution would be 15 meters, and the maximum range would be 7.5 km with sufficient maximum velocity for all meteorological targets. The device is normally operated bistatically and is not equipped with a correlation receiver.

3.1.5 Random Noise Radar

A random noise radar has been constructed at Purdue University (McGillem *et al*, 1968). Its potential for excellent spatial resolution and velocity resolution have been demonstrated on discrete, coherent targets. The random signal radar transmits short pulses of wideband noise at a high pulse repetition rate. The high repetition rate eliminates the velocity ambiguity associated with conventional pulsed Doppler radars and range ambiguities are avoided because each transmitted pulse is independent. The wideband noise transmitted allows excellent range resolution. In principle this radar is capable of measuring the same parameters that a conventional radar of the same wavelength measures but with the desirable characteristics noted above. The principal disadvantage of this radar is that when the radar scatterers occupy a large range interval (as they will for rain for example), there will be more than one radar pulse at one time

in the space between the target and the radar. Therefore energy will be received from targets at various ranges at the same time. The receiver, a correlation receiver as in the pseudorandom radar, views the return from ranges other than the one being examined as additional noise. This "uncorrelated clutter" is a crucial limitation of this radar for meteorological targets since its magnitude can be many times as large as the signal. Thus random signal radar, as the pseudorandom coded radar, may require long integration times. The potential of this radar needs to be explored. It can use the same antenna for transmitting and receiving, a distinct advantage for scanning systems.

3.1.6 Coded Radar

The FM/CW radar, the pseudorandom noise radar, and the random noise radar are specific examples of a broad class of radar devices using coded modulation schemes. Their application to meteorology is just starting to be explored. The immediate applications envisioned for those radars in meteorology are in the boundary layer where limitations in range resolution and minimum range of pulsed radars are not sufficient to observe turbulent structure. A boundary layer radar capable of measuring the wind field in clear air to 1 km altitude, using either refractive index fluctuations or aerosol particles, may be possible. It is clear that these radars are in the research stage and will be for some time.

3.1.7 Special Problems for Buoy Operation

Some of the problems of a radar operating unattended from a buoy have been referred to in previous paragraphs. Even though weather radars have been operational for years, buoy operation would require entirely new engineering solutions. The major problems are summarized in this section.

(a) Antenna stabilization - The antenna system must be stabilized if optimum use is to be made of the data. Radar systems that use two antennas, are steerable, and require good isolation between antennas, will present special difficulties. Two-meter antennas for a 10-cm radar would yield reasonable beamwidth (4°). Shorter wavelength radars with comparable beamwidths would be easier to accommodate.

(b) Calibration - Radar systems are able to make quantitative measurements only after careful calibration. The buoy radar could be calibrated prior to installation but a method of checking the calibration on the buoy would be needed. This is particularly necessary for the hostile antenna environment of the buoy.

(c) Power Consumption - The power required by various radar systems and the power available will be a factor in deciding the type of radar, the mode of operation, peak power, etc. The power available on the buoy may be the major factor determining system performance.

(d) Data Processing - The data rate of most radars will be too large to record and store raw video data except for short samples. Limitations on data storage or transmission to shore will require extensive preprocessing of data.

(e) Other significant problems are cost, reliability, and the hostile environment. Consideration must be given to the systems that will utilize the radar data, particularly if many buoys are to be radar equipped or if vast quantities of data are obtained from even one radar.

3.2 Sea State Measurements with Buoy-Mounted Radars

The most desirable quantitative measure of sea state in a given localized area (e.g., a 20 km diameter patch) is the two-dimensional waveheight spatial spectrum. This quantity -- call it $S(\kappa_x,\kappa_y)$ or $S(\kappa,\phi)$ -- provides a measure of the strengths (or heights) of waves of various spatial lengths ($L=2\pi/\kappa$) and moving in various directions, as denoted by ϕ. By integrating the spectrum over ϕ, one obtains the nondirectional spectrum $S(\kappa)$; upon integrating this again over the remaining independent variable, κ, one can obtain the rms (or significant) waveheight of the sea, H. The latter two quantities ($S(\kappa)$ and H) are isotropic or nondirectional, which means that one has no knowledge of the direction in which the ocean waves are moving from $S(\kappa)$ and H alone.

There are several methods of measuring $S(\kappa)$ and H. A short-pulse satellite radar altimeter will measure H at the suborbital point (Barrick, 1972). Buoys are now commercially available -- equipped either

with vertical accelerometers or submerged dynamic pressure transducers -- which can measure the sea waveheight at the buoy vs time. From this quantity, $S(\kappa)$ and H can be readily computed. There are presently no straightforward techniques for measuring the directional spectrum, $S(\kappa,\phi)$. Both Stillwell photography (involving optical signal processing) and a multi-course airborne laser profilometer can provide estimates of $S(\kappa,\phi)$. Since they require manned aircraft, they are quite costly, complicated, and are fair-weather techniques; hence they are ill-suited to remote sensing applications. Arrays of buoys have been used in rather disappointing attempts to measure the directional spectrum (Kinsman, 1965); the complications and expense of such floating arrays appear to preclude any further use of this technique. Interest recently has turned to the use of buoys with orthogonal inclinometers to measure tilts (or wave slopes) vs time (Saenger, 1969). Such buoys can give only gross directional characteristics (e.g., they have about 90°-120° azimuthal resolution), and have not yet been experimentally validated in deep water.

It is quite important to measure sea directionality -- especially the directions of the longest gravity waves present -- for these are the essence of sea state. The directions of these waves can be used to infer the wind pattern history above the sea area. In addition, a knowledge of wave directionality will permit forecasting of sea state propagation, and also degeneration of high wind waves into swell which is seen later thousands of miles distant from storm areas. Hence, this report concentrates only on those buoy-mounted radar techniques which offer the prospect of providing directionality, i.e., $S(\kappa,\phi)$. If one wishes only nondirectional data, i.e., $S(\kappa)$ or H, he is much better off using buoy-mounted accelerometers or pressure transducers; the technology behind them has already been developed, they are less costly, and are more reliable than radar techniques.

Of the radar techniques suggested here, only the MF/HF frequency region is considered promising for buoy-mounted applications. While surface-based microwave radars are constantly plagued with sea scatter (or clutter), there has been almost no success -- either theoretically or experimentally --

in relating near-grazing microwave sea scatter to sea state. In contrast, the mechanism behind HF sea scatter is well understood, has been established theoretically, and verified experimentally. Simply stated, the sea wave-trains at HF appear to the radar as a superposition of diffraction gratings; backscatter at grazing thus occurs from only those sets of waves moving toward and away from the radar with spatial period precisely one-half the radar wavelength. The strength of the average scattered power is proportional to the heights of the waves present at this wavelength. By spectrally processing the received signal, the direction of wave movements can be established. Section 3.2 examines three buoy-mounted MF/HF radar concepts which have been initially explored. These concepts can all give direct measures of $S(\kappa,\phi)$, the directional ocean waveheight spectrum.

3.2.1 Buoy-Satellite Bistatic HF Sea Sensor

Under a recent study for NASA (Ruck, Barrick, Kaliszewski, 1972), the feasibility of a technique for measurement of the sea waveheight directional spectrum, $S(\kappa,\phi)$, was examined. This technique involves transmission of an HF signal from the buoy and reception/processing aboard an orbiting satellite. This situation is shown in Fig. 3.2.1 for the case when the satellite is directly overhead for simplicity in explaining the concept.* Both the direct signal and the signal scattered from the sea at a given time delay, $t_D \simeq R_T/c$ are received at the satellite (c is the free-space radio wave velocity). This sea-scattered signal for a given, fixed range gate corresponds to the return from a ring around the buoy, which would typically be 10-20 km in radius. The signal from this range gate is then Doppler-processed, using the direct signal between buoy and satellite as a reference both for amplitude and Doppler. Typically, for satellite velocities of about 8000 m/s, the required Doppler resolution is about $\pm$ 0.5 Hz.

---

* It is not necessary that the satellite be overhead, or even orbit in a plane which contains the buoy. The pulse-Doppler relationships for this more general configuration are analyzed in the above reference.

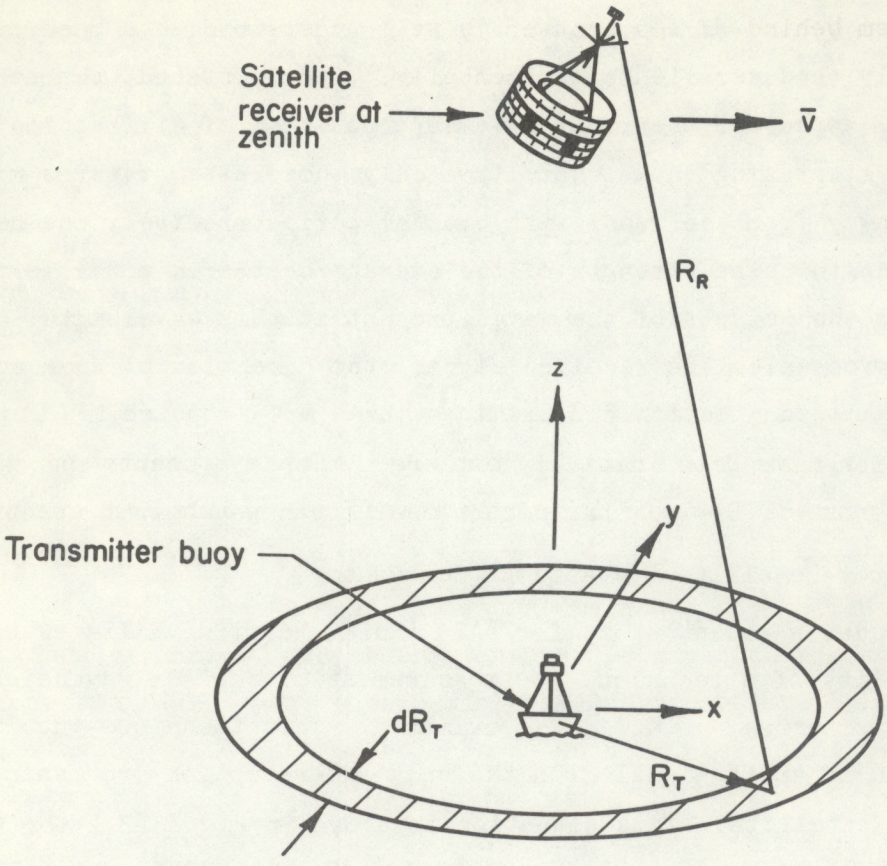

Fig. 3.2.1 Bistatic HF buoy-to-satellite radar

The principle behind this concept is as follows. By the diffraction grating mechanism discussed previously, only those ocean waves crossing the circle radially and of length approximately the radar wavelength are seen by the receiver. The large satellite velocity imparts different Doppler shifts to scatter from each point around the ring; typically at 10 MHz, these Dopplers lie between $\pm$ 14 Hz, the largest coming from that portion of the ring in the orbital plane in front of the satellite. One thus steps (or sweeps) the carrier frequency, f_0, through the HF region (from about 3 to 30 MHz), sampling the ocean wave spectrum at wavenumber

$\kappa = 2\pi/\lambda = 2\pi f_0/c$; the waveheight spectrum at angle ϕ is obtained by examining the receiver signal spectrum at Doppler Δf. For the geometry shown here $\Delta f/f_M = \cos\phi$, where $f_M \simeq f_0(R_T/R_R)(v/c)$. The spectral amplitude can be known precisely because any path attenuations in passage through the atmosphere/ionosphere are also present on the direct signal, which is received and used as a reference.

Antenna requirements for the satellite and buoy are simple: omni-directional broadband dipoles/monopoles or loops. Either a pulse or phase-coded/FM signal can be used here. The above referenced study shows that 10 watts peak pulse power provides an adequate signal-to-noise ratio. Reception aboard the satellite (rather than aboard the buoy) is considered desirable because the data can then be pre-processed, recorded, and relayed to ground at a convenient point in orbit, eliminating the problem of data telemetry from the buoy. Buoy motions will not degrade the signal appreciably at HF. The ionosphere does restrict transmissions during the daytime at the lowest HF frequencies; the extent of this limitation is examined in the above report. Since the lower HF frequencies are measuring the longest ocean waves, having build-up and decay time constants of the order of 12 hours, daytime operation restrictions would not appear to hamper the utility of this concept.

3.2.2 Buoy Backscatter MF/HF Sea Sensor Using Directional Antennas

A backscatter MF/HF radar at the sea surface also observes the scatter from a circular annulus, as shown in Fig. 3.2.1, corresponding to a time delay $t_D = 2R_T/c$. To radiate, propagate, and scatter effectively above the sea, vertical polarization must be used. If the radar is stationary (i.e., not aboard a moving vessel), the first-order return from the sea waves of length $L = \lambda/2$ moving radially across the circular annulus occurs at discrete Doppler shifts $\Delta f = \pm\sqrt{g/\pi\lambda}$; this arises because the phase velocity of ocean waves of length L is $v = \sqrt{gL/2\pi}$, where g is the acceleration of gravity (9.81 m/s^2). Thus, using a non-directional, stationary antenna, it is not possible to tell which part of the ring is producing the scatter, and hence the directionality of the ocean waves cannot be established.

The use of directional antennas would permit one to "look" at only one part of the ring in azimuth. Highly directional antennas at low HF are huge, however. Moderately directive antennas are possible, having approximately a cosine-squared azimuth pattern. One such antenna is a vertical loop antenna. Two such vertical loops, crossed and fed independently as shown in Fig. 3.2.2, can produce a fat beam (~ 90° half-power beamwidth) which can be scanned in azimuth by amplitude control at the terminals. A single loop can scan by mechanical rotation. The use of a backscreen and/or parasitic elements can remove one of the two lobes produced by a loop, solving the backlobe ambiguity.

Similar scannable cosine-squared patterns can be produced by other electrically small antenna configurations. Several such antenna alternatives should be considered for implementation aboard a buoy. Factors which will eliminate some of the candidates are: (1) the requirement that the carrier frequency by stepped (or swept) over nearly a decade in bandwidth (to permit measurement of the ocean wave spectrum over its significant lower end); (2) electrical differences in efficiency for the element when used as a transmitting and as a receiving element at MF/HF; (3) operation under salt spray conditions and near a highly conductive sea.

Even though the ultimate pattern achieved at a buoy can probably be no better than the 90° (cosine-squared) beam, greater angular accuracy than 90° can be achieved if the received signal-to-noise ratio is high. By scanning the beam with time, the antenna pattern can be deconvolved from the directional pattern of the sea scatter. The angular accuracy achievable in measuring the directional waveheight spectrum thus increases with the signal-to-noise ratio and with the number of independent samples employed in the processing.

Such a buoy/backscatter system has the advantage of being self-contained, rather than depending upon a satellite for reception. The ionosphere poses no problems to this system. Buoy motion does not significantly degrade the signal. As with the preceding concept, data from only one range cell (~ 10-20 km from the buoy) need be processed.

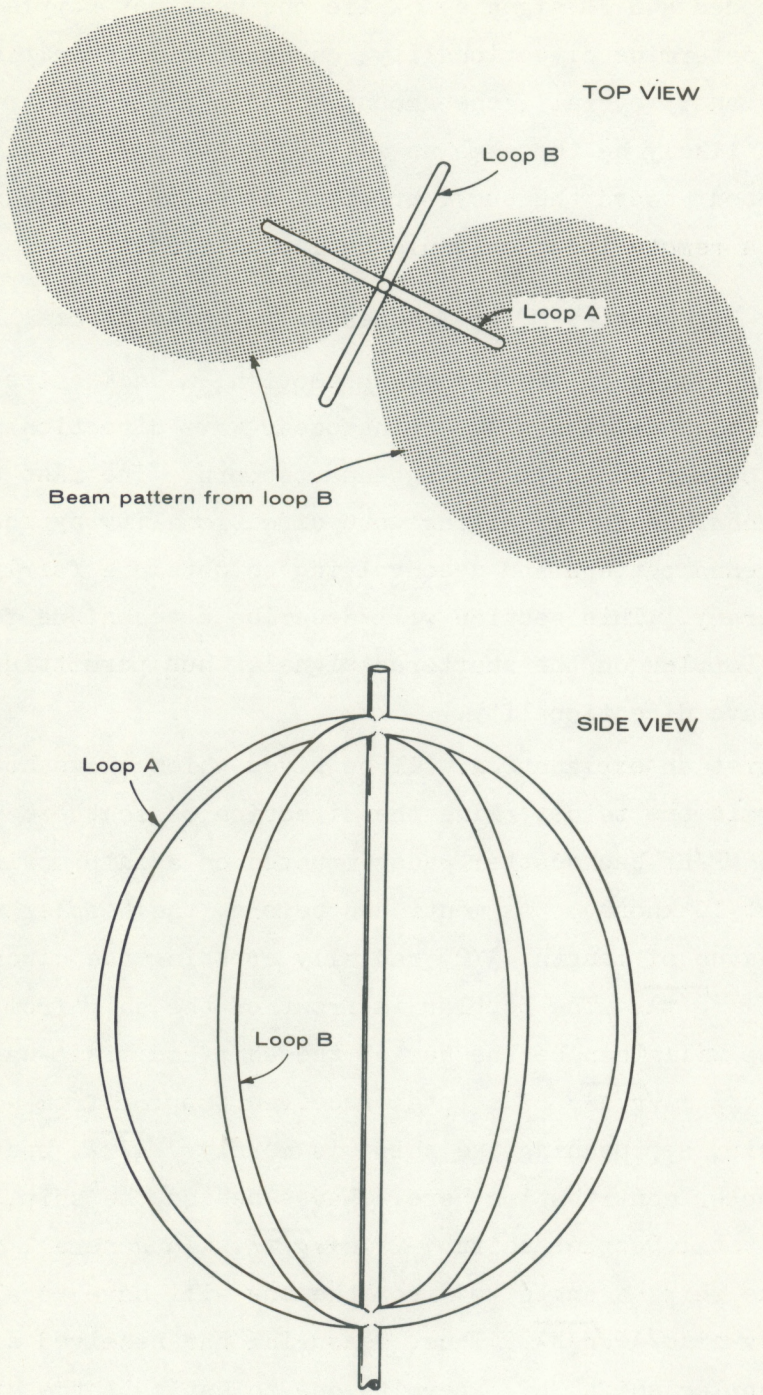

Fig. 3.2.2 Independently-fed crossed loop antenna configuration

The system must be pulsed to avoid feed-through problems inherent with longer phase-coded and FM signals. While one need not Doppler process the signal to determine directionality, one must sample in time as the antenna beam scans; overall, the amount of data collected, processed and recorded would likely be the same as in the preceding system. Since the data is collected aboard the buoy, problems of relaying the information to shore from a remote location would be encountered.

3.2.3 Buoy Backscatter MF/HF Sea Sensor Using Artificial Doppler

As mentioned in the preceding section, a backscatter radar at the surface of the sea cannot determine ocean-wave directionality if it is stationary or has an isotropic antenna pattern. The last section described a technique for obtaining wave directionality by scanning a broad-beam antenna pattern and deconvolving to obtain a fairly narrow azimuthal accuracy. This section will describe a technique for inducing an artificial Doppler on the scattered signal, thus permitting one to obtain ocean-wave directionality.

First an explanation will be given which shows how a moving radar will permit one to determine the direction of scatter. Consider for example an MF/HF backscatter radar mounted on a ship moving at velocity v (e.g., about 10 knots). As mentioned before, the Doppler shift produced by sea waves of length $\lambda/2$ radially crossing the circular range-ring is $\Delta f = \pm \sqrt{g/\pi\lambda}$. The Doppler in front of the ship from waves moving toward the ship will then be the sum of the ship and ocean-wave Dopplers, i.e., $\Delta f_T = 2v/\lambda + \sqrt{g/\pi\lambda}$. The total received Doppler from waves at the side of the ship, approaching the ship, is merely $\sqrt{g/\pi\lambda}$, because there is no ship Doppler contribution here. Waves behind the ship, approaching the ship have total Doppler shift $-2v/c+\sqrt{g/\pi\lambda}$. In general, ocean waves approaching the ship at angle ϕ from the bow will have total Doppler shift $\Delta f_T = 2v \cos\phi/\lambda+\sqrt{g/\pi\lambda}$. Thus, measuring the received signal spectral strength at Doppler shift Δf_T permits one to estimate the directional ocean waveheight spectrum at angle ϕ from the ship heading. An omni-directional antenna is most desirable here (e.g., a vertical monopole) so that the antenna pattern will not distort the signal spectrum.

A novel approach can be employed to simulate the effect of a moving ship. Suppose three omnidirectional stationary antennas were arranged in a row. The antennas are then used in sequence, i.e., the first is used for transmission and reception for T seconds, then the second, and then the third. If the spacing between antenna elements were s, then the whole radar would appear to be moving at a velocity $v = s/T$. Hence, the sea-scattered signal spectrum would have the same Doppler bias introduced on it as discussed in the preceding paragraph for a moving radar. If the switching between elements were abrupt, Doppler sidelobes would appear at the switching frequency. By proper element spacing, proper switching frequency, and by amplitude-tapering the switching (rather than abrupt switching), these Doppler sidelobe problems can be eliminated.

This system has fundamentally the same advantages and disadvantages as the preceding concept. All three techniques produce ambiguities; here there is an ambiguity in $\pm \phi$ because of the cosine. In the preceding technique there was an ambiguity in the front-back direction unless some type of screen were used to remove one-half of the double-lobe cosine-squared antenna pattern of a small loop. In the first system, an ambiguity exists in $\pm \phi$ about the orbital path, for much the same reason as in the artificial-Doppler system described here. All of these double-sided ambiguities can be removed by a variety of techniques; the added equipment complexities in eliminating the ambiguities will help determine which of the three techniques is most cost-effective.

3.3 Recommendations

3.3.1 Meteorological Radar

Table 3.1 summarizes the present status of radar devices for meteorological measurements. Two types of radar systems for buoys merit further consideration: a search radar, (possibly with Doppler capability or with the option of adding Doppler) for precipitation measurements to a range of 200 km and a boundary layer radar for refractive index fluctuation measurements, precipitation measurements, and velocity fields to an altitude of about 2 km. The implementation of the search radar requires extensive

engineering; the implementation of the boundary layer radar requires extensive research.

Two recommendations are therefore made:

(1) The first steps should be taken toward the development of a precipitation measuring radar operating from a buoy. A detailed study of the feasibility of installing a search radar on a buoy needs to be performed. The study should examine the technological feasibility, the data processing alternatives, and the measurement accuracies expected. The study would couple the radar and the buoy and as such would require close coordination with the buoy specifications. If a radar is to be installed on a buoy in 1976-1978, that study needs to be performed in FY 73. A 40 K effort for 6 months is estimated. The study would conclude with a report on the feasibility and method of implementation of a weather radar on a buoy. If the study indicates a system can and should be built, the next step would be to determine system specifications.

(2) The development of a boundary layer radar for buoy operation will require research support. Very little effort has been spent on coded radars and they should be explored. Support for the development of a boundary layer radar is recommended. A brief study should be made to examine which radar offers the best promise for boundary layer measurements, particularly wind. The ability of the FM/CW radar to obtain Doppler velocity should be ascertained. The use of marine aerosols as Doppler tracers should be examined.

The following program is recommended:

- a 3-month study for selecting the most promising boundary layer radar for buoy use followed by
- an 18-month development program of a boundary layer radar capable of obtaining Doppler velocity in the clear air.

Funding required - 20 K for 3 months, 2-man study
- 240 K for 18-month radar development
120 K for 2-man effort
120 K for other objects

The study would conclude with a report detailing the optimum approach to be used in developing a boundary layer radar, what parameter can be measured, and what accuracy and range can be expected.

3.3.2 Development of Buoy-Mounted Radar for Sea State Sensing.

The relationship between first-order MF/HF scatter from the sea and the directional waveheight spectrum has been derived theoretically and successfully verified experimentally in a variety of shore-based monostatic and bistatic configurations. What remains to be done is to examine alternatives for installation aboard a stationary unmanned buoy, select the optimum design, and implement an experiment to ascertain the utility of such a buoy as a remote sensor of sea state. Consequently, WPL recommends a two-phase effort over a period of 20 calendar months.

The first phase, lasting 8 calendar months, is to compare the alternative concepts discussed in Section 3.2 on an engineering basis. Equipment requirements for each concept will be examined, based upon the attendant constraints imposed by operation on a buoy (e.g., power limitations, on-board data processing limitations, space limitations, salt-spray environment, etc). Close interaction between WPL and NDBC personnel will be maintained in order to ensure that realistic buoy constraints are employed. Performance and measurement accuracy will be estimated for each concept; digital simulation of operation in a noisy environment may be used -- if necessary -- to assess the performance. Finally, Phase I will select one of the alternatives as a preferred approach; communication of results along the way with NDBC will be maintained, and their guidance will be solicited in making the final selection.

Phase II will consist of: 1) The final design -- down to equipment specifications -- of the selected technique; 2) procurement of the required equipment from a commercial manufacturer; 3) assembly and calibration of the gear at WPL; and 4) installation and operation of the gear aboard a moored buoy in deep water. In connection with Item 4), other sea-state sensors will be used in the area (e.g., wave staff, vertical accelerometer) to provide ground-truth data for comparison with the buoy-radar output.

Phase I will require 8 man-months, and will cost approximately $40K for labor and other items. Phase II will require approximately 16 man-months of WPL support; approximately $120K will be needed for labor, equipment purchase, and conduct of the sea-based experiments.

3.4 References

Atlas, D. (1964), Advances in radar meteorology, Advan. Geophys. *10*, 317-478.

Barrick, D. E. (1972), Remote sensing of sea state by radar, Chapter 12 of *Remote Sensing of the Troposphere*, V. E. Derr, Ed., U. S. Government Printing Office, Washington, D. C.

Bean, B. R., R. E. McGavin, R. B. Chadwick, and B. D. Warner (1971), Preliminary results of utilizing the high resolution FM radar as a boundary layer probe, Boundary Layer Meteorology *1*, 466-473.

Browning, K. (1972), Atmospheric research using the Defford radar facility, Weather *27*, No. 1., 2-13.

Chadwick, R. B., and B. D. Warner (1971), Potential capabilities of four lower atmosphere remote sensing techniques

Kinsman, B. (1965), *Wind Waves*, Prentice-Hall, Inc., Englewood Cliffs, N. J., 472-483.

Lhermitte, R. (1970), Dual-Doppler radar observations of convective storm circulation, 14th Radar Meteorology Conference, Tucson, Arizona.

McGillem, C., G. Cooper, and W. Waltman (1969), Use of wideband stochastic signals for measuring range and velocity, EASCON Conference, Sheraton Park Hotel, Washington, D. C.

Miller, L. J. (1972), Dual-Doppler radar observations of circulation in snow conditions, 15th Radar Meteorology Conference, Champaign-Urbana, Illinois.

Reid, M. S. (1969), A millimeter wave pseudorandom coded meteorological radar, IEEE Trans. on Geosci. Electronics, *GE7*, No.3, 146-156.

Richter, J. H. (1969), High resolution tropospheric radar sounding, Radio Sci. *4*, No. 12, 1261-1268.

Richter, J. H. (1972), New developments in FM-CW radar sounding, Boundary Layer Meteorology (to be published).

Ruck, G. T., D. E. Barrick, and T. Kaliszewski (1972), Bistatic radar sea state monitoring, Battelle Technical Report, Columbus, Ohio.

Saenger, R. A. (1969), Measurement of the statistical properties of the ocean surface with instrumented surface floats, parts I and II, Hudson Laboratories Technical Reports, Columbia University, New York, N. Y.

Table 3.1 Types of Radar For Remote Sensing From Buoys

Type	λ	Parameters Measured	Present Status	Remarks
Incoherent-pulsed	10 cm	Rainfall Rates Total precipitation Sea clutter-?	Operational(NWS)	250 n mi range-typical 150 m resolution-typical 2° BW -typical
	3 cm	Rainfall rates Total precipitation Sea clutter-?	Operational(NWS)	Attenuation by hydrometeors limits maximum range and accuracy of precipitation measurements.
	8.6mm	Rainfall rates Total precipitation Sea Clutter-? Liquid H_2O of clouds and fog	Research tool (significant met. results)	Poor accuracy of rainfall range and total precipitation, except at short range
	3 mm	Rainfall rates Total precipitation Sea clutter-? Liquid H_2O of clouds and fog Large aerosols	Research device (no sig. met. results)	Has not been used in meteorological applications. Would not be useful for accurate precipitation measurements except at very short range.
Coherent-Pulsed	10 cm	Rainfall rate Total precipitation Sea clutter-? Spectrum of radial velocity Wind field in hydrometeors under same conditions	Research tool (NSSL and others)	60 n mi range 150 m resolution $\pm$ 30 m/sec velocities 0.8° BW 28' antenna
	3 cm	Rainfall rate Total precipitation Sea clutter Spectrum of radial velocity Wind field under same conditions	Research tool (WPL and others)	40 n mi range 60 m resolution $\pm$ 16 m/sec velocities 0.8° BW 12' antenna

Type of radar	λ	Parameters Measured	Present Status	Remarks
Multiple Doppler	3 cm	Wind field deduced from particle velocity	Research tool (WPL)	2 Doppler radars separated by 20-40 n mi to measure 2-dimensional velocity fields mobile system for various applications
	10 cm		Under construction (NSSL)	2 Doppler radars separated by 20-40 n mi to measure 2-dimensional velocity field Convective thunderstorm application
FM/CW	10 cm	Boundary layer C_n^2 Cloud tops for some clouds	Research tool	Vertical pointing-2 antennas-1500 m range 2 m resolution
		Rainfall rate Total precipitation Sea clutter-?	Conceptual	Information available but not used in any present application
		Velocity of boundary layer structure and hydrometeors	Conceptual	Information may be available-method for obtaining velocity from distributed targets is not known
Pseudorandom coded	8.6mm	Precipitation parameters(drop size distb. velocity) Velocity of hydrometeors Liq. H_2O of clouds	Under construction (NITR, So. Africa)	Results expected in 1972
Random noise	3 cm	Precipitation parameters Hydrometeor velocities	Under development Purdue Univ.	Has demonstrated excellent range and velocity resolution on coherent targets
Coded Radars	10 cm	Boundary layer C_n^2 and velocity of turbulent structure Velocity of hydrometeors Precipitation parameters	Conceptual	Range to about 2.5 km Range resolution of 10 m

Type of radar	λ	Parameters Measured	Present Status	Remarks
Coded radars (continued)	8.6mm	Liquid H_2O of clouds and fogs Velocity of hydrometeors Precipitation parameters	Conceptual	
	3 mm	Wind by velocity of aerosol sprays	Conceptual	

Section 4 APPLICATIONS OF LIDAR REMOTE SENSING TO DATA BUOYS

V. E. Derr and R. B. Slusher

Section 4 APPLICATIONS OF LIDAR REMOTE SENSING TO DATA BUOYS

V. E. Derr and R. B. Slusher

4.0 Introduction

The characteristics of lasers have made possible many new methods of remote measurements of environmental parameters. Coherence of the radiation from lasers allows velocity measurement by Doppler shifts. The large spectral and spatial brightness of the laser permits the use of backscatter of laser beams from even the tenuous atmosphere, and the wide range of frequencies available allows spectroscopic interaction with individual molecules. Such interaction permits remote positive identification and concentration measurements of atmospheric and oceanic constituents to an accuracy generally not possible with other methods.

Laser systems operate in many temporal modes: pulsed, continuous, modulated in time or frequency. Thus they may be used for distance measurement and determination of constituent concentrations as functions of range, similarly to the way the more familiar forms of microwave radar are used.

Thus, in the atmosphere, measurements of temperature, humidity, wind velocity, aerosol and hydrometeor content, cloud heights, CO_2 concentration and other quantities may be made as functions of position in a hemisphere whose radius is equal to the maximum effective range of the lidar system. The same lidar system, aimed at the water, can measure temperature of the surface and the first few tens of meters into the water. Laboratory studies and a few field studies have shown the feasibility or potentiality of measuring chlorophyll content, dissolved oxygen, fish oil traces, oil spillages, red tide and other ocean constituents.

Laser technology progresses rapidly and further potentialities open frequently in laser remote sensing. However, it is doubtful that the principal limitation of laser radiation, its strong attenuation by liquid

water, either in the form of fog or clouds or ocean waters, will be overcome. For the near future, certainly, laser remote sensing is severely range limited in fog and limited to a few tens of meters penetration of the ocean. However, many characteristics of importance occur in the upper ocean.

The applicability of laser techniques to data buoy missions is clear because of their ability to measure profiles of atmospheric parameters such as temperature, humidity, winds, cloud heights and water-ice ratios, visibility, and ocean constituents and temperature to several tens of meters. Exact precision, sensitivity and maximum range determination are only possible after laboratory and field research is complete. Until that time the competitiveness of these techniques with other candidates is not determinable. In the next subsections laser methods will be reviewed; in the final subsection research is recommended to lead to a final determination of the usefulness of lasers in this application, prior to engineering specifications.

Detailed discussion of the methods described herein may be found in Chapters 23, 24, of Derr (1972) and Derr and Little (1970) and the references contained therein.

4.1 Measurement of Atmospheric Parameters

The measurement of concentrations of H_2O, temperature and aerosols, by lidar systems has been well established (Strauch et.al., 1971 and 1972; Derr, 1972), and the system formulae have been frequently verified in field tests. Therefore, the extrapolation to problems of data buoy use can be made with confidence. No field tests have been made on CO_2 detection by this means, but extension of the system analysis to this constituent is justified by careful laboratory measurements of its cross section for Raman scattering. (For a discussion of Raman Scattering see 4.1.4.2.) The problems discussed in this subsection are the measurements of wind velocity and of the concentrations of aerosols, H_2O, CO_2 and temperature by buoy based lidar systems.

4.1.1 Wind Velocity by Eddy Correlation

In the real atmosphere, the variation of temperature, humidity, and composition observed by use of a point sensor shows inhomogeneity of these passive tracers that are carried along by the prevailing wind. To the degree that the structure of the eddies persists, they can be observed at two points separated by a known distance. Even in strong mixing conditions, the eddy structure remains recognizable for useful distances. Thus, by some kind of pattern recognition process, such as cross correlation, we can compare the signals at two points in the wind stream, determining velocity from the passage time of eddies.

Active and passive correlation methods have been effective in wind tunnels, passive methods have been used in the field, and active methods with searchlights, have been studied by Newstein. Active wind sensing methods using lasers are under investigation by Derr at NOAA. There are many possible geometrical configurations of the crossed beam technique. Figure 4.1 shows a simple scheme used to test the method. It is, however, too cumbersome to use in practice, since the wind direction changes constantly. An alternative method is to use a coaxial transmitter and receiver (or closely coupled parallel axes) as in Fig. 4.2. The beam is conically scanned with sufficient frequency so that no turbulence crosses the cone

Fig. 4.1 Crossed Beam Wind Sensing Test Configuration

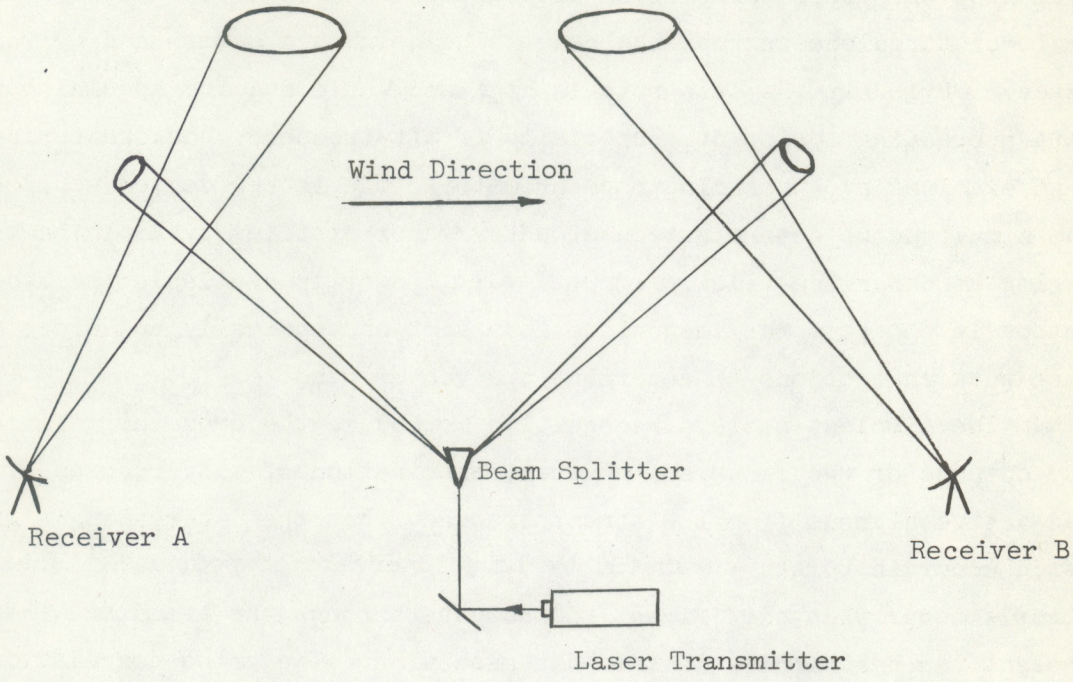

Fig. 4.2 Conically Scanned Wind Sensing Configuration

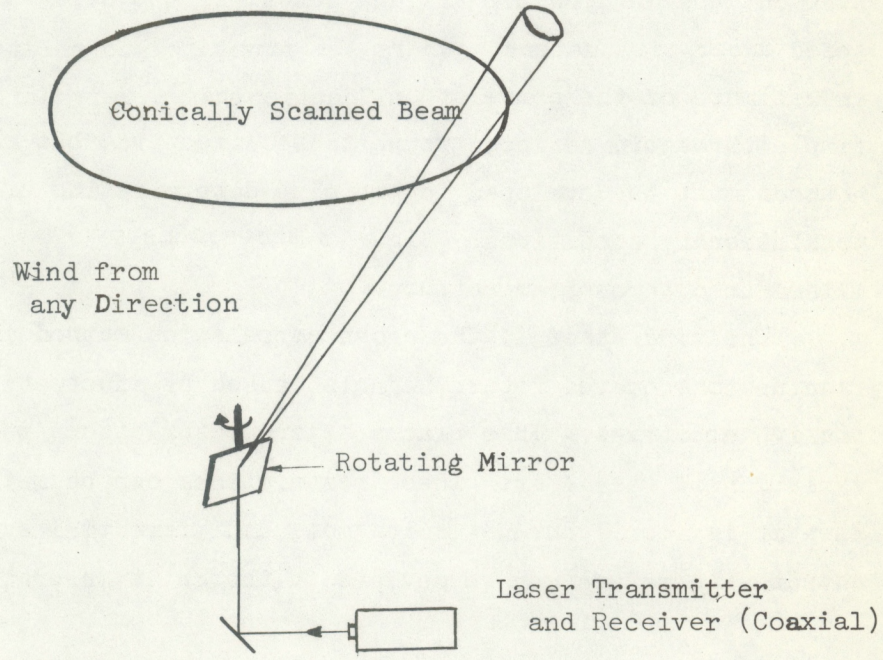

unilluminated and with sufficiently high pulse repetition frequency so that the turbulent spectrum is properly sampled. The cone is divided into elements, and cross correlation between elements is used to detect the drift of turbulence across the cone. The height is determined by range gates. Obviously the data rate is high and would require special purpose data processing equipment, especially if off-frequency backscattering is also examined by a scanning monochromator. The latter device would allow the simultaneous determination of water vapor profiles by Raman backscattering as described below. If sufficient power is available the best method is to split the image into four sections optically and cross correlate between sections to determine the vector wind.

The simplest pattern recognition method is the cross correlation of the outputs of two sensors. However, examination of many records of passive and active signals from the atmosphere show that the interesting signals often occur in bursts separated by long intervals of poor SNR. These signals occur when significant eddies pass through the beams and they represent the best indications of the mean wind. The cross correlation function is diluted by the intervening high noise record and the accuracy of its indication of wind speed is diminished. As a result an observer of the dual trace output of correlation crossed beam receivers can frequently, by eye, pick out the delayed signals and determine the delay and, hence, the wind speed under circumstances where the truncated correlation function used as an estimate of the correlation function has a very large uncertainty. A simple threshold has been found to be effective, but more sophisticated methods must be developed to optimize determination of wind speed under nonstationary conditions. Fig. 4.3 shows some typical records of active, laser illuminated, crossbeam outputs.

The wind speed in the cross correlation method is determined by small fluctuations on the return signals caused by fluctuations in the atmospheric passive additives. This places severe restrictions on the tolerable power variation of the laser. These restrictions can be met by existing lasers. When it is nearly but not quite met, a differential system of comparison of output with return can be devised, although it is preferable to avoid this

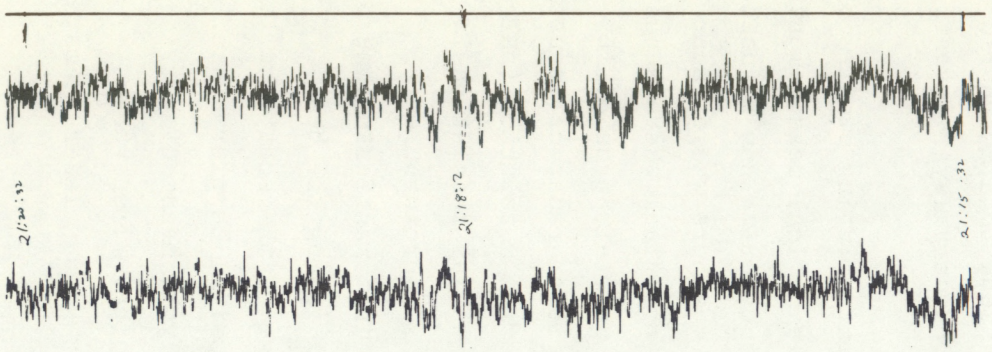

DATA

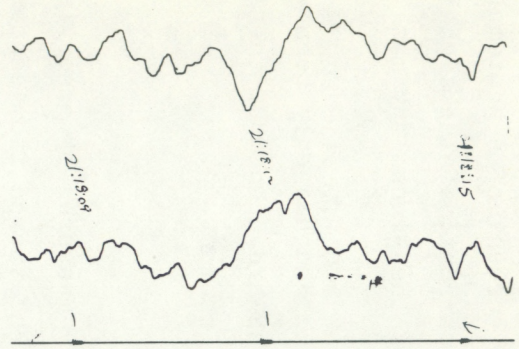

Expanded Data Section

(Voltages reversed)

Average anemometer speed = 10.9 mph

.64 sec delay ⇒ ≈ 12 mph

CW Argon laser

10-foot delay

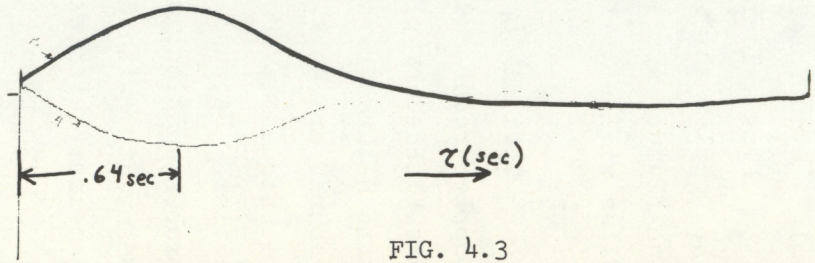

Cross correlation

21:18:12 ± 3.2 sec of data

8 March 1970

FIG. 4.3
Wind Velocity Measurement by Eddy Cross Correlation

complexity. As has been pointed out above, an ultimate limitation on the range at which wind can be measured by correlation techniques arises from the unavoidable random fluctuations on the signal current of a photomultiplier. Even in the absence of background noise and dark current, if the signal is small (photon counting), the Poisson shot noise of the signal may mask the fluctuations of the atmosphere.

At present the use of the eddy correlation method has only been verified to tower heights (150 ft.) and further studies are needed of the signal-to-noise ratios achievable in an ocean environment.

4.1.2 Wind Velocity by Doppler Methods

Flow velocities in some fluids are routinely measured by observing the Doppler shift in the frequency of laser light scattered from centers in the fluid. Applications of the optical Doppler technique to atmospheric flows will significantly enhance WPL capability in boundary layer investigations.

Optical Doppler velocity measurements complement existing studies of Doppler radar and acoustic Doppler techniques. While optical measurements are blocked by clouds or dense hydrometeors, laser scattering can be used with natural aerosol markers in a nominally clear atmosphere where radar returns are weak. Optical Doppler measurements are practical where acoustic techniques may be limited by ambient noise, such as near airports or in cities. Because of a much shorter wavelength than either radar or acoustic probes, optical scattering allows extremely high spatial resolution (narrow beamwidth) with practical transmitter sizes. Such spatial resolution is necessary, for example, in studies of water spouts or microturbulence.

Two theoretically similar but practically distinct manifestations of optical Doppler principles are useful. Longitudinal (along the beam) velocities cause a spectral shift or frequency change of the scattered laser light from the incident photon frequency in the classical Doppler sense. This Doppler frequency shift may be detected directly by means of very high resolution spectroscopy or by optical heterodyning. Transverse velocity components are measured utilizing two intersecting laser beams,

which generate an interference fringe pattern with fringes parallel to the beam bisector. Individual scattering centers or fluctuations in the density of scatterers will yield an intensity modulated scattering signal as the scatterers pass through the interference pattern. The frequency of the modulated signal is proportional to the particle (and hence flow) velocity component perpendicular to the fringes. With the addition of a third beam, two orthogonal sets of fringes are formed, allowing both transverse wind components to be measured.

In principle, a combination of the frequency shift and intensity modulation forms of optical Doppler allows simultaneous measurement of three orthogonal wind components from a single backscatter lidar system. This is an attractive prospect for boundary layer studies. Pulsed signal ranging has not yet proven useful for Doppler lidar. We suggest study of an AM-FM-CW technique where a CW laser carrier is amplitude modulated (AM) with a swept modulation frequency (FM). Range information is then obtained as in the case of **FM/CW radar.**

4.1.3 Clouds and Hydrometeor Measurements

Cloud parameters such a height and velocity may be measured with the same lidar system as that needed for wind velocity measurements. The Raman scattering of liquid water is substantially different from water vapor and may be used to measure the temperature of the clouds, since the response is quite temperature sensitive. This method has been tested in the laboratory, but has not received a field test. Preliminary tests of ice Raman scattering have indicated that there may be substantial differences in its spectrum. If further tests verify the phenomenon, the ice-water ratio of the bottom layer clouds may be determinable by lidar methods.

Cloud height laser altimeters are now a standard mode of operation. Further laboratory and field research is needed to determine the feasibility of the other methods discussed.

4.1.4 Other Atmospheric Measurements

In this section the concepts of measurement of aerosols, water vapor

and temperature as functions of altitude by lidar are presented. Section 4.1.4.4 contains a discussion of maximum ranges attainable by specific lidar systems. CO_2 detection is discussed in 4.1.4.5.

4.1.4.1 Aerosols

Determination of the presence of aerosols was the earliest use of lidar in the atmosphere. Any attempted quantitative measurement of the absolute air density by on-frequency laser radar backscattering is strongly affected by the presence of aerosols in the lower troposphere. At visible wavelengths, in the lower troposphere, the contribution to atmospheric scattering by aerosols is usually greater than that due to molecular scattering. Hence, air density measurement requires knowledge of the ratio of molecular and aerosol scattering to molecular scattering. Moreover, when laser radar measurements are being used for the exploration of the aerosol content in the air, this ratio must be known to deduce the molecular scattering from a measurement of the total scattering. This ratio, known as the "turbidity" is, therefore, one of the very first properties of the atmosphere that must be determined to evaluate quantitatively any laser echo.

The principal limitations lie in the interpretation of the lidar return signals since they do not give a unique solution of the lidar equation for the backscattering coefficient and the attenuation coefficient when they arise from an unknown distribution of sizes and shapes.

Two additional pieces of information have been investigated to aid in distinguishing between molecular and aerosol scattering, viz., the specifically molecular information inherent in Raman scattering and the doppler spectrum of the on-frequency backscattering. The latter method depends on the difference in the doppler spectrum of air molecules and the much heavier and, on the average, slower, aerosol particles.

An important new development in remote laser measurements of aerosols is the tunable laser such as the dye laser. With these tunable sources, independent information on scattering intensity as a function of wavelength increases greatly the amount of information available for solution of the equations for the distribution of sizes of aerosols.

With these developments, the knowledge of the presence and opacity of atmospheric aerosol layers can be supplemented by further details of the nature of the aerosols, reducing the number and stringency of assumptions needed in an atmospheric model used to interpret the data. Details of this discussion may be found in Derr (1972, Chapter 23).

The laser has early demonstrated its capacity for sensing aerosols. Now developments of theory and technology move toward a solution of the problem of measuring size distributions. We recommend that these studies be advanced in the area of marine aerosols.

4.1.4.2 Water Vapor

Two kinds of spectroscopic scattering may be used to identify individual molecular species, fluorescent scattering and Raman scattering.

Fluorescent scattering can occur only when the frequency of the incident radiation is in an absorption line or band in the sample material. Transition to a state of higher energy may then occur, followed by relaxation and emission of light at frequencies equal to or less than the incident frequency. This is called Stokes fluorescence; anti-Stokes fluorescense, in which the light of higher frequency is emitted, is weaker by a factor of 10^{-3}. The emitted (and absorbed) radiation frequencies are dependent on the detailed structure of the molecular energy level diagram and hence are characteristics of the molecule. Since the absorbed light is required to be at a frequency fixed by the molecular characteristics, the source of illumination must, barring lucky accidents, be tunable. The emitted radiation can then be used to identify uniquely the molecule responsible for the scattering. Fluorescence has characteristic re-emission times of the order of 10^{-8} sec to 10^{-1} sec. The mean time between air molecule collisions in the troposphere is usually so short ($\approx 10^{-9}$ sec) that the fluorescent emission is quenched or perturbed, and it is rarely observed at atmospheric pressure. Fifteen kilometers altitude is, with few exceptions, a lower limit on the observation of fluorescence. Two exceptions are NO_2 and SO_2, which have been observed at atmospheric pressure in mixtures with N_2 and with air. The cross sections for

fluorescent interactions can be much larger than Rayleigh cross sections- as large as 10^{-16} cm^2/sr.

Raman scattering, although the weakest of the phenomena considered here, is useful because it is a means of identifying scattering molecules, and because it occurs regardless of the irradiating frequency. The radiation frequency need not be matched with molecular resonances to allow transitions of the molecule; thus it can be used with fixed frequency laser sources. If the incident radiation is of frequency ν, Raman lines occur at a series of frequencies $\nu \pm \nu_1$, $\nu \pm \nu_2 \cdots$; the lower frequencies are called Stokes lines, the higher anti-Stokes lines. The latter are not considered here because they are weaker under tropospheric conditions. The frequency displacement is related to the rotation-vibration spectrum of a molecule, but selection rules differ from those operating in infrared spectra.

Although fluorescence will be found useful in identifying biological materials, it does not occur usually in the troposphere and consequently scatter systems must depend on Raman spectra. By its Raman scattering we can obtain profiles of H_2O in the atmosphere using lidar systems.

4.1.4.3 Temperature

The principal contribution to atmospheric pressure is from the oxygen and nitrogen content. Water vapor accounts for less then 1% of the mass in a column through the atmosphere. In a static atmosphere the pressure at ground level is due to the total mass of gas, and the minor departures from this in nonstatic situations can usually be ignored. The perfect gas law, $p = \rho RT/M$, where p is the pressure, ρ is the density, R is the universal gas constant, M is the molecular weight, and T is the absolute temperature, is locally applicable, but if ρ and p are known as functions of height then T is also known as a function of height h. But p(h) can be obtained from the hydrostatic equation

$$p(h) = p_o - \int_o^h g\rho(z)dz,$$

if $\rho(z)$ can be obtained from the Raman lidar data. Thus we can calculate the temperature profile.

$$T(h) = \left[p_o - g\int_o^h \rho(z)dz\right] \Big/ (\rho(h)R/M),$$

where g is the acceleration due to gravity. The pressure at ground level p_o can be obtained from a local barometer reading.

Since the errors of range measurement can be made small, the important source of error in determining the temperature arises from the errors in $\rho(z)$. Random and systematic errors in $\rho(z)$ will contribute in different ways to temperature errors. Random errors, assumed of zero mean, are serious when the term $\rho(h)$ in the denominator is small. Systematic errors will contribute to the integral of the density more than to the density term in the denominator. As a measure of the error in the calculated temperature, we can calculate the variance of the temperature, σ_T^2. The variance of

$$I = \int_o^h \rho(z)dz$$

can be shown to be much less than the variance of $\rho(z)$ under time-bandwidth conditions normally true for lidar systems, and hence can be ignored. Under this condition it is easily shown that

$$\sigma_T^2 / \langle T \rangle^2 = \sigma_\rho^2 / \langle \rho \rangle^2,$$

where σ_ρ^2 is the variance of ρ and the brackets indicate ensemble averages. Each of the quantities in this equation is a function of time (or range). We may most easily obtain some numerical results by assuming an exponential falloff for the density, i.e., $\rho(z) = \rho_o e^{-\lambda z}$. If we choose $p_g = 1.013 \times 10^6$ dyn cm^{-2}, $\rho_o = 1.77 \times 10^{-3}$ g cm^{-3}, then for z = 1 km, T = 295.6 K. Simulating an inaccuracy in ρ, if we replace $\rho(z)$ by $\rho(z) + 10^{-2} \times \rho(z)$, T changes to 268.2 K. Only if the measurement of ρ is accurate to better than a few percent is this method of temperature measurement very useful in tropospheric probing.

The proportion of N_2 to O_2 in the troposphere is nearly constant. Hence a measure of the amount of N_2 as a function of altitude serves to determine the temperature profile.

4.1.4.4 Maximum Ranges of Specific Lidar Systems

The maximum range of a lidar system for water vapor Raman scattering, nitrogen Raman scattering, or aerosol scattering with ruby, doubled neodymium, doubled ruby, nitrogen, or quadrupled neodymium laser systems was computed.

The lidar system consists of a pulsed laser system and a receiver system. It is most convenient to consider the characteristics of the laser and receiver separately since we will be considering more than one laser system for the same receiver system.

Each laser system considered is one which is commercially available and in all cases is the best "state of the art" device obtainable at this time to the best of our knowledge. In this context best "state of the art" is actually a compromise between maximum energy per laser pulse and maximum pulse repetition frequency (PRF). As can be seen in Table 4.1, three ruby systems are considered, starting with the largest energy per pulse. With smaller energy per pulse the PRF can be increased. For those systems which use frequency doublers we have assumed a 10 per cent conversion efficiency of the input laser pulse which is incident on the doubler. Table 4.1 shows the assumed power in and out of the doubler crystal.

Table 4.2 gives the features of the receiver system. It should be noted that the wavelength of the laser must be considered in choosing the proper system parameters from Table 4.2. The instrument transmission is the product of the mirror reflectivity and the filter transmission. The background radiation for day time (Clark, 1969) is assumed to be that for a bright clear day, and for night time a reasonable assumption is 10^{-7} times the daytime irradiance. All data for atmospheric attenuation was obtained from Elterman (1968). In all cases the integration time used is 10 seconds. Therefore, the systems will not (in these calculations) be able to see events on a time-scale less than 10 seconds.

Table 4.1

LASER SYSTEMS CONSIDERED

System	Energy/Pulse (Joules)	PRF (pulses per second)	Output λ (Å)
Ruby	100	.0033 - 1p/5 min.	6943
"	10	1	"
"	1	10	"
Nitrogen	.001	500	3371
Doubled Ruby	.1(1 into doubler)	10	3472
Doubled Neodymium	1(10 into doubler)	1	5300
Quadrupled Neodymium	.1(10 into first doubler 1 into second doubler)	1	2650

A vertical profile with the sea level receiver system was calculated for each laser system. The range increment used was 500 m and the maximum range for aerosol scatter, water vapor Raman scatter was plotted as a function of the signal-to-noise ratio for each system (Appendix 4.I). Note that the maximum range was given to within ±250m. This uncertainty is due to the chosen range increment and does not include variations due to uncertainties in other variables such as background and atmospheric attenuation, etc. For those calculations which use a 50m range increment the uncertainty was ±25m. An intercomparison of each of the systems was made and from this the systems were chosen which gave the maximum range for different constituents and for three signal-to-noise ratios. The results of this analysis are shown in Table 4.3.

Table 4.2

RECEIVER SYSTEM PARAMETERS

Laser Type	Ruby	Doubled Neodymium	Doubled Ruby	Nitrogen	Quadrupled Neodymium
Wavelength	6943	5300	3472	3371	2650
Det. Quant. Eff.	.04	.17	.25	.25	.25
Det. Quant. Eff. @ H_2O Raman Wavelength	.017	.05	.25	.25	.25
Det. Quant. Eff. @ N_2 Raman Wavelength	.03	.08	.25	.25	.25
Det. Current Gain	10^7	10^7	10^7	10^7	10^7
Det. Dark Current (amp.)	7.5×10^{-9}	7.5×10^{-9}	7.5×10^{-9}	7.5×10^{-9}	7.5×10^{-9}
Filter Bandwidth (Å)	10	10	10	30	80
Filter Transmission (%)	70	70	35	30	25
Mirror Reflectivity (%)	90	90	80	80	80
Instrument Transmission (%)	63	63	28	24	20
Background Radiation (Watts-M^{-2}-$Ster^{-1}$-$Å^{-1}$)	.01	.0125	.005	.005	0
Integration Time (sec)	10	10	10	10	10

Ground-based Lidar Telescope: Telescope Diam. 3.05m (assumed 4-60" diam. mirrors with 7m focal length)
Telescope Beamwidth 2.85 milliradians (T.B. = limiting aperature/focal length = 2cm/700cm)

Table 4.3

MAXIMUM RANGE FOR VARIOUS TRANSMITTERS, SIGNAL TO NOISE RATIOS, GROUND BASED SYSTEM

H_2O Vapor-Raman		N_2-Raman		Aerosols	
Day	Night	Day	Night	Day	Night
Quadrupled Neodymium R = 1.2 km E/pulse=.1j @ 1pps	Doubled Ruby R = 2.2 km E/pulse=.1j @ 10pps	Quadrupled Neodymium E/pulse=.1j @ 1pps or Ruby 10j/pulse @ 1pps R = 2.2 km	Ruby 1j @ 10pps or 10j @ 1pps R = 9.2 km	Ruby 10j @ 1pps R = 7.7 km	Ruby 1j @ 10pps or 10j @ 1pps R >20 km
" R = 1.7 km	" R = 3.2 km	" R = 3.2 km	All systems considered excluding Ruby 100j@1p/5min N_2.001j@500pps and Quadrupled Neodymium had R >20 km	" R = 8.2 km	" R >20 km
" R = 3.7 km	" R = 5.7 km	" R = 5.7 km	All systems considered excluding Quadrupled Neodymium had R >20 km	" R = 9.7 km	" R >20 km

The following is an example of a particular lidar system's ability to determine absolute temperature versus maximum range for various signal-to-noise ratios. By use of the hydrostatic equation and the pure gas law, the temperature profile may be obtained from the nitrogen density profile. For both day and night conditions we assume the system is looking vertically from sea level into a model atmosphere. On the right side of Figure 4.4 the average temperature is given versus altitude. To the right of this are the uncertainties which arise when using the nitrogen Raman return at night and during the day to measure temperature. These are calculated in the following way. Consider, as an example, the night time case for S/N = 100. Since we have specified the signal-to-noise ratio as 100 the maximum range obtainable is 5.5 km at which the approximate daytime temperature is 256K. With this signal-to-noise ratio we will have a 1% uncertainty in our measurement which corresponds to 2.6K.

4.1.4.5 CO_2 Measurement

Since atmospheric CO_2 is approximately 330 parts per million of the atmosphere, it is more difficult to detect by its Raman scattering than the other constituents discussed. However, since CO_2 is well mixed in the atmosphere and its variation small, local measurements from a data-buoy-based lidar would be sufficient to obtain the information needed.

The maximum range of a lidar system for measuring CO_2 has been calculated, using the appropriate Raman cross section.

The laser systems and receiver systems considered were identical to those used for N_2, H_2O vapor and aerosols except for the following differences:

a. 50m increment was used to get better spatial resolution since range is small
b. Quantum efficiency of detector at CO_2 Raman wavelength is different
c. Background radiation differs.

For all three cases considered the maximum ranges were much less than those obtained for H_2O vapor, N_2 and aerosol. Table 4.4 shows the system (doubled ruby) which gives the maximum range for each lidar configuration.

Fig. 4.4 Temperature Measurements Using N_2 Raman Scattering

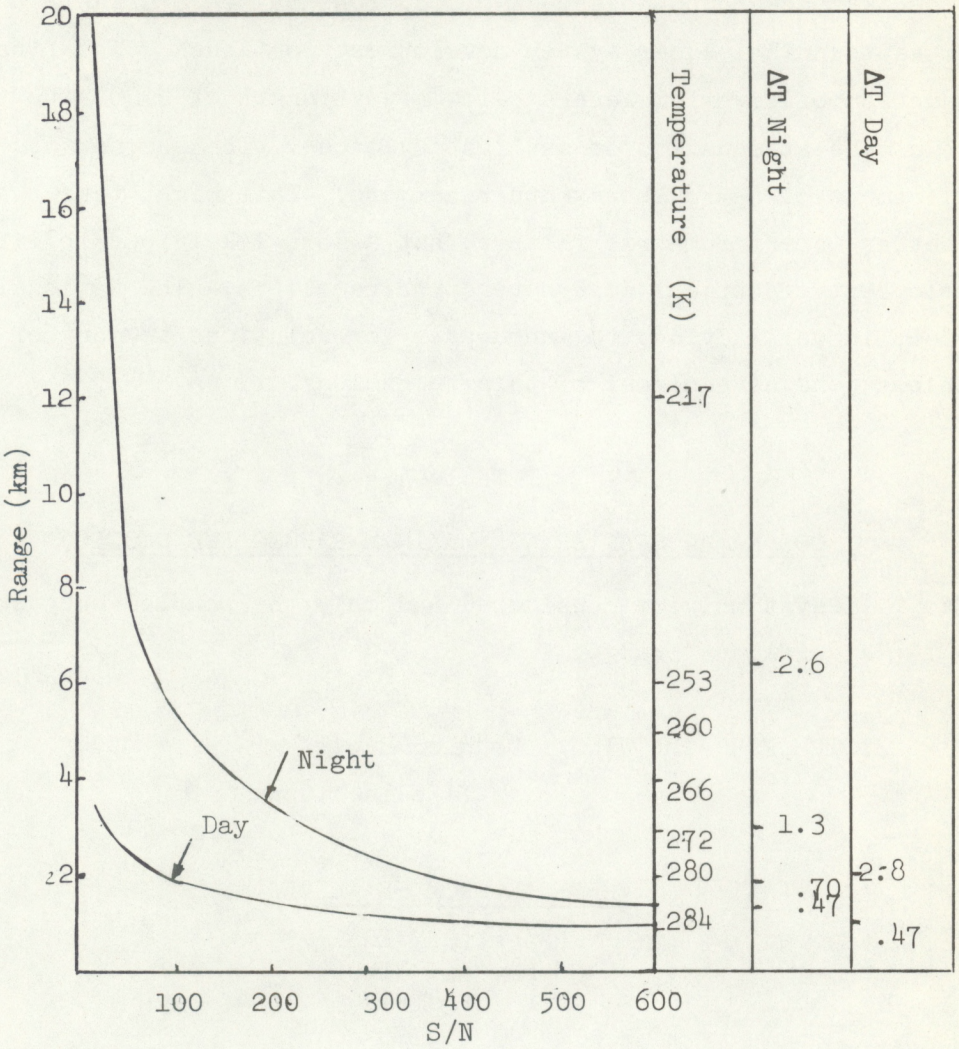

SYSTEM PARAMETERS

SYSTEM TYPE RUBY

Energy per pulse (Joules) 10
Telescope Diameter (Meter.) 3.05
Telescope Beamwidth FWHM (Milliradians) 2.85
Filter Bandwidth (Angstroms) 10
Integration Time (Sec) 10
Range Increment---Min Length (Meters)
Rep Rate (PPS) 1
Instrument Transmission .63

Consideration of the results just presented shows that a principal limitation on the employment of lidar systems in atmospheric measurements is the sky background noise. Two solutions may be **available** to this problem as technical laser system development continues. The first is the production of powerful lasers below a wavelength of 2900 Å to take advantage of the attenuation of sunlight by ozone. The second solution is the development of narrow bandwidth receivers. This might take the form of better interferometric filters, but a more likely possibility is the development of optical superheterodyne receivers. The National Buoy Project is well advised to encourage, for solutions to many of its problems, the advancement of this technology.

Table 4.4

CO_2 RAMAN SCATTERING (MAXIMUM RANGES AND SYSTEM)

NOTE: All systems were considered and only the Doubled Ruby showed a "significant" range.

SYSTEM FOR FOLLOWING: Doubled Ruby
.1J/pulse 10pps

VERTICAL FROM SEA LEVEL

Range (S/N=10)
Day and Night
1.8km

Range (S/N=100)
Day and Night
0.27km

4.2 Measurement of Ocean Parameters

Although some applications of lidar to the sensing of atmospheric parameters have been demonstrated, the potential application to ocean constituents and parameters has been explored generally only in the laboratory. One notable exception is the use of fluorescense scattering in the determination of chlorophyll content. However, laboratory studies have indicated that temperature profiles to depths of a few tens of meters may be obtained by lidar systems. Further, materials such as fish oil, certain bacteria (application to the red tide), spilled petroleum, certain dissolved salts and plant constituents exhibit large Raman scattering signals and may be detected by some of the same temporarily downward directed laser systems described in the preceding sections.

In the following sections the maximum range down into the ocean is computed for chlorophyll detection, temperature profiles and dissolved oxygen content. In the ensuing LIDAR computations a configuration was assumed in which the transmitter (laser) and receiver (mirror) are at sea level looking down through a smooth air-sea interface (Table 4.5). Four laser transmitters were considered and only one receiver system.

Much of the data which was used in these calculations was obtained by extrapolation and the following assumptions. The content of dissolved O_2 in sea water ranges from 10.31 ml/l @ $0^{\circ}C$ to 5.6 ml/l @ $30^{\circ}C$. The value assumed is 6 ml/l. From this the effective Raman cross section is determined assuming that the cross section for dissolved O_2 is the same as for O_2 in the gas phase. Since no data is presently available for the Raman scattering cross section for liquid H_2O it has been assumed that it is approximately equal to the cross section for H_2O vapor. Due to the lack of absolute data on chlorophyll Raman cross sections we have assumed the value to be 10^3 times that of acetone. Comparisons between acetone and chlorophyll Raman cross sections have in this laboratory shown that resonance effects in chlorophyll produce at least this increase. We have assumed the Raman cross sections of acetone and benzene are comparable. The cross section of benzene has been measured.

4.2.1 Chlorophyll

Using the four lidar systems described in Table 4.5 the maximum range

Table 4.5

LASER SYSTEMS CONSIDERED

System	Energy/Pulse (Joules)	PRF (pulses per second)	Output λ (Å)
Ruby #1	100	.0033-1p/5min	6943
Ruby #2	10	1	"
Ruby #3	1	10	"
Doubled Neodymium	1(10 into doubler)	1	5300

SYSTEM PARAMETERS

Laser Type	Ruby	Doubled Neodymium
Wavelength (Å)	6943	5300
Det. Quant. Eff.	.017	.05
@ H_2O Raman Wavelength	.017	.05
Det. Quant. Eff.	.034	.11
@ O_2 Raman Wavelength	.034	.11
Det. Quant. Eff. @ Chlorophyll Raman Wavelength	.035	.1
Det. Current Gain	10^7	10^7
Det. Dark Current (amp.)	7.5×10^{-9}	7.5×10^{-9}
Filter Bandwidth (Å)	10	10
Filter Transmission (%)	70	70
Mirror Reflectivity (%)	90	90
Instrument Transmission (%)	63	63
Background Radiation (Watts-m^{-2}-$Ster^{-1}$-$Å^{-1}$)	.0001	.00012
Integration Time (sec)	10	10

Telescope Diameter .76m (30" diam. mirror with 2m focal length)
Beamwidth 2.85 milliradians

of detection of chlorophyll below the ocean surface has been plotted in Figure 4.4 and Figure 4.5. Two concentrations, .1mg/m^3, a low (clear water) value, and 15 mg/m^3, a relatively high (green water) value.

The ruby systems are not as useful in this application as the frequency doubled neodymium system, which offers greater depth penetration. If we require a S/N of 100, we see that a depth of 22 meters is possible in daylight (15 mg/m^3). The curves show what is intuitively clear, the dominating factor is ocean water attenuation. We see that at night the percentage improvement is not large, i.e. the effect of background noise is not as pronounced as in the case of atmospheric lidar probing. Also the effect of changing the concentration to lower values does not strongly effect the maximum range; a daylight range of 10 meters is available for detection at the .1 mg/m^3 chlorophyll concentration.

The lidar systems considered here are not optimized for ocean measurements. Further laboratory studies are needed to determine maximum resonant cross sections available. Optimizing the choice of frequency for maximum penetration is also important. When these two requirements do not lead to the same choice of frequency an optimum compromise must be made.

4.2.2 Temperature Profile

The temperature of water can be determined from the shape of its Raman scattering intensity plotted versus frequency. Thus a measure of the ability to measure temperature of ocean water as a function of depth is again the maximum depth of sensing the Raman scattering as a function of S/N. If Figure 4.6 is shown the maximum range as a function of S/N. By this method we may measure with S/N = 100, to a maximum range of 21 m, a profile of temperature. (The range resolution was here chosen to be 2 m.)

Improvements to this method will be in the direction of using on-frequency scattering and line shapes of Rayleigh and Mie scattering from hydrosols.

4.2.3 Dissolved Oxygen

Oxygen dissolved is sea water is an important parameter for biologists. As shown in Figure 4.7 the doubled neodynium system allows determination

Fig. 4.4 Chlorophyll (.015g/m^3)

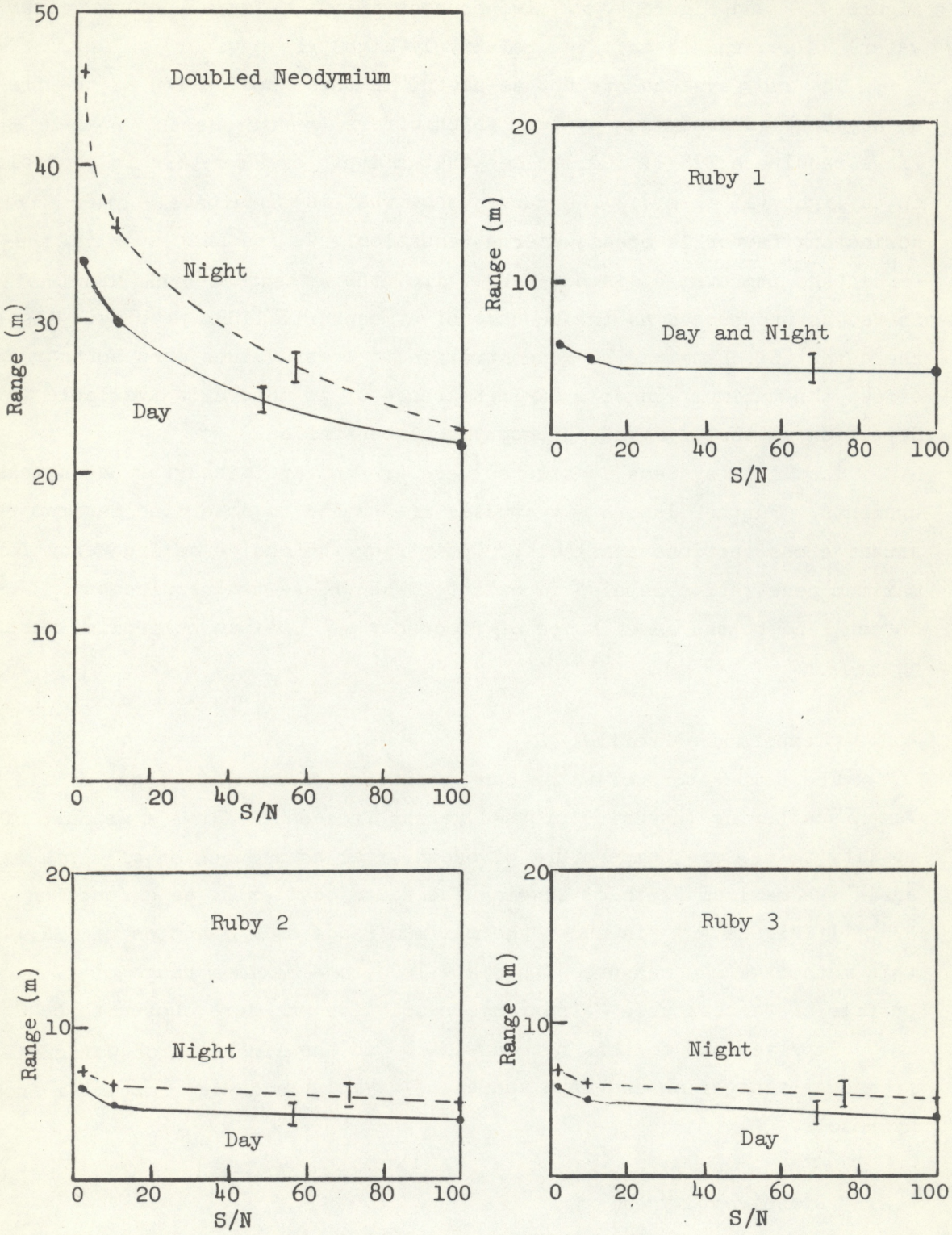

Fig. 4.5 Chlorophyll (.0001g/m^3)

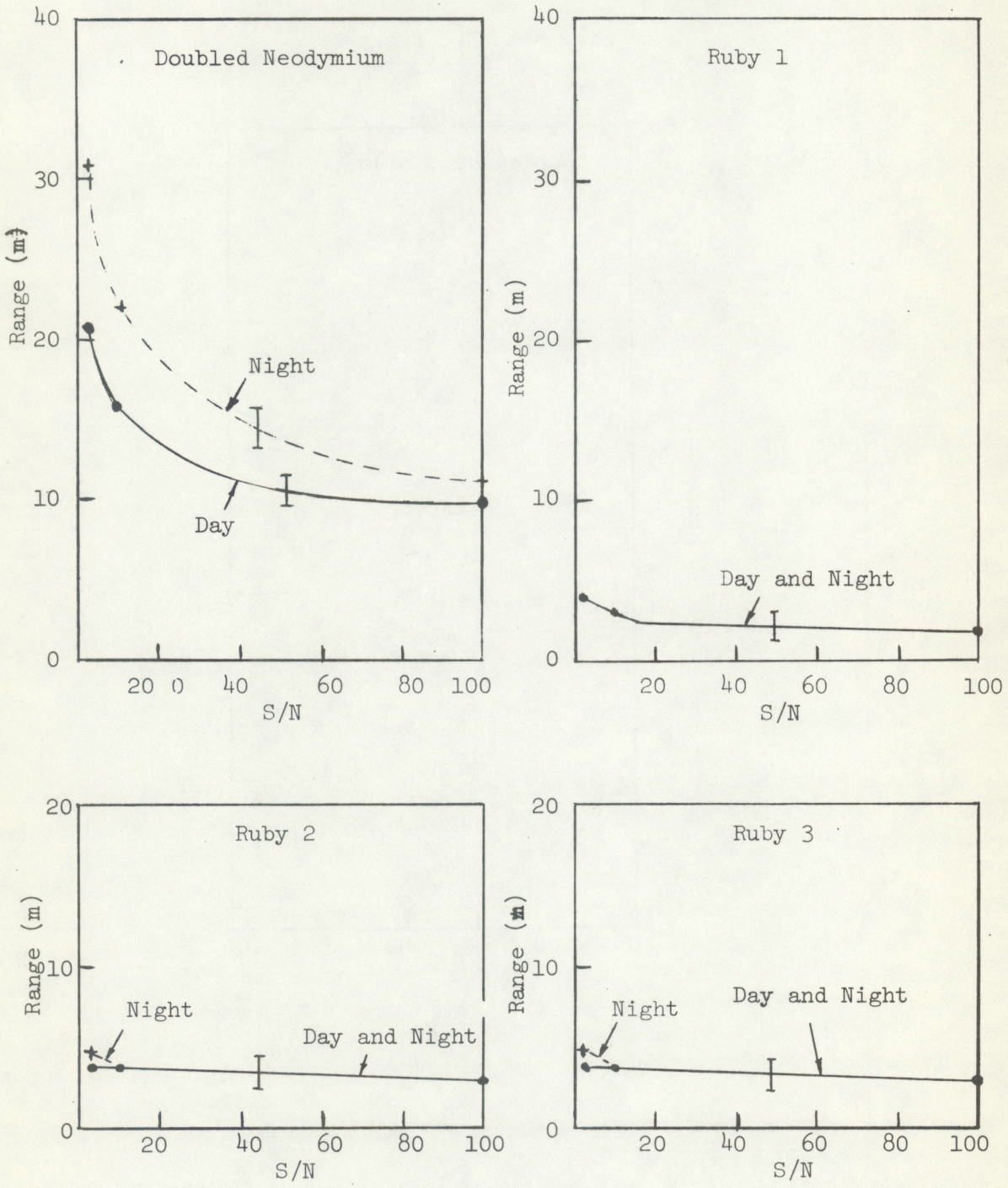

Fig. 4.6 H_2O Raman

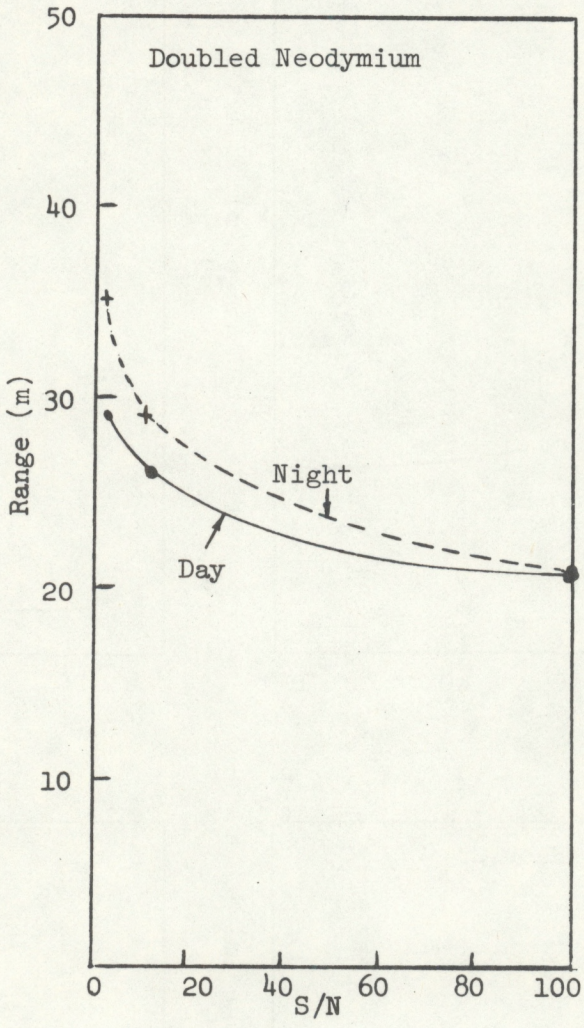

Fig. 4.7 O_2 Raman (6ml/l) In H_2O

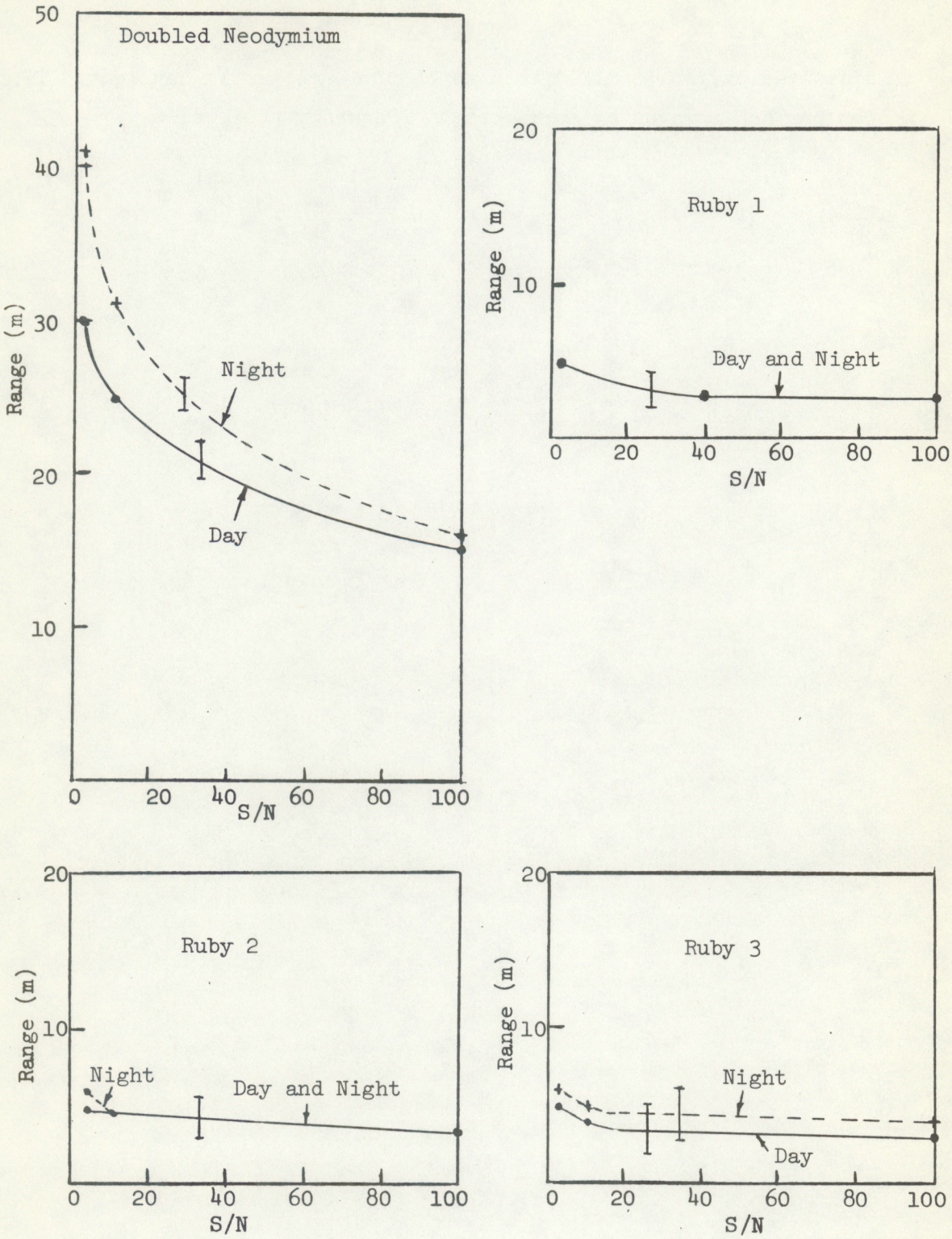

of dissolved oxygen (6 ml/l) to a depth of 18 meters in daylight. This system can be improved by more optimum frequency choices.

4.3 Safety and Environmental Problems

A question often raised about laser usage in untended areas concerns the possible dangers to human health. The only danger of any importance is that to the eye. If the eye is irradiated by the total output of lasers considered for these applications (say 10 Joules per pulse) severe damage or blindness could result. Thus the laser output window should be mounted (perhaps on top of a long tube) well above the height working personnel normally occupy and protected by a simple ring barrier.

Above the output window the beam is dispersed in angle so that above a few hundred meters the power density is below the maximum permissible exposure. A danger area exists from the output window to a height of, say, 400 meters. From that point up the eye would observe a very bright, short (10^{-6}s) flash, without danger. The flash could be seen by pilots of aircraft but even at night should not affect vision. The calculations for these estimates are based on radiation hazard standards revised by a committee of the American National Standards Institute.

These estimates assumed the use of visible lasers, the most dangerous kind. The move toward ultraviolet lasers is very likely and in that case the glass of an aircraft cockpit would greatly attenuate the laser beam.

If the low probability of danger to low flying aircraft pilots who fly over the buoy and look directly down into the beam at the moment a pulse is produced is still deemed too high, the lidar must be shut off when low flying aircraft approach. If a microwave radar is aboard, it can be programmed to shut off the lidar at the approach of aircraft. If not, a simple inexpensive low power lidar system can be devised to surround the main beam and turn off the transmitter at the approach of a low flying aircraft.

The difficult environment of the ocean requires careful engineering and sealing. These have been accomplished in many laser systems in the ocean environment and the techniques are well known. Even the problem of keeping the output window clean has effective although not very elegant solutions. A more difficult matter is the large receiving mirror. Here we must assume some degradation of reflectivity over several months period, but this can be minimized by windows and seals.

4.4 Recommendations

Because of the great versatility of laser systems it is strongly recommended that the National Data Buoy Project plan to employ laser systems as part of the facilities aboard data duoys. In order to accomplish this a program of laboratory and field testing is required. In some areas the Wave Propagation Laboratory will continue its researches, but no funds are available for ocean applications and NDBP is requested to support research and field trials in WPL.

The Atmospheric Spectroscopy Program Area requests a five year period of research on the application of laser ranging techniques to data buoy measurement problems, commencing November 1, 1972.

The first phase of the project would occupy three years and would be devoted to the evaluation in the laboratory and in the field of the feasibility, accuracy, sensitivity, range, and temporal and spatial resolution of each of the measurement techniques listed below. During this period, and especially at the end of it, a determination of the applicability of the techniques would be made. The first phase would include, no later than the third year, shipboard testing of breadboard equipment. The second phase of the project would be devoted to the engineering development, specification and procurement of appropriate equipment for trial buoy use. During this period the Wave Propagation Laboratory would be active in specification of optimum equipment. Of especially great importance would be the design of transmitter, receiver and data processing equipment in an integrated unit which would perform the largest possible variety of measurements compatible with data buoy needs.

The following techniques will be studied:

1. Aerosol identification, concentration and size distribution (other than hydrometeorology)
   - Estimated range > 10 km.
   - Multiwavelength, multipolarization measurements.

   Employment of new inversion techniques (such as Strand-Westwater and Backus-Gilbert mathematical inversion techniques).

- Determination of turbidity by combined on-frequency and Raman scattering from N_2, serving as a visibility measure.
- Identification of aerosol composition by inelastic scattering spectroscopy.

2. Measurement of gaseous concentration in the troposphere
   - Estimated range-up to 10 km.
   - Use Raman and fluorescent scattering.
   - Measure H_2O vapor, N_2, and O_2.
   - At short ranges measure CO_2 content.
   - Optimize laser pump frequency for each component (see 4 below)
3. Measurement of tropospheric temperature profiles
   - Estimated range-up to 10 km.
   - Use Raman scattering (N_2 density technique) and/or
   - Use Rayleigh line shape technique.
4. Laboratory investigation and field application of resonance Raman scattering
   - Enhancement of Raman cross sections by many orders of magnitude.
   - Requires increased use of tunable lasers.
   - Requires investigation of scattering cross sections for ultraviolet laser pumps.
5. Remote measurement of wind
   - Eddy correlation method for horizontal wind
   - Doppler method for longitudinal wind
   - Interference fringe scatter method for transverse wind.
6. Cloud parameter measurement
   - Temperature by Raman scattering
   - State (ice or water) by polarization or Raman scattering.
   - Thickness, quite limited in depth.
   - Height by Mie scattering.
   - Eddy correlation method for cloud velocity.

7. Ocean water characteristics

- Temperature profile (depth $\leq$ 50m) by variations in scattering spectra.
- Salinity and other solute measurement.
- Chlorophyll content by Raman scattering

It is anticipated that all the above measurements would be performed by the same transmitter and receiver, operating in various modes as commanded by a minicomputer.

Funding requirements and schedule are outlined below:

Task	FY 73	FY 74	FY 75	FY 76	FY 77
1	18	21			
FT-1		20	30	5	
2	10	10			
FT-2		25	20	5	5
3	15	15			
FT-3		25	20		
4	25	25	25	15	
FT-4					
5	10	20			
FT-5	5	35	15		
6	30	30	20		
FT-6		30	40	30	15
7	25	35	35	15	
FT-7		35	45	35	15

FT = Field trial Amounts in thousands of dollars

At the conclusion of field trials engineering specifications would be prepared. It is assumed in these budgets that shipbound trials and buoy tests would be aboard equipped and manned vessels supplied by NDBP or other NOAA elements. The budgets do include salary, travel and shipping costs for such field trials.

4.5 References

Clark, W. M. (1969), "High Altitude Daytime Sky Radiance", S.P.I.E. Jour. Vol. 7.

Derr, V. E., Little, C. G. (1970) Appl. Optics, 9, 1976.

Derr, V. E. (Editor) (1972), "Remote Sensing of the Troposphere", Supt. of Documents (0323-0011), Government Printing Office, Washington, D.C.

Elterman, L. (1968), "UV, Visible, and IR Attenuation for Altitudes to 50Km", AFCRL-68-0153 Env. Research Papers No. 285.

Krause, F. R., Derr, V. E., Abshire, N. L., Strauch, R. G. (1969), Proc. 6th Intl. Symp. Remote Sensing Environ. 1, 327, Ann Arbor.

Strauch, R. G., Derr, V. E., Cupp, R. (1971), "Atmospheric Temperature Measurement Using Raman Backscatter", Appl. Optics, 10, p. 2665.

Strauch, R. G., Derr, V. E., Cupp, R. (1972), "Atmospheric Water Vapor Measurement by Raman Lidar", Rem. Sens. of Env., 2, p. 101.

Appendix 4.I Calculation of Maximum Lidar Range

If the laser emits N_o photons per pulse, the number of photons at range R is

$$N_o e^{-\alpha R},$$

which is equal to $(N_o e^{-\alpha R}/\Omega_T R^2)$ photons per unit area. α is an atmospheric attenuation coefficient and Ω_T is the solid angle of the laser beam. The number of photons scattered from the beam back into a solid angle Ω_R by a single particle through a process represented by a differential cross section $\sigma(\Omega)$ is

$$\frac{N_o \sigma(\Omega) \Omega_R e^{-\alpha R}}{\Omega_T R^2}$$

The number of particles at a density $\rho(R)$ in the volume defined by the laser beam and a range increment ΔR is

$$\rho(R) \Delta R \Omega_T R^2,$$

so that the number of photons scattered back into a telescope of area A from the particles in the range increment R is

$$\frac{N_o \sigma(\Omega) \rho(R) \Delta R A e^{-2\alpha R}}{R^2}$$

The signal, S, is taken to be the number of photoelectrons generated by n laser pulses transmitted through an optical system of transmission β to a photocathode of quantum efficiency η. Thus

$$S = \frac{\beta \eta n H_o \sigma(\Omega) \rho(R) \Delta R A e^{-2R}}{R^2}$$

The detector photocathode current is composed primarily of three components:

1) Signal current, i_s (the information carrier).
2) Dark current, i_d (the current present with no light on the detector), and

3) Background current, i_b (the current generated by sunlight scattered from the earth's atmosphere into the detector).

The relative magnitude of these components, along with their spectral and temporal characteristics and the type of signal processing performed determine the signal-to-noise ratio at the output of the signal processor.

The DC component of background and dark current can be rejected or substracted from the total current, so that the receiver sensitivity is ultimately limited by the magnitude of the statistical fluctuations in the photocathode current. Assuming Poisson statistics, this limitation may be represented by an effective noise current at the photocathode which generates N electrons in time n_τ according to the equation

$$N = \sqrt{\frac{n\tau}{e}(i_s + i_d + i_b)},$$

e being the electron charge. The quantity $n\tau i_s/e$ is just the signal S. It is usually more convenient to represent i_d by

$$i_d = I_d/G,$$

where I_d is the anode dark current and G the detector current gain. The background photocathode current i_b can be obtained from the background radiant flux through the relation

$$i_b = \frac{\beta\eta B_\lambda A\Omega_R \Delta\lambda\, e}{hc}$$

where

B_λ = background radian flux (watts - cm^{-2} - $ster^{-1}$ - Å^{-1})

λ = wavelength (cm)

$\Delta\lambda$ = filter optical bandwidth (Å)

h = Planck's constant (6.63×10^{-34} joule-sec)

c = velocity of light (3×10^{10} cm/sec)

Substituting this into the equation for N produces an effective noise of

$$N = \sqrt{S + n\tau\left(\frac{\beta\eta B_\lambda A\Omega_R \lambda \Delta\lambda}{hc} + \frac{I_d}{eG}\right)} .$$

The following expressions relate some of the system parameters to more readily available quantities:

$N_o = \frac{J\lambda_o}{hc}$, where J is the energy per laser pulse

$n = (PRF) \times T$, where (PRF) is the pulse repetition rate and T is the observation time

$\tau = \frac{2\Delta R}{C}$, assuming the receiver is closed except when returns from the range increment ΔR arrive

$\Omega_R \cong \frac{\pi\phi^2}{4}$, where ϕ is the receiver telescope beamwidth (FWHM)

$A = \frac{\pi D^2}{4}$, where D is the diameter of the receiver telescope

Combining these quantities and substituting the values of the constants generates the following expression for the system signal-to-noise ratio

$$\frac{S}{N} = \frac{3.95 \times 10^{10} J\lambda_o \sigma(\Omega)\rho(R)\Delta R\beta\eta D^2 (PRF) T e^{-2\alpha R}}{R^2\sqrt{S + 0.667(PRF)T\Delta R\left(3.1\beta\eta B_\lambda D^2\phi^2\lambda\Delta\lambda + \frac{6.25 \times 10^{10} I_d}{G}\right)}}$$

where J = laser energy (joules)

λ_o = laser wavelength (Å)

$\sigma(\Omega)$ = interaction cross-section (cm^2/steradian)

$\rho(R)$ = particle density (cm^{-3})

ΔR = range increment (meters)

β = transmission of receiver optics

η = detector quantum efficiency

D = receiver telescope diameter (meters)

PRF = laser pulse repetition frequency (sec^{-1})

T = observation time (sec)

α = extinction coefficient (km^{-1})

R = range (km)

B_λ = background flux (watts - cm^{-2} - $ster^{-1}$ - $\mathring{A}^{-1}$)

ϕ = receiver telescope beamwidth (milliradians)

λ = wavelength of maximum receiver transmission ($\mathring{A}$)

$\Delta\lambda$ = receiver optical bandwidth ($\mathring{A}$)

I_d = detector anode dark current (amps)

G = detector current gain

SECTION 5 APPLICATION OF RADIOMETRY TO DATA BUOYS

M. T. Decker and E. R. Westwater

5.0 Introduction

In this section, we discuss the possible application of microwave and infrared radiometers to remote sensing of atmospheric and ocean surface parameters from a buoy. Before presenting promising areas of radiometric remote sensing, a brief discussion of radiometers and atmospheric radiation will be given.

The fundamental quantity describing the atmospheric radiation field is the radiance, I_ν, describing the flow of spectral power density through a unit area and solid angle. The radiance is a function of position, viewing direction, wavelength, and is sensitive, in general, to the state of the atmosphere and surface conditions. The radiance is related to parameters of a medium by (Snider and Westwater, 1972)

$$I_\nu(0) = I_\nu^{ext}\, e^{-\tau_\nu(0,\infty)} + \int_0^\infty J_\nu\, e^{-\tau_\nu(0,s)}\, ds$$

where I_ν^{ext} is the radiance incident at the opposite boundary of the medium, J_ν is the source function, $\tau_\nu(0,s)$ is the optical depth from the origin to the point s, ds is a unit of path length and ν is the frequency. In the (usual) case, J_ν is given by

$$J_\nu = \alpha_\nu B_\nu(T)$$

where α_ν is the absorption coefficient and $B_\nu(T)$ is the Planck function of temperature T. Remote sensing of the atmosphere using radiance measurements is possible because the dependence of α_ν on composition (water vapor, clouds, ozone, etc.) and B_ν on temperature. Surface properties are usually inferred from measurements of I_ν^{ext}. Specific applications of these techniques will be discussed later. Before this is done, a brief description of radiometers is appropriate.

Both microwave and infrared radiometers are sensitive instruments for measuring the radiance incident on an aperture. Because of the rapid variability of absorption with frequency, radiometers used for remote sensing usually require narrow spectral resolution. This is in contrast to broad band radiometers used in radiation budget studies. In many (but not all) techniques, ground-based determination of composition and temperature profile requires measurements of the angular variation of I_ν. Such measurements require a narrow beam width (usually $\sim 0.5^\circ$), an accurate knowledge of pointing angle, and, in general, a stable platform on which to operate. In any anticipated buoy experiment, the radiometers optics and antenna system would be enclosed in a radome. The long and short term effect of an ocean environment on such a radome is an important consideration. In the following sections, we will describe techniques of passive remote sensing that, except where noted, have been field tested on land-based platforms.

5.1 Temperature and Water Vapor Profiles

Measurements of downwelling radiance from the clear atmosphere are a source of information about vertical temperature and humidity profiles. Temperature information is obtainable from measurements in the 5 mm band of O_2, and the 4.3 and 15 μm band of CO_2.

Water vapor may be studied from measurements at 183 GHz, and several IR bands of H_2O, such as 6.4 μm. Profile recovery from passive measurements requires solution of an inversion problem. Before discussing specific techniques of temperature and water vapor profiling, our inversion technique should be mentioned.

The difficult problem of recovering atmospheric profiles from indirect observations has received much attention in the past. Application of statistical estimation techniques to the inversion problem (Westwater and Strand, 1968) has led to successful retrieval of temperature profiles from satellite observations, and from ground-based measurements (Westwater, 1972; Snider, 1972). Below, we discuss the application of this technique to ground-based microwave inference of temperature profiles. The method, however, is quite general and is applicable to water vapor profiling, as well.

Statistical inversion techniques require knowledge of the statistical characteristics of atmospheric profiles to construct a physically significant and stable solution to the inversion problem of radiative transfer. The estimation of the required statistical matrices can be formed from a past history of directly measured profiles, such as a backlog of radiosonde observations. The a priori knowledge is then combined with transmission characteristics and radiometer noise levels to yield a minimum-variance data processing scheme. In Fig. 5.1, an example is given of the predicted achievability in temperature sensing by applying statistical techniques to microwave radiometer data. The curve labeled σ_T represents the a priori standard deviation in temperature which could be achieved by using only the measured surface temperature as a statistical predictor. The three dashed curves represent the residual standard deviation when the indicated angular scan measurements are used. Thus, for this climatology, angular measurements of the given noise levels and frequencies, can infer temperature profiles with a rms error of less than 1 K up to about 3 km.

Applying statistical inversion techniques to profile inference assumes that the a priori mean profile and covariance matrix are representative of the local environment of the radiometer. Since it is frequently desired to place radiometers in locations where a priori data have not been gathered, it is quite important to determine the sensitivity of inversion results to errors in estimating the representative statistics. Reasonable profile recoveries using statistical information gathered 50 to 60 miles from the radiometer location have been achieved, and results to date have indicated that profile recovery is insensitive to errors in representative statistics.

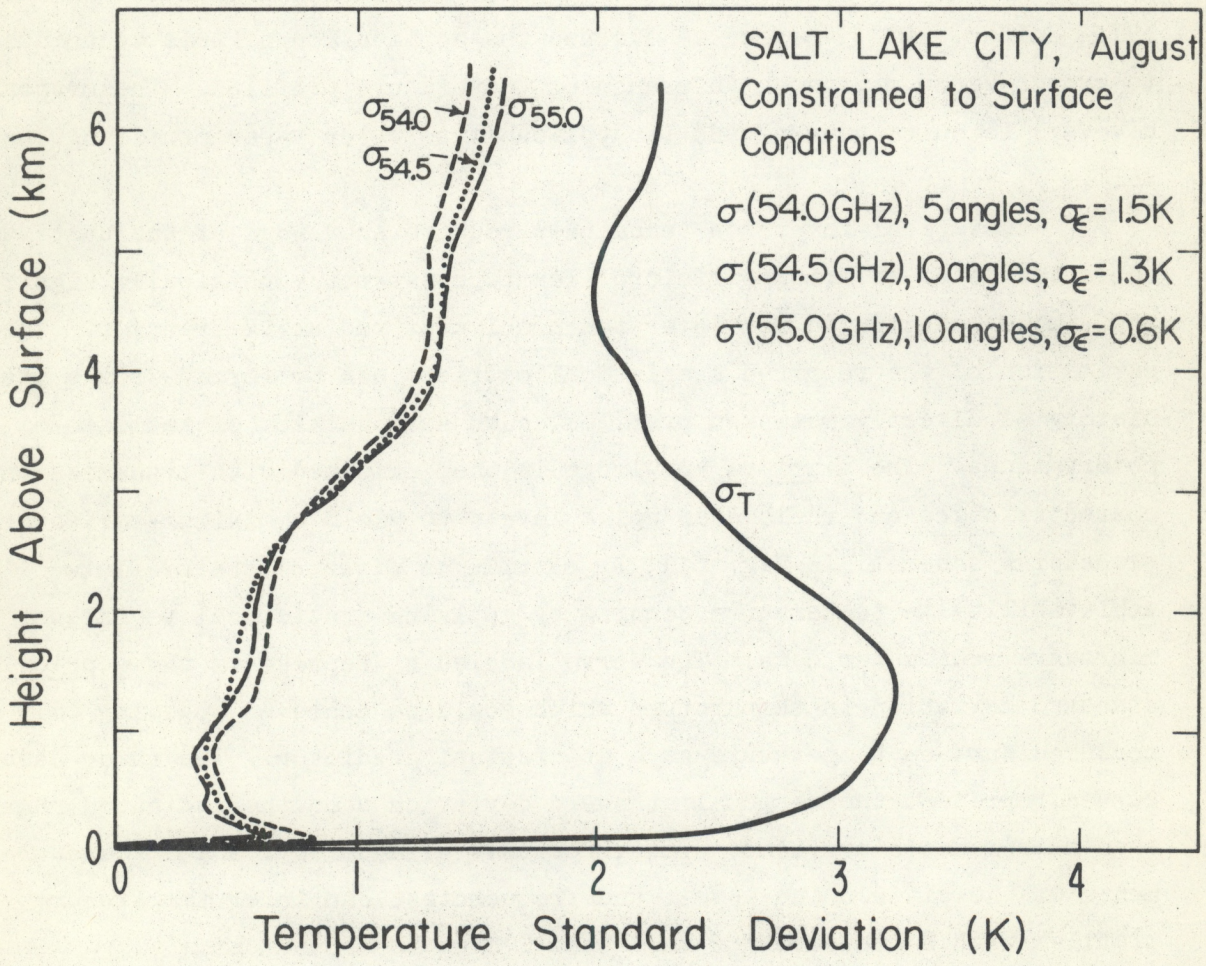

FIG. 5.1. PREDICTED ACHIEVABILITY in determining vertical temperature profiles by inversion of microwave radiometer data.

A passive technique which has received much experimental and theoretical effort is recovery of temperature profiles from microwave emission measurements in the 5 mm (60 GHz) band of O_2. The emission at any frequency and any angle is the weighted spatial average of the temperature profile over a distance whose optical depth is roughly equal to unity. Typical weighting functions are shown in Fig. 5.2. By varying the optical depth (by angular or frequency diversity) a set of brightness observations are generated that are sensitive to different layers of the temperature profile. The temperature profile is then recovered from the brightness measurements by inversion of an integral equation (see Westwater and Strand, 1972, for a discussion of inversion techniques).

A multi-channel mm wave radiometer has been constructed to implement the temperature profiling technique. Major objectives in the design of the radiometer were capability of operation in both angular-scan and multi-spectral modes, simultaneous operation on 3 or 4 frequencies from a common antenna, high angular resolution in the antenna system, good spectral resolution, and the greatest possible sensitivity consistent with the other design goals.

The radiometer enclosure and its 1.2 m diameter conical horn antenna are installed on an elevation over azimuth antenna mount which provides the capability of angular scan operation. (See Fig. 5.3). The antenna position is read out remotely at the data recording position. A relatively large antenna aperture was employed to obtain a high angular resolution while the conical horn configuration was selected to minimize stray radiation into the back and side lobes and thereby simplify the conversion of antenna temperature to brightness temperature. It should be realized, however, that the use of a smaller aperture would be desirable for a buoy application. Some research in antenna design is certainly needed here.

A summary of the essential radiometer characteristics is presented Table 5.1.

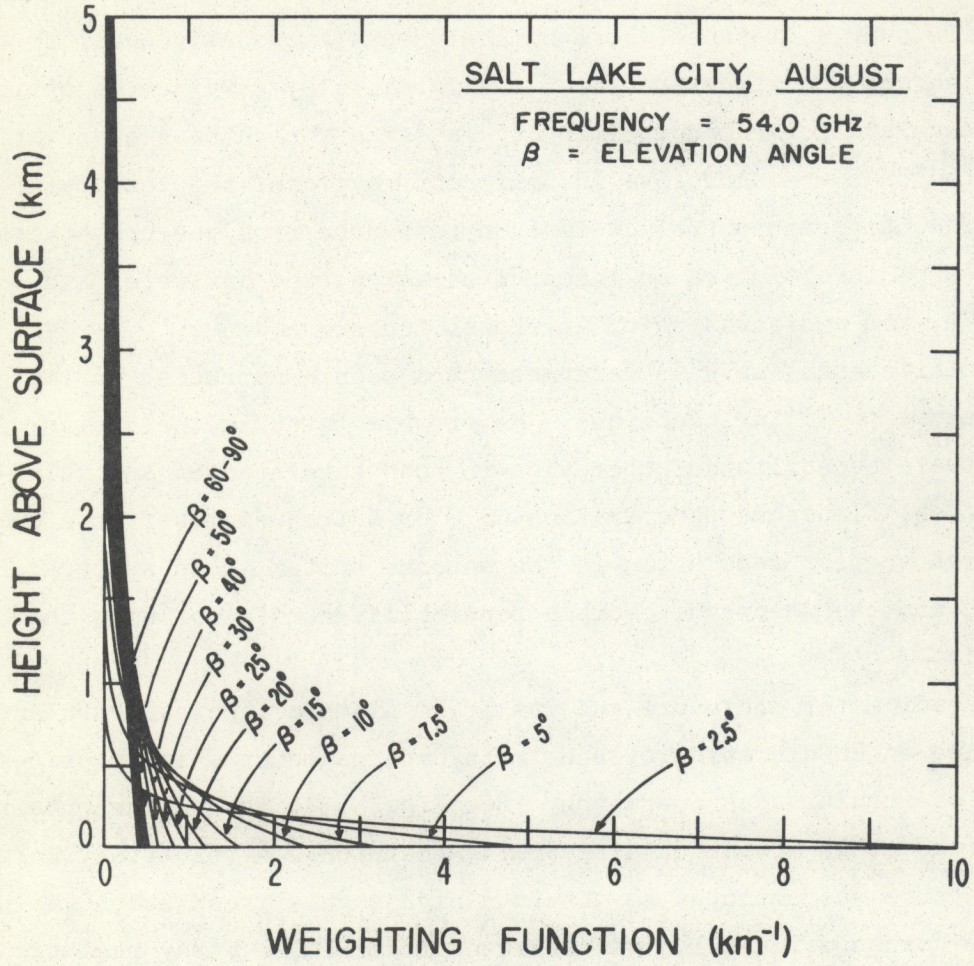

FIG . 5.2. WEIGHTING FUNCTIONS FOR ANGULAR PROBING

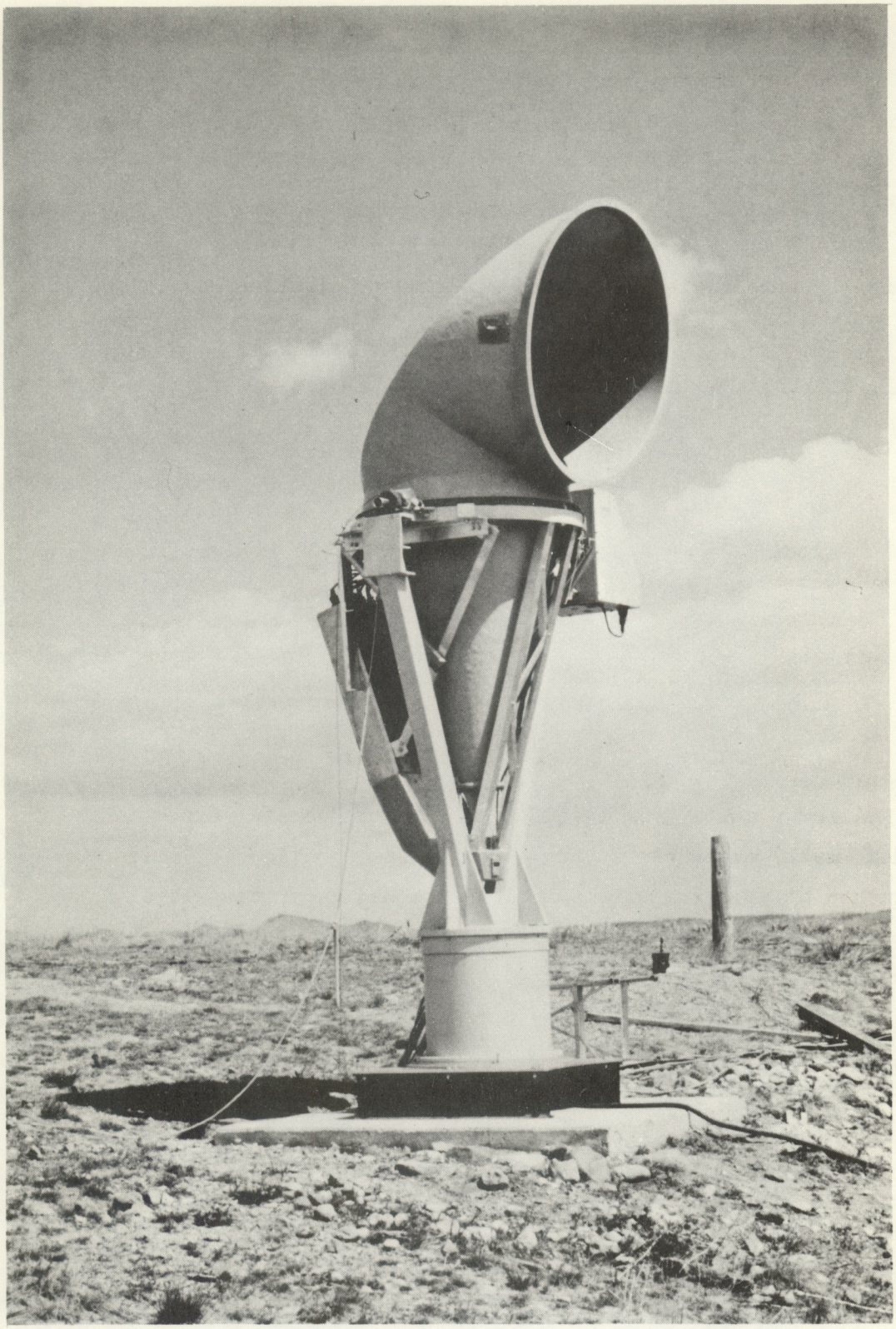

Fig. 5.3. Four frequency radiometer and conical horn antenna.

Table 5.1 Multi-frequency radiometer characteristics

Operating frequency	- 52.5, 53.5, 54.5, 55.5 GHz
Antenna Characteristics	- 1.2 meter diameter conical horn, 3 dB beamwidth 0.3°
Receiver type	- Dicke switching radiometer, dual-conversion superheterodyne 1st IF: 4 to 8 GHz 2nd IF: 60 MHz center frequency, noise bandwidth approx. 30 MHz
Sensitivity	- Approx. 1 K for 60 s integration time

A few results from a recent temperature sensing experiment (Snider, 1972) are shown in Fig. 5.4. These profile recoveries were determined by applying statistical techniques to multispectral and multiangle data gathered by the radiometer described above. As is evident from inspection of Fig. 5.4 the correspondence between the temperature profiles measured by a radiosonde and by the radiometer is good.

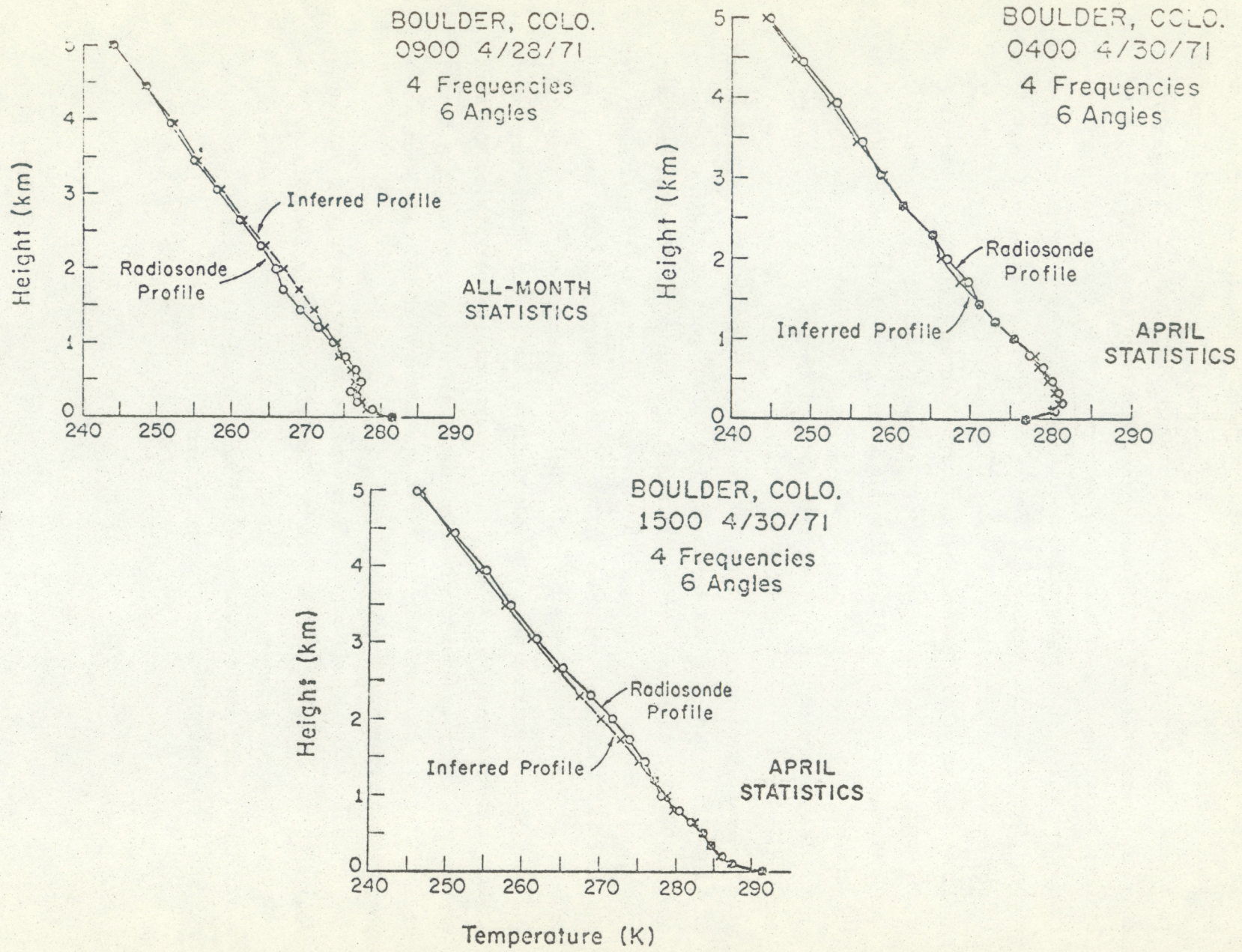

Fig. 5.4 Inferred and measured temperature profiles using combination of angle-scan and multi-spectral input data.

The alternative to microwave ground-based passive temperature profiling is from infrared CO_2 measurements. Although little has been published in this area, the technique is both theoretically and technologically feasible. Much developmental work in IR radiometers has been done because of satellite applications. Because of the large variation of IR absorption with frequency, a zenith viewing multi-frequency radiometer could provide an alternative to angular scanning. The major problem with the IR technique is the extreme sensitivity to clouds, a limiting factor in satellite applications as well. An experiment was conducted recently by Barnes Engineering Company and the Wave Propagation Laboratory in which a 15 μm band radiometer and a 60 GHz radiometer were operated simultaneously. The results of this experiment should be available in about three months.

The determination of humidity profiles from gound-based passive techniques has not received as much attention as the temperature problem. Nevertheless, the same techniques of recovering profiles from measurements of downwelling radiance can be used. Promising spectral regions include the 183 GHz H_2O line and several infrared H_2O bands. In the IR, radiometer technology already exists, again because of satellite techniques. However, the spectral locations would be different than currently used satellite channels. A variety of theoretical studies are needed in this area, (a) what accuracies and height resolutions are obtainable from currently available measurement techniques? (b) what inversion techniques are most appropriate to ground-based humidity sounding? (c) can a humidity profile be obtained without knowledge of the temperature profile? (d) what are the optimum frequency locations?

In IR sensing schemes, the temperature and/or water vapor channels should be supplemented with a "window channel" to aid in identifying emission data contaminated with clouds. A simple optical arrangement would also permit sea surface observations. From these observations, sea surface temperature could be easily inferred.

5.2 Precipitable Water

Microwave radiometric techniques can be used for an indirect measurement of the total precipitable water in the atmosphere. This line integral of water vapor density is easier to obtain than the height distribution of vapor, so that the simpler measurement is appropriate where the profile information is not required. Both single channel and multiple channel techniques have been proposed (Gaut, 1968; Naumov, 1968; Waters and Staelin, 1968) and a number of experiments performed that indicate the feasibility of the method. Related studies of the correction of range measurement errors introduced by water vapor (Westwater, 1967; Schaper, et al., 1970; Guiraud, et al., 1971) also indicate the potential of the method.

A single channel measurement will be adequate for many meteorological purposes, and a simple method for analysis is given here. The thermal emission from the atmosphere is measured at an appropriate wavelength near the 1.35 cm water vapor absorption line, the wavelength being chosen to minimize the effect of the spatial distribution of vapor on the observed radiation. This condition is met at wavelengths of 1.28 and 1.46 cm for

reasonable tropospheric distributions of water vapor. The total absorption at either of these wavelengths due to water vapor is then directly proportional to the total precipitable water along the line of observation. With an estimate of the mean radiating temperature, T_m, of the atmosphere, the observed thermal emission (in terms of a brightness temperature, T_b,) may be written

$$T_b = T_m (1 - e^{-kW - \tau_d})$$

where W is precipitable water, k is an absorption coefficient and τ_d is the total absorption due to the dry constituents of the atmosphere. Reasonable estimates of T_m, k, and τ_d can be made using surface temperature values, and hence with a measurement of T_b, the precipitable water can be determined.

Evidence supporting this technique comes from both simulated observations and from field measurements. For example, the precipitable water and the corresponding computed zenith brightness temperature at 1.46 cm have been determined from 73 Hawaiian radiosondes, and the two variables are correlated with a coefficient of unity. Measurement errors were not introduced in this computation. Waters and Staelin (1968) have estimated that the integrated water content can be determined to 0.1 g/cm^2 from a two-channel measurement of zenith emission. Indirect evidence of the ability of the microwave radiometer is contained in experiments performed by the Wave Propagation Laboratory in 1968 and 1971. Fluctuations of electrical range on a mountain top to sea level path in the Hawaiian Islands are compared to observed sky brightness temperatures on an adjacent path. The range fluctuations in the microwave region result primarily from the changes in integrated water vapor along the path, and as such represent variations of interest here. A series of 1230 simultaneous measurements of these two quantities during a 16-day period in 1971 resulted in a correlation of 0.9, where both clear and cloudy atmospheres are included. Fig. 5.5 is an example of a one-day comparison of range fluctuations measured directly and inferred from radiometric observations.

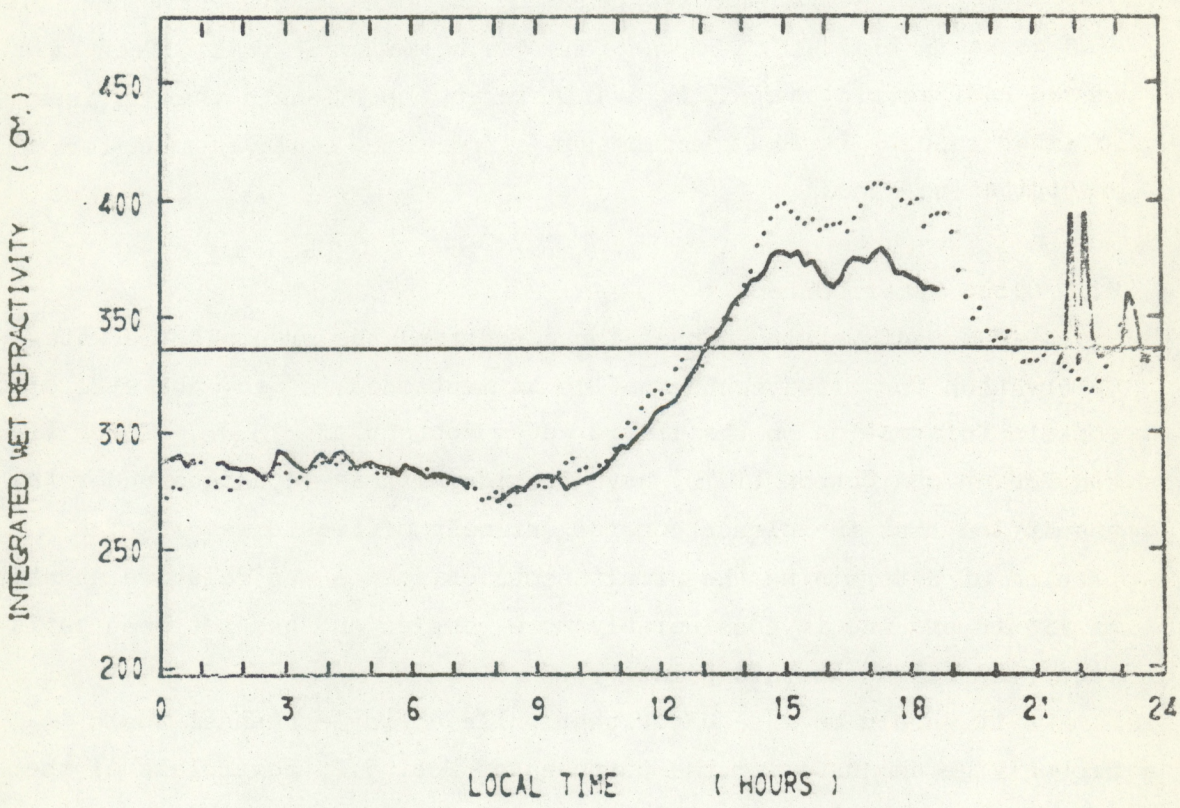

FIG. 5.5. Comparison of fluctuations in electrical range (dotted curve) with the same quantity derived from radiometric measurements (solid curve), for data collected 8/27/71.

Application of the technique to a buoy platform would require pointing direction be known and probably stabilized near the zenith for the period of measurement. Pointing to a high degree of accuracy would not be required in this case. A single measurement could be made in about ten seconds, depending on radiometric sensitivity.

Clouds represent a contaminating source of radiation to this measurement as can be seen in the two peaks in the radiometric curve near time 2200 hours in Fig. 5.5. Corrections can be made for this effect if a second radiometric channel is available at a wavelength that is insensitive to water vapor. It is expected that corrections could be made for all but precipitating clouds.

5.3 Cloud Water Content

The radiometric channel for correcting the precipitable water observation for cloud contamination as mentioned in Sec. 5.2 will also contain information on the liquid water content of clouds. Toong (1967) and Decker and Dutton (1970) have considered this technique under the assumption that the clouds consist entirely of liquid water. The problem of determining the simultaneous existence and relative quantities of liquid and ice is considerably more complex and has not been satisfactorily solved at this point.

It should be made clear that while a single channel would probably be adequate for the purposes of Sec. 5.2, regardless of the ice-liquid ratio in non-precipitating clouds, additional information would be required if the total condensed water substance is to be measured. The degree to which the quantities can be resolved with additional radiometric channels and under various meteorological conditions is currently being studied.

5.4 Surface Properties

Remote sensing of a number of ocean surface properties has been proposed, primarily for satellite and airborne applications (see, for example, Hansen, 1972). Many of these properties could be point sampled directly from a buoy, but it might also be desirable to adapt some of the remote sensing techniques, and a few examples are mentioned here. Potential advantages include the fact that area averages may be obtained that are more representative than direct point measurements. Techniques have been suggested for detecting water surface temperature, salinity, pollution, ice, sea state, and albedo. The difficulty of making a good surface temperature measurement by direct means suggests that an IR radiometer would be appropriate here. Considerable work has been done on the effects of sea state on microwave brightness temperatures, including theoretical calculations by Stogryn (1967) and experimental work from surface based platforms by Hollinger (1971) and Shipley and Torok (1969). The various results are not completely consistent and further evaluation would be required.

5.5 Recommendations

A number of proposals are made here for evaluation of several promising buoy-based remote sensing techniques. In general, each of these require a certain amount of theoretical or modeling study to show their viability in the marine environment, followed by experiments on a stable platform, and then adaptation to the buoy platform. Cost estimates reflect this sequence, but could require some modification as results become available. The cost estimates are given in the categories of (1) Theoretical or modeling studies, (2) Equipment costs, (3) Experimental operation and analysis, (4) Consultation.

5.5.1 Proposal for Evaluation of Precipitable Water Measurement in a Cloudy Atmosphere

While considerable evidence exists regarding the feasibility of the radiometric measurement of precipitable water under clear or nearly clear sky conditions, we would propose additional theoretical and experimental work on correction techniques for cloud contamination. Theoretical work would consist of model computations of the cloud effect to determine (1) the appropriate wavelength for a radiometer, (2) the best method for utilizing the data in a correction process, and (3) the degree to which a successful correction could be made under various meteorological conditions. Following this an experimental effort is proposed in which a two-channel radiometric system would be tested at a suitable land based site and the resulting data compared with radiosonde data. Portions of the required equipment are available in the Wave Propagation Laboratory, but some additional equipment will be required, depending in part on the outcome of the theoretical work. Approximately two weeks of experimental recording are proposed not including time for preparation and analysis. Further experimental evaluation in the buoy environment is proposed following successful land based operation.

Estimated costs are

	FY 73	FY 74	FY 75	FY 76	FY 77
(1)	15.0 K	(3) 45.0 K	(3) 50.0 K	(4) 15.0 K	(4) 5.0 K
(2)	40.0 K	(2) 80.0 K			
Total	55.0 K	125.0 K	50.0 K	15.0 K	5.0 K

5.5.2 Proposal for Theoretical Study of Passive IR Profiling

Because of the large variation in IR atmospheric transmission, multi-spectral buoy-based passive radiometric measurements can recover both temperature and humidity profiles. Before an experimental program appropriate to a buoy can be mounted, many theoretical questions must be answered. Among these are: (a) how many channels are necessary to give desired results? (b) what frequencies should be selected? (c) what inversion algorithms are appropriate for simultaneous humidity and temperature profiling from ground-based IR measurements? (d) can a volume averaged surface measurement of sea temperature be incorporated in the instrument package?

A series of experimental evaluations as determined by the theoretical work would be carried out, probably in conjunction with those of Proposal 5.5.3.

Estimated costs are

	FY 73	FY 74	FY 75	FY 76	FY 77
(1)	30.0 K	(2) 50.0 K	(3) 20.0 K	(4) 15.0 K	(4) 5.0 K
		(3) 45.0 K			
Total	30.0 K	95.0 K	20.0 K	15.0 K	5.0 K

5.5.3 Experimental Study of 5 mm Passive Temperature Profiling

Temperature profile recovery from ground-based 5 mm radiometric observations has been achieved (see Sec. 5.2). Multichannel radiometers have been field tested by the Wave Propagation Laboratory at several locations, all of which possessed a stable platform. Before a buoy or a ship-based experiment can be adequately proposed, further questions relevant to antenna design and platform stability must be investigated.

It is proposed that these questions be answered by a modeling study in which the different parameters can be varied in a simulated marine environment. Equipment specifications will result and procurement can then be initiated. Experimental evaluation would probably be in conjunction with tests of Proposal 5.5.2.

Estimated costs are

	FY 73		FY 74		FY 75		FY 76		FY 77
(1)	15.0 K	(3)	45.0 K	(3)	45.0 K	(4)	15.0 K	(4)	5.0 K
(2)	110.0 K	(2)	50.0 K						
Total	125.0 K		95.0K		45.0 K		15.0 K		5.0 K

5.5.4 Proposal for Investigation of Determination of Cloud Cover Using Passive IR Radiometry

Measurements of IR emission in a "window" channel are insensitive to background fluctuations of clear atmospheric variables (temperature, pressure, and moisture). Clouds, however, radiate nearly as black bodies, and their contribution to the emission within a given solid angle will be roughly proportional to percentage cloud cover within this angle. We propose to investigate the accuracy with which cloud cover can be inferred from a single, broad beam, IR emission measurement. Important considerations of this investigation are:

a) The effect of scattering from aerosols

b) The degree to which "clear" emission can be predicted in the presence of clouds

c) The effect of varying cloud heights.

Following this investigation a cloud monitoring program utilizing the radiometric technique coupled with time lapse photography would be initiated at the Wave Propagation Laboratory. An experimental effort would be conducted in the buoy environment if the technique proves successful.

Estimated costs are

	FY 73		FY 74		FY 75		FY 76		FY 77
(1)	12.0 K	(3)	25.0 K	(3)	25.0 K	(4)	10.0 K	(4)	5.0 K
(2)	25.0 K	(2)	10.0 K						
Total	37.0 K		35.0 K		25.0 K		10.0 K		5.0 K

5.5.5 Proposal for Lightning Flash Counters on an Ocean Buoys

A lightning flash counter is an instrument for counting the number of lightning discharges that occur within a certain distance of the unit during a given period of time. There are perhaps a thousand or more instruments of this type in use around the world employing various electromagnetic methods of sensing a lightning discharge and of recording the information. A typical instrument has an antenna, a triggering device and a counting unit.

Each unit would supply information on the occurrence of thunderstorms in the vicinity of the buoy. Such information would be valuable in the interpretation of data concerning the lower atmosphere and the sea state. It would also be useful in short term weather forecasting, in supplying data on the world-wide distribution of thunderstorms, for obtaining statistical data on radio noise, and for aiding atmospheric electricity studies of the earth-ionosphere global electric circuit. A decision on the relative importance of these uses must be made before selecting a particular design of the antenna, triggering unit, and counting device.

A design and development program is proposed with a following experimental evaluation in the data buoy environment.

Estimated costs are

FY 73	FY 74	FY 75	FY 76
20.0 K	30.0 K	15.0 K	10.0 K

References

Decker, M. T., and E. J. Dutton (1970), Radiometric observation of liquid water in thunderstorm cells, J. Atmos. Sci., Vol 27, No. 5, 785-790.

Gaut, N. E. (1968), Studies of atmospheric water vapor by means of passive microwave techniques, Massachusetts Inst. of Tech. Cambridge Research Lab. of Electronics, Tech. Rept. 467, Dec. 20, 1967.

Guiraud, F. O., M. T. Decker and E. R. Westwater (1971), Experimental investigation of the correction of electrical range errors by passive microwave radiometery, NOAA Technical Report, ERL 221-WPL 19.

Hanson, K. J. (1972), Remote Sensing of the Troposphere, Chap. 22, Remote sensing of the ocean, CU-NOAA (1972).

Hollinger, J. (1971), Passive microwave studies, Third annual Earth Resources Program Reviewer, Vol. III, Sect. 69, NASA, MSC, Houston, Texas.

Naumov, A. T. (1968), Izv., Atmospheric and Oceanic Physics, Vol. 4, No. 2, 170-181.

Schaper, L. W. Jr., D. H. Staelin and J. W. Waters (1970), The estimation of tropospheric electrical path length by microwave radiometry, Proc. IEEE, Febr. 1970, 272-273.

Shipley, D. G., and K. J. Torok (1969), Passive microwave measurememts of sea surface temperature, RCA Defense Electronic Products, Princeton, N. J., Rept. No. AED-R-3525.

Snider, J. B. (1972), Ground-based sensing of temperature profiles from angular and multi-spectral microwave emission measurements, J. Appl. Meteorology, Vol. 11, No. 6, 958-967.

Snider, J. B., and E. R. Westwater (1972), Remote Sensing of the Troposphere, Chap. 15, Radiometry, CU-NOAA (1972).

Stogryn, A. (1967), The apparent temperature of the sea at microwave frequencies, IEEE Trans. Ant. Prop. AP-15, 2, 278-286.

Toong, H. D. (1967), Interpretation of atmospheric emission spectra near 1-cm wavelength, Proc. Northeast Electronics Research and Engineering Meeting (NEREM), Boston, Mass., Nov. 1967, 214-215.

Waters, J. W., and D. H. Staelin (1968), Statistical inversion of radiometric data, Massachusetts Inst. of Tech. Cambridge Research Lab. of Electronics, Quarterly Progress Rept. 80.

Westwater, E. R. (1967), An analysis of the correction of range errors due to atmospheric refraction by microwave radiometric techniques, ESSA Tech. Rept. No. IER 30-ITSA 30.

Westwater, E. R. (1972), Ground-based determination of low altitude temperature profiles by microwaves, Monthly Weather Review 100, 1, 15-28.

Westwater, E. R., and O. N. Strand (1968), Statistical information content of radiation measurements used in indirect sensing, J. Atmos. Sci., Vol 25, No. 5, 750-758.

Westwater, R. R., and O. N. Strand (1972), Remote Sensing of the Troposphere, Chap. 16, Inversion Techniques, CU-NOAA (1972).

Section 6 LINE-OF-SIGHT METHODS

R. S. Lawrence

6.0 Introduction

Line-of-sight techniques exist for measuring, with laser beam and/or microwaves, the integrated turbulence, the average crosswind, and the total amount of water vapor along a line of sight. (See Section 5 for further mention of the water-vapor problem.) Most of these techniques, as they have been developed and used on ground-to-ground paths, require equipment at both ends of a line-of-sight. Since it is our understanding that the data buoys will normally be used singly rather than in pairs, we shall not describe in detail the possible applications of these methods.

6.1 Measurement of Winds Aloft

One line-of-sight technique that does seem promising is the observation of starlight to measure winds aloft. Winds aloft are an essential ingredient for numerical weather forecasting, and present methods of balloon observation give insufficient continuity. Our proposed optical method relies upon the fact that turbulence, always present throughout the atmosphere, produces an irregular pattern of intensity of starlight on the earth's surface. The pattern moves across the earth as the winds aloft carry the turbulence. The result is the familiar twinkling (scintillation) of stars, and simple apparatus can be devised to measure the rate of the motion.

It is more difficult to infer the height of the wind that is being measured, and to separate winds blowing at different velocities at different heights. The simplest method of making such a determination

relies on the fact that the scale-size of the scintillation pattern depends upon the distance between the observer and the turbulence. Turbulence near the observer produces fine-scale patterns, while that at greater heights produces larger patterns. The pattern size increases as the square-root of the height, and is about 10 cm for turbulence at the height of the tropopause. Using this fact, it is possible to design receiving telescopes to respond primarily to the winds from any desired height or, by the use of multiple receiving apertures (spatial filtering), to measure separately the winds at several heights. Ochs and Clifford (1972) have demonstrated that such a system, using four small telescopes (about the size of ordinary binoculars) to observe Polaris, measures winds that are well correlated with rawinsonde observations of upper winds.

There are two difficulties with the spatial-filtering method, using a small number of simple apertures. First, the effective filters are very broad, giving poor height resolution. Typical resolution is about 30 percent in height, i.e. the winds can be measured independently at only three separate, slightly overlapping, height ranges in the atmosphere. Second, the height range being measured varies somewhat with the vertical profile of turbulence that happens to be present in the atmosphere. Thus, the height range varies from day to day, and it is not possible to define it exactly for any particular observation.

6.2 Recommendation for the Development of a More Accurate Method

Both of the difficulties mentioned above can, in principle, be avoided by the use of photodiode arrays to achieve high-resolution spatial filters and the use of nearby pairs of stars and receivers spaced about a meter apart to, in effect, triangulate on the turbulence. While these methods are understood theoretically (see Harp, 1971), they have not been attempted in practice. We recommend that a ground-to-mountaintop path be established using artificial light sources as "stars" and that this path be used to test the performance of the method and to optimize the parameters of the instrument. The mountaintop location for the sources has several obvious advantages over the use of actual stars. In particular, tracking apparatus will not be required and the sources can be varied at will.

Using the facilities and equipment already available in the Wave Propagation Laboratory, the supplementary resources required establish an appropriate path, to test the performance of the method, and to optimize the parameters of the instrument are listed below.

The immediate result of such an effort would be a report giving a definite statement of the feasibility of measuring winds aloft from ground-level observations of starlight and a description of the ground-based apparatus. No attempt would be made to design the tracking and acquisition equipment required to operate such a system on a moving buoy, nor would such environmental factors as the effect of salt spray on lenses be considered at this time. Presumably the tracking and acquisition equipment could resemble the star-trackers used for spacecraft navigation.

The first twelve calendar months of the WPL effort would involve the following supplements to funds and equipment that are presently available:

Labor	$58,100
Interfacing equipment between existing photodiode array and existing minicomputer	4,500
Report	1,000
Miscellaneous expenses	1,200
NOAA Support Services	4,900
	$69,700

The entire project would probably extend over portions of five fiscal years as follows:

FY 73	Set up equipment and make initial tests of feasibility	$35,000
FY 74	Complete feasibility tests and prepare report	85,000
FY 75	NOAA personnel to consult with a commercial supplier to make a detailed engineering design	40,000
FY 76	NOAA personnel to work with NDBP personnel to help with operation and interpretation of data	10,000
FY 77	Complete the work of FY 76	5,000
	Five-year total	$175,000

6.3 References

Harp, J. C. (1971), Resolving the motions and turbulent structure of the atmosphere from line-of-sight propagation measurements, NATO Adv. Study Inst. on Statistical Methods and Instrumentation in Radiometeorology, Ch. 5.

Ochs, G. R. and S. F. Clifford (1972), Measurement of atmospheric winds by observation of stellar scintillations, presented at 1972 USNC/URSI-IEEE Spring Meeting, Washington, D. C.

Section 7 SUMMARY AND RECOMMENDATIONS

C. G. Little and V. E. Derr

7.0 Introduction

A large number of concepts for the remote measurement of atmospheric or oceanic parameters from ocean buoys have been discussed in the previous sections. It now remains to bring these concepts together, to summarize and evaluate them, and then to develop recommendations as to which concepts seem worthy of implementation or further study.

The process we have used to achieve this evaluation is as follows. The different remote sensing concepts were tabulated in broad categories of Acoustic echo-sounding, Lidar, Radar, and Passive techniques respectively, with each category broken down into atmospheric and ocean remote sensing. For each technique, the parameters to be measured were identified. Each concept was then evaluated numerically according to (a) the importance of the parameter(s) being measured, (b) the estimated probability that the system could work successfully in the buoy environment, (c) the absence of any other existing measurement system (such as a satellite system) capable of measuring the parameter.

Examination of the numerical ratings showed that the concepts should be divided into two categories, (a) those for which the hardware had been sufficiently tested on land that one could appropriately go straight to the development phase, and (b) those for which research funds would first be required, because of important uncertainties as to the feasibility of the system (due either to engineering problems, or to uncertainties in the physical principles involved).

Based on the above analysis, the different concepts were rank-ordered in relative priority for Development or for Research funding. Tentative budgets have been drawn up for a five-year period for each concept, and are summarized below.

7.1 Concepts Recommended for Development Funding

Priority 1 Atmospheric Acoustics

Considerable research has been conducted in recent years in acoustic echo-sounding, both by the Wave Propagation Laboratory and by other groups. This has shown that acoustic echoes are readily obtained in the atmospheric boundary layer, and can be used to monitor the internal structure (e.g., convective plumes, temperature inversions) of the atmosphere. Moreover, Doppler and phase angle of arrival techniques can be used to measure wind profiles. The ability to remotely sense both the wind profiles and the internal structure and processes of the atmospheric boundary layer from ocean buoys would seem to be extremely important, and for this reason we give top priority to this concept for development funds. The tasks proposed are outlined in some detail in Section 2; the estimated budget requirements for the tasks to be undertaken by WPL are as follows.

Proposed Budget

Fiscal Year	$K
73	30
74	153
75	200
76	20
77	10

Priority 2 Microwave Temperature Profiling

As discussed in Section 5, research and development work in WPL and in industry has shown that atmospheric temperature profiles can be readily measured using microwave radiometric techniques in the 5 mm O_2 absorption band. A commercially developed unit, (the Thermosonde) is potentially

available, and the next task would appear to be to undertake the necessary development studies which will permit eventual operation in the buoy environment. The physical limitations of this technique - contamination of data by clouds, and rather poor height resolution - prevent our giving it top priority, but at this time it does appear to offer good promise for the routine measurement of temperature profiles. The details of the proposed development tasks are given in Section 5; the proposed expenditures by fiscal year are as follows.

Proposed Budget

Fiscal Year	$K
73	125
74	95
75	45
76	15
77	5

Priority 3 Sea Scatter

As described in Section 3, the spectrum of sea waves can be remotely sensed by HF radar techniques. The theory and experimental hardware involved are well understood, and because of the obvious importance of being able to routinely monitor the sea state for some hundreds of kilometers around the buoy, we recommend this technique for development funding. The proposed phasing of these studies is outlined in Section 3; the proposed fiscal year breakdown of WPL expenditures is as follows.

Proposed Budget

Fiscal Year	$K
73	30
74	110
75	20

Priority 4 Precipitation Radar

Almost since the first development of radar, it has received some use for remote sensing of precipitation. In recent years, the advent of solid

state devices has greatly increased the operational reliability of radars, and it is now widely used by the National Weather Service for routine monitoring of severe storms and precipitation. Because of the advanced state of this technology, and the obvious value of routine monitoring of precipitation out to 200 km from the buoy for weather forecasting and research purposes we recommend this concept for development funding. The proposed tasks are also identified in Section 3; the proposed WPL expenditures by fiscal year are given below.

Proposed Budget

Fiscal Year	$K
73	40

7.2 Concepts Recommended for Research Funding

The following research tasks are recommended for funding in the amounts shown. The highest priority is listed first, but the difference in importance between the highest and lowest priority is not great.

Priority 1 Ocean Acoustic Sounding Research

Very extensive use of underwater acoustic ranging has been made for detection of man-made targets, but its use in environmental probing is only beginning. Data developed principally by the Navy shows a potential for measuring physical parameters such as temperature structure, currents and sea surface state and biological entities such as seaweed and fish. Only acoustic waves have the potential to study the complex internal wave and turbulent structure of the ocean because of their small attenuation and large interaction. The position of the thermocline and upwelling areas is also detectable by acoustic sounding, as well as regions of heavy sedimentation. A five-year research effort by WPL is recommended, funded as below; the details of the proposed tasks are given in Section 2.

Proposed Budget

Fiscal Year	$K
73	15
74	210
75	200

Priority 2 Optical Lidar Applications to Data Buoys

The potential multiple applications of lidar to the atmosphere and to the ocean, using the same basic system, are the reasons for a strong recommendation for research in this area to extend presently-known capabilities and explore new ones. At present, in the atmosphere, temperature and humidity profiling have been shown feasible; in the oceans the lidar has been used for chlorophyll concentration measurement. Preliminary studies have shown that the measurement technique should be extendable to wind, cloud parameters, aerosols and high level atmospheric constituents in the atmosphere; in the ocean, temperature profiles, O_2 content, biological material, fish and fish oils should be measurable. This is a tremendous range of measurements with one instrument and could create a major expansion of the capability of data buoys. A five-year program is proposed, research to continue throughout that time. On some techniques development can begin as early as the second year.

Proposed Budget

Fiscal Year	$K
73	138
74	326
75	250
76	95
77	35

Priority 3 High Sensitivity, Continuous Wave Radar

As discussed in Section 3, recent developments in continuous wave radars show considerable promise for remote monitoring of atmospheric structure and dynamics. The FM/CW technique has already been fully demonstrated; pseudo-random or random noise modulated radars which offer the possibility of Doppler measurements of wind velocity would appear to be even more valuable. Therefore, research funding is requested to permit undertaking the tasks identified in Section 3.

Proposed Budget

Fiscal Year	$K
73	60
74	160
75	40

Priority 4 Passive Techniques

a. Passive Infrared Radiometry

Passive techniques have great advantages of simplicity, low cost and low power consumption. Infrared radiometry, using variable frequency techniques has a potential for measuring water vapor and temperature profiles. A study of the technique and a field evaluation is recommended.

b. Measurement of Winds Aloft by Star Scintillation

The profile of high altitude winds is of great importance in medium and long range weather forecasting. The stargazer technique is a simple means of determining this parameter in clear weather. A program of research and field evaluation is required to precede a development program for buoy use.

Proposed Budget

	a. Passive IR	b. "Stargazer"
Fiscal Year	$K	$K
73	30	35
74	95	85
75	20	40
76	15	10
77	5	5

7.3 Concepts Not Recommended for Funding At This Time

Among the concepts discussed in Section 5 are two which are not recommended for funding at this time. These are (a) measurement of precipitable water by microwave radiometry at about 20 GHz, and (b) measurement of cloud cover by infrared techniques. Although both are valid

techniques, similar data are potentially available on a global basis by satellite techniques; for this reason we do not recommend them for funding at this time.

7.4 Concluding Remarks

In closing this Summary and Recommendations Section, it is important to stress the very preliminary nature of its conclusions. As emphasized in the Introduction, it is based on a brief 3 month $15K study, as opposed to the 3 man year $90K originally planned. Although the conclusions reached and recommendations given are, of course, believed valid, the potential importance of the decisions reached as to the role of remote sensing in the National Data Buoy Project is so large that it is obvious that further studies of this problem should be undertaken. Since the eventual expenditures of public funds in the NDBP program will probably exceed 10^8 dollars, the accurate identification of optimum array of sensor systems is obviously very important. The role of remote sensing of the oceans and marine atmosphere from data buoys is clearly going to be a critical one; we feel that this first study, although hopefully a valuable one, must be followed by other more detailed ones if the right scientific technological and management decisions are to be reached. For example, in addition to specific analyses of individual measurement concepts, there is an important need for a critical look as to specifically what parameters should be measured by ocean buoys of the late 1970's or the '80's, and who will be the users of the data, and for what purposes. For example, this preliminary report has not considered the measurement of the very important energy exchange processes between the atmosphere and the ocean. Detailed analysis might well come up with methods for the routine monitoring of the fluxes of heat, momentum and water vapor (evaporation), which, so far as we are aware, are not among the parameters presently listed as planned for measurement by NDBP. Similarly, analysis is needed as to how networks of buoys might be used to measure the mesoscale divergence and convergence so important to the GATE and GARP programs.